NTNU – Trondheim
Norwegian University of
Science and Technology

Validation of material model for polypropylene (PP)

Kristin Sælen

Master of Science in Product Design and Manufacturing
Submission date: June 2012
Supervisor: Arild Holm Clausen, KT
Co-supervisor: Marius Andersen, KT

Norwegian University of Science and Technology
Department of Structural Engineering

Department of Structural Engineering
Faculty of Engineering Science and Technology
NTNU- Norwegian University of Science and Technology

ACCESSIBILITY

OPEN

MASTER THESIS 2012

SUBJECT AREA:	DATE	NO. OF PAGES:
POLYMER ENGINEERING	10.06.2012	96+50

TITLE:

Validation of material model for polypropylene (PP)

Validering av materialmodell for polypropylen (PP)

BY:

KRISTIN SÆLEN

SUMMARY:
A hyperelastic-viscoplastic material model intended for thermoplastics has been developed by SIMLab at NTNU. This model formed the basis of the thesis, where a material model for the polymer polypropylene was calibrated and validated. Four rounds of material testing were carried out. Tension and compression tests formed the basis for a calibration of the material model. Two different component tests were used for validation; stretching of a plate with a hole and plate impact tests.

The calibrated model was implemented as a user-defined material model in the non-linear finite element code LS-DYNA, and numerical simulations of the tension and compression tests were carried out in order to verify the calibrated parameters. The component tests were numerically simulated with the purpose of controlling the ability of the model to predict the behaviour of the material when subjected to more complex loading cases.

The calibrated material model was able to capture the main characteristics of the experimental tests. The model does, however, have limitations, as it was not able to correctly predict all strain rate effects of the material at high strain rates, like viscoelasticity. A partly recalibration of the material model was carried out to enable the model to predict the material's behaviour at high strain rates.

RESPONSIBLE TEACHER: Professor Arild H. Clausen

SUPERVISORS: Arild H. Clausen, Marius Andersen, Anne Serine Ognedal

CARRIED OUT AT: SIMLab, Department of Structural Engineering, NTNU

MASTEROPPGAVE 2012

Kristin Sælen

Validation of material model for polypropylene (PP)

(Validering av materialmodell for polypropylen (PP))

As a part of the development of the finite element method, significant effort has been devoted to propose new material models which are able to represent the material behaviour at different conditions. Relevant parameters involve strain level, strain rate, temperature, and the material at hand may also exhibit anisotropy, viscoelasticity etc. Today, material models for metals are in general more accurate than models for e.g. polymers. This is a general tendency for all non-linear finite element programs, including Abaqus and LS-DYNA. SIMLab is involved in the development of improved models for thermoplastics. A model applicable for ductile polymers was ready in 2010, and the research work continues with other classes of models.

All new models need to be validated against experimental benchmark tests for different types of polymers. Validation involves also calibration, requiring material tests on the material at hand. This master thesis is concerned with a PP material produced by the German company SIMONA. The selected benchmark tests are tension of a plate with a hole and impact tests on small plates. Subsequently, the test results are to be compared with numerical predictions applying the material model for ductile thermoplastics.

Some keywords for activities related to this master thesis project are:

- Literature: Polymers in general, relevant test results, material models.
- Experimental tests: Material and component tests. Presentation of test results.
- Calibration: Identify the coefficients of the material model.
- Numerical modelling: Simulation of experimental tests. Evaluation of the model.

The candidate may agree with the supervisors to pay particular attention to specific parts of the investigation, or include other aspects than those already mentioned.

The thesis is to be organized as a research report, recognising the guidelines provided by Department of Structural Engineering.

Supervisors: Arild H. Clausen, Marius Andersen and Anne Serine Ognedal

The report is to be handed in at Department of Structural Engineering not later than 11 June 2012.

NTNU, 18 January 2012

Arild H. Clausen

faglærer

Sammendrag

En hyperelastisk-viskoplastisk materialmodell beregnet for termoplaster er utviklet av SIMLab ved NTNU. Modellen var grunnlaget for denne masteroppgaven, der en materialmodell for polymeren polypropylen ble kalibrert og validert. Fire runder med materialtester ble gjennomført. Strekk- og trykktester dannet grunnlaget for en kalibrering av materialmodellen. To forskjellige komponenttester, strekk av plater med et hull og fallende last på en plate, ble brukt som valideringstester.

Den kalibrerte modellen ble implementert i det ikke-lineære elementmetode-progammet LS-DYNA som et brukerdefinert materiale, og numeriske simuleringer av strekk- og trykktestene ble gjennomført for å verifisere de kalibrerte parametrene. Testene med strekking av plater med hull og fallende last på en plate ble numerisk simulert for å sjekke materialmodellens evne til å forutsi oppførselen til materialet når det ble utsatt for komplekse lasttilstander.

Den kalibrerte materialmodellen var i stand til å fange opp hovedtrekkene til de eksperimentelle testene. Modellen klarte imidlertid ikke å forutsi alle tøyningshastighetseffekter i materialet under store tøyningshastigheter, som for eksempel viskoelastisitet. En delvis rekalibrering av materialmodellen ble gjennomført slik at modellen kunne forutsi oppførsel ved høye tøyningshastigheter.

Acknowledgement

This thesis was written at the Structural Impact Laboratory at the Department of Structural Engineering at NTNU from January to June 2012.

I would especially like to thank Professor Arild H. Clausen for excellent supervising, and for always being willing to help. I would also like to thank co-supervisors PhD students Marius Andersen and Anne Serine Ognedal for good and helpful advice.

The experimental tests were done in collaboration with students Tonje Hegni, Torgrim Østen and Kjetil Vange. I would like to thank them for helpful discussions and cooperation during the work with this thesis.

Many thanks also to Senior Engineer Trond Auestad for great help during the material testing in the laboratory.

Kristin Sælen

Trondheim, June 2012

Table of Contents

1 Introduction

The use of polymers has increased the last decades, especially in the structural and automotive industry. Polymers are resistant to corrosion, easy to form, rather cheap, light and durable, and these attractive characteristics have resulted in polymers replacing metals in many cases. Polymers are experiencing an increased use in load carrying components, and this is due to the low density and high energy absorption skills of the polymers [1].

Since the use of polymers in components subjected to mechanical loading increases, careful design of these components is required. Numerical simulations involving finite element analysis of the polymer components are applied. However, most of the material models in commercial finite element codes available are based on the behaviour of metals.

As the mechanical behaviour of polymers can be more complex than the behaviour of metals, different constitutive models are required. Among the three groups of polymers; thermosets, elastomers and thermoplastics, there exist rather accurate models for the first two. However, a material model for thermoplastics still needs improvements [2,3].

Structural Impact Laboratory (SIMLab) at the Department of Structural Engineering at NTNU has been involved in research and development of improved material models for thermoplastics. SIMLab is a Centre for Research-based Innovation, and this thesis is written in cooperation with SIMLab. In 2010, SIMLab introduced a constitutive model for thermoplastics [4], and this thesis is a study of that model.

The scope of the thesis is to calibrate a material model for the polymer polypropylene, and further validate this model. The ability of the model to correctly predict the behaviour of the material polypropylene was to be evaluated as well. The model consists of several parameters determined from a range of experimental tests.

The thesis will firstly give an account of polymers and polypropylene in Section 2. The most important theory behind the constitutive material model is also explained. Further, material tests in tension and compression are described in Section 3, and the results are presented and evaluated. Section 4 gives an account of the calibration process, and Section 5 outlines the numerical simulations of the tension and compression tests.

Furthermore, tension tests on plates with a hole and plate impact tests are explained in Section 6. The section presents the results from the experimental tests, as well as an evaluation of the numerical simulations of the validation tests. The thesis is in Section 7 concluded, and recommendations for further work are outlined. Data from the experimental tests, as well as MATLAB scripts and LS-DYNA keywords are shown in the appendices.

2 Theory

This chapter will shortly present the theory behind polymers and further introduce the polymer polypropylene. The theory of hyperelasticity and viscoplasticity is shortly described, before the constitutive model for thermoplastics is introduced.

2.1 Polymers

A polymer is a material that consists of molecular chains. These molecular chains are made up of 1000 to 100 000 identical units called monomers. The process where monomers are linked together to molecule chains is called polymerization, and the main building block in the molecular chains is carbon atoms. All molecules that can link to form a chain can be a monomer. Therefore an enormous amount of different polymers exists. The properties of a polymer depend on the structure of its monomer [5].

Polymers can be divided into three groups; thermosets, elastomers and thermoplastics. Polypropylene is a thermoplastic. The difference between these groups is the bonding between the molecular chains. Thermoplastics consist of only weak van der Waals bonds between the molecular chains [1]. Elastomers and thermosets can also have covalent bonds between the chains, called cross-links. In elastomers, cross-links occur at a rate of about 1 per 1000 atoms, and thermosets have a higher density of covalent cross-links [6].

Thermoplastics are semi-crystalline because they consist of both crystalline and amorphous regions. In the crystalline regions, the chain molecules are regularly arranged, like the simplified model in Figure 2-1 shows. In between the crystalline areas, there are amorphous regions. These regions do not have a regular structure [5]. Figure 2-2 illustrates the principle of the semi-crystalline structure with crystalline and amorphous regions.

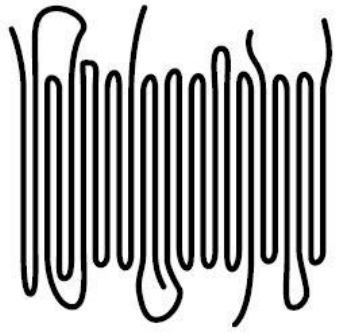

Figure 2-1. A crystalline region of a polymer [5].

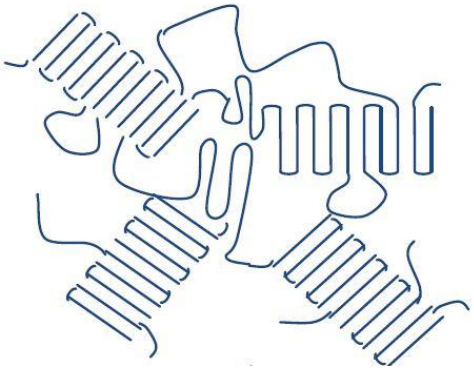

Figure 2-2. Semi-crystalline structure with crystalline and amorphous regions [3].

The schematic drawing in Figure 2-3 illustrates the deformation behaviour in thermoplastics. First, the amorphous regions are uncoiled, and then the crystalline areas are rotated and separated. Thermoplastics can take large plastic deformations because the chains can slide relative to each other [5]. The crystalline regions give the thermoplastics strength, while the amorphous areas provide flexibility to the material [3].

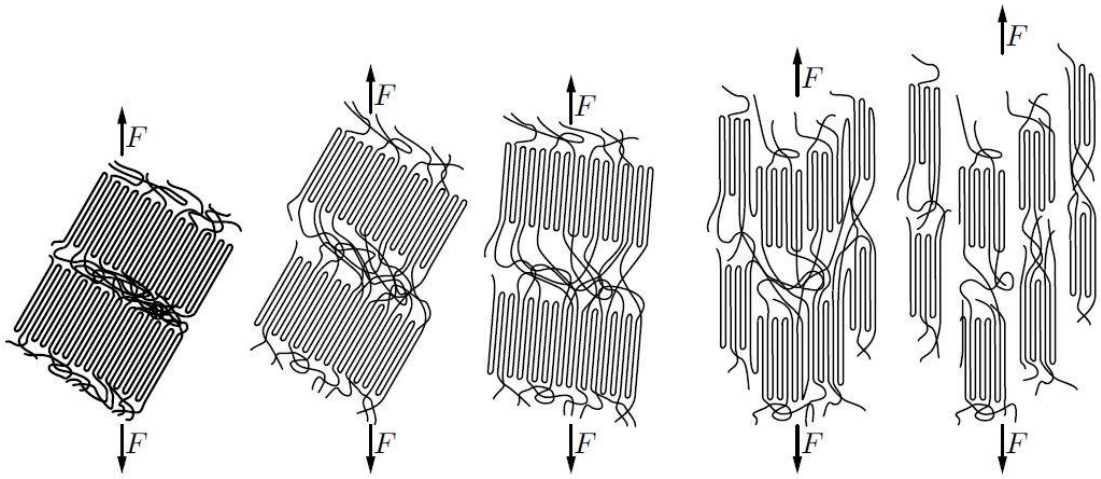

Figure 2-3. A simplified model of the deformation in polymers [5].

2.2 Polypropylene

Polypropylene is a semi-crystalline thermoplastic polymer. It was developed in 1959 and is used in a variety of different areas and industries. Typically polypropylene is defined as a lightweight and rigid material, with excellent chemical resistance [7]. The short form of the name, PP, is used from here on. The chemical structure of PP is seen in Figure 2-4, where the PP monomer is repeated *n* times.

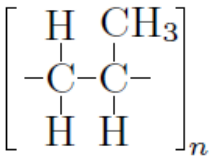

Figure 2-4. Chemical structure of polypropylene [5].

2.3 Material models for thermoplastics

Materials can be described by a material model with the purpose of representing the behaviour of the material when subjected to loading. This section will describe three material models; viscoelasticity and viscoplasticity, as well as hyperelasticity.

2.3.1 Viscoelasticity and viscoplasticity

A viscoplastic model includes strain rate dependency in the plastic area. Figure 2-5 illustrates elastic-viscoplastic behaviour in one dimension, where the yield stress increases with the strain rate $\dot{\varepsilon}$. σ_0 represents the yield stress at a quasi-static strain rate. The viscous stress, σ_v, is the rise in yield stress because of increased strain rate [8]. The elastic area is not sensitive to the strain rate, and a constant Young's modulus is applied in elastic-viscoplastic models. Polymers exhibit strain rate sensitivity in the plastic regime, and should hence be described by a viscoplastic model [9].

A viscoelastic model on the other hand, has strain rate dependency in the elastic area. Polymers can experience large plastic deformations, and hence viscoelasticity is less important in polymer models.

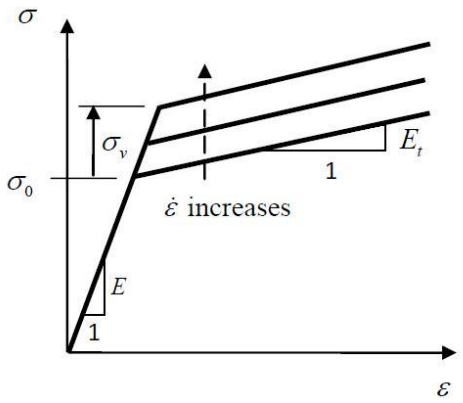

Figure 2-5. Elastic-viscoplastic behaviour with linear work-hardening [8].

2.3.2 Hyperelasticity

A hyperelastic model is derived from a strain energy function, which results in path independent stress states. In contrast, hypoelastic models are formulated in rate form, and may dissipate elastic energy [10].

2.4 A hyperelastic-viscoplastic model for thermoplastics

The hyperelastic-viscoplastic material model for thermoplastics introduced by Polanco-Loria et al. [4] is seen in Figure 2-6 and Figure 2-7. The model was developed for explicit finite element analysis. This material model was calibrated for PP in this thesis, and evaluated in LS-DYNA.

The model assumes that the resistance of the material to deformation is divided into two parts. Part A represents the intermolecular resistance to deformation, while part B represents the intramolecular resistance [6]. The intermolecular resistance to deformation corresponds to forces between the molecular chains. Intramolecular resistance on the other hand means a stretching of the molecular chains in the polymer [11]. This section will give an account of the main equations and principles of the model.

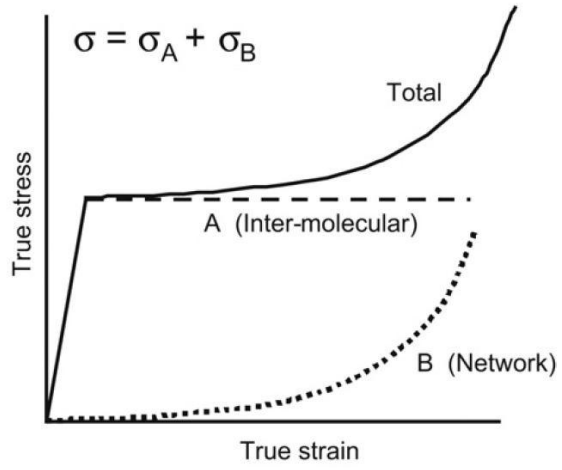

Figure 2-6. Hyperelastic-viscoplastic constitutive material model for thermoplastics [4].

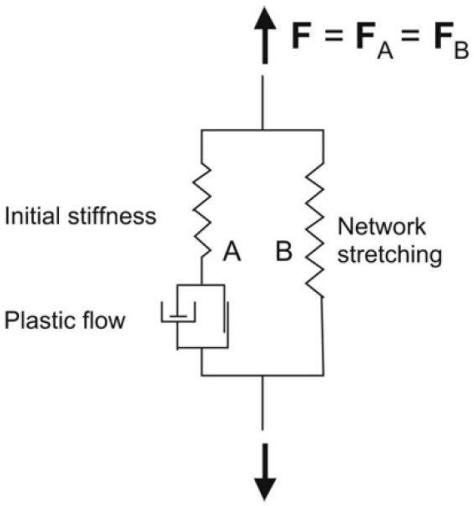

Figure 2-7. Rheological model for the material model [4].

Part A - Intermolecular resistance

Part A is represented by the left side of the rheological model in Figure 2-7. The friction plates in the figure describe the plastic flow, where Equation (2-1) is the modified Raghava yield criterion.

$$f_A = \bar{\sigma}_A - \sigma_T - R = 0 \tag{2-1}$$

σ_T is the yield stress in uniaxial tension and $\bar{\sigma}_A$ is the equivalent stress introduced by Raghava et al. [12]. $\bar{\sigma}_A$ is defined in Equation (2-2) where the coefficient α describes the pressure sensitivity of the material. When α is higher than 1, the material has a higher yield stress in compression than in tension, and the material is pressure sensitive. A pressure sensitive material has different material properties in tension and compression.

$$\bar{\sigma}_A = \frac{(\alpha - 1)I_1 + \sqrt{(\alpha - 1)^2 I_1^2 + 12\alpha J_2}}{2\alpha} \tag{2-2}$$

The variable R is defined in Equation (2-3) and is representing hardening or softening, depending on whether σ_S is larger or smaller than σ_T. σ_S is the saturation stress. The hardening parameter H controls the stress between the yield stress and saturation stress. ε^P is the plastic strain [6].

$$R(\varepsilon^P) = (\sigma_S - \sigma_T)\left[1 - e^{-H\varepsilon^P}\right] \tag{2-3}$$

The flow rule potential defined by Raghava et al. [12] was modified by Polanco-Loria et al. [4] and is seen in Equation (2-4). The coefficient β controlling the plastic dilatation was introduced.

$$g_A(\beta) = \frac{(\beta - 1)I_1 + \sqrt{(\beta - 1)^2 I_1^2 + 12\beta J_2}}{2\beta} \geq 0 \tag{2-4}$$

The elastic response of Part A is described by the spring on the left side of the rheological model in Figure 2-7. This spring involves two coefficients; Young's modulus E and Poisson's ratio ν. The strain rate dependency is represented by the dashpot, including the strain rate sensitivity parameters $\dot{\varepsilon}_{0A}$ and C [2]. The relationship between these parameters is described by Polanco-Loria et al.[4] and seen in Equation (2-5).

$$\bar{\sigma}_A = \sigma_T \left(1 + C \cdot \ln\left(\frac{\dot{\varepsilon}_A^P}{\dot{\varepsilon}_{0A}} + 1\right)\right) \tag{2-5}$$

Part B - Intramolecular resistance

The right side of the rheological model in Figure 2-7 represents Part B, and this part is controlled by the parameters C_R and $\bar{\lambda}_L$. C_R is the initial elastic modulus for Part B, and $\bar{\lambda}_L$ is the locking stretch. The locking stretch is related to the maximum possible deformation of the material [4]. The locking stretch is reached when the molecular chains are oriented in the stretch direction, and this is illustrated in Figure 2-8.

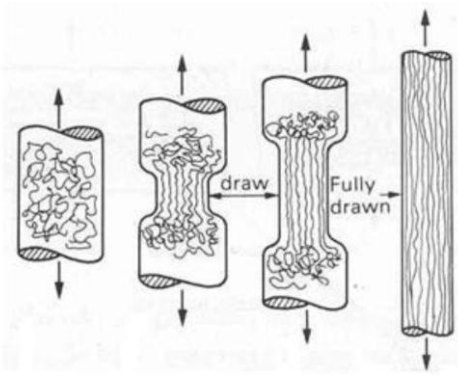

Figure 2-8. Illustration of the stretching of the molecular chains [2].

Equation (2-6) represents the stress state in Part B.

$$\boldsymbol{\sigma}_B = \frac{1}{J_B}\frac{C_R}{3}\frac{\bar{\lambda}_L}{\bar{\lambda}}\mathcal{L}^{-1}\left(\frac{\bar{\lambda}}{\bar{\lambda}_L}\right)\left[\boldsymbol{B}_B^* - \bar{\lambda}^2\boldsymbol{I}\right] \tag{2-6}$$

$\mathcal{L}^{-1}$ is the inverse of the Langevin function, which is defined as $\mathcal{L}(x) = \coth(x) - \frac{1}{x}$. The effective distortional stretch, $\bar{\lambda}$, is defined as $\bar{\lambda} = \sqrt{\frac{tr(\boldsymbol{B}_B^*)}{3}}$, where $\boldsymbol{B}_B^*$ is the distortional left Cauchy-Green deformation defined $\boldsymbol{B}_B^* = \boldsymbol{F}_B^*(\boldsymbol{B}_B^*)^T$ and $\boldsymbol{F}_B^* = J^{-\frac{1}{3}}\boldsymbol{F}_B$ is the distortional part of the deformation gradient $\boldsymbol{F}_B$. The Jacobian determinant is defined $J_B = J = \det(\boldsymbol{F})$.

3 Material testing

A wide range of material tests on the material polypropylene were carried out. This chapter will describe the test material, the experimental program and the Digital Image Correlation technique. Furthermore, tension and compression tests are presented.

3.1 Material

The material studied in this thesis was extruded plates of type PP-DWU from the German company SIMONA AG, and they were delivered right before the testing was carried out.

The plates were delivered with dimensions 2000 x 1000 mm, and with two different thicknesses, 5 mm and 10 mm. The test specimens for all the tests were cut out of these plates, at least 100 mm from the plate edge.

The material properties of PP-DWU as provided by the supplier are shown in Table 3-1. The supplier describes the material by characteristic properties like high corrosion resistance, low density when compared to other materials, high surface hardness, long life span, low water absorption, good processing properties and universal application [13].

It is common for the manufacturers of polymers to add particles to the material in order to improve the properties. Mineral or rubber particles are the most common fillers, and the particles usually have a size of 1 μm [11]. For PP, the mineral filler talc is typically used to improve the mechanical strength. An increase in the mineral filler content will however decrease the fracture toughness [3]. As the material is yielding, the particles will loosen from the rest of the material, and during hardening the voids where the particles were fastened will grow. This will lead to volume increase [14]. The suppliers do not provide information about the content of particles, and it is assumed that mineral or rubber particles are present in the material.

Table 3-1. Material properties of PP-DWU [13].

Density	910	kg/m^3
Yield stress	32	MPa
Elongation at yield stress	8	%
Elongation at tear	70	%
Tensile Young's modulus	1400	MPa

3.2 Experimental test program

Tests were carried out in tension and compression at different strain rates. A servo-hydraulic Dartec M1000/RK testing machine with a capacity of 20 kN was used for the tension and compression tests, as well as for the component tests on a plate with a hole. The applied velocity was constant in each test. An Instron CEAST 9350 Drop Tower machine was used in the plate impact tests. The machines recorded the cross-head displacement and force. The test samples were carefully measured before and after testing with a digital caliper.

The geometries of the test samples, and the angle that the samples were cut from the plate with respect to the extrusion direction, are shown in Figure 3-1. In reality there were two PP plates, one of thickness 5 mm and one of thickness 10 mm, and the figure is a simplified model showing all the test specimens in the same plate.

Uniaxial tension tests were carried out the two test samples with different thickness named T in Figure 3-1. Compression tests were done on the two different types of circular test samples named C. The circular sample with the length axis parallel with the extrusion direction had a height of 8 mm while the other specimen had a height of 5 mm. In addition, tension tests were carried out on the two different types of 5 mm thick test samples with a hole in the middle, named H in the figure. These samples had a different diameter of the holes. The 5 mm thick square specimen named D was used in plate impact tests in the Drop Tower machine.

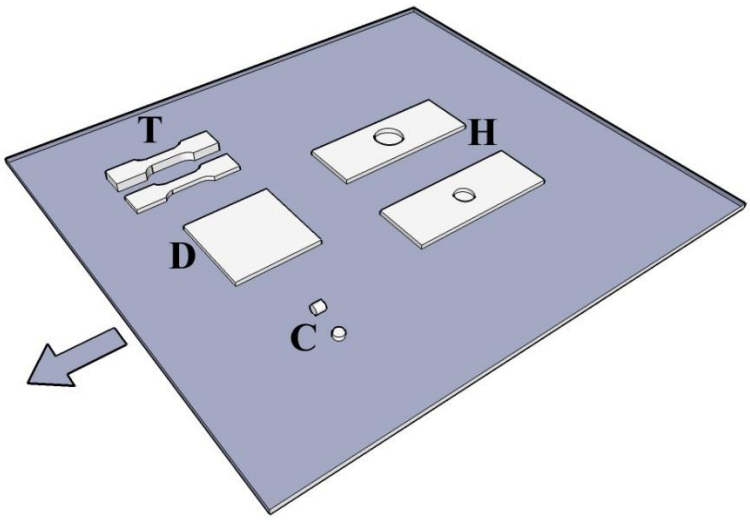

Figure 3-1. Layout of the test samples cut from the plate. The arrow indicates the extrusion direction.

3.3 Digital Image Correlation

A Digital Image Correlation (DIC) technique was used to measure the strains and displacements in the test specimens during testing. DIC is an optical technique that tracks changes in images taken during the tests to determine measurements. An extensometer was not used in the testing because the displacements were too large.

The test samples were covered in white paint with a random pattern of black spots before the test, like seen in Figure 3-2. This was done to ensure that the changes in the specimen were recognizable in the pictures. The painting was done right before the testing to ensure that the paint was still wet, so it would deform with the test specimen without any cracking [1]. A digital camera was used during the tests, taking pictures with a frequency adapted to the cross-head velocity, ensuring that each test was documented by circa 200-300 pictures.

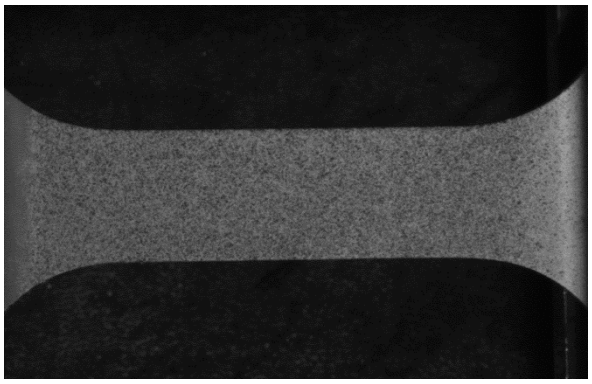

Figure 3-2. Tension test specimen covered with paint.

The pictures from the camera were post-processed by the DIC software 7D. This software can extract the desired data from the test, for example the deformation or strain field. 7D works in the way that a grid is made on the test specimen in the area where data is needed, like seen in Figure 3-3, and the program is then able to follow this grid throughout all the pictures by recognizing the paint pattern on the specimen in each picture. Figure 3-4 shows the grid when the test sample is stretched. The paint pattern is compared to the pattern in the first picture, and 7D will measure how many pixels each point has moved. These data can be further processed in MATLAB where the deformation in pixels can be transferred into millimeters. The force and displacement data from the machines was synchronized with the DIC pictures, facilitating calculation of stresses and strains at a common time axis.

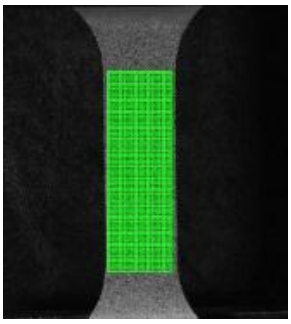

Figure 3-3. The grid on a test specimen in the software 7D.

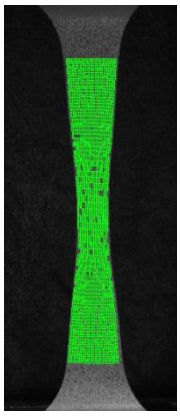

Figure 3-4. The grid following the deformation in the test specimen in 7D.

3.4 Uniaxial tension tests

11 uniaxial tension tests were carried out, and they consisted of test samples of two different thicknesses, 5mm and 10 mm. The geometry of the specimens is shown in Figure 3-5. The parallel area had a length of 33 mm and a width of 12 mm. The test specimens were all cut out from the plates in the extrusion direction as shown in Figure 3-6.

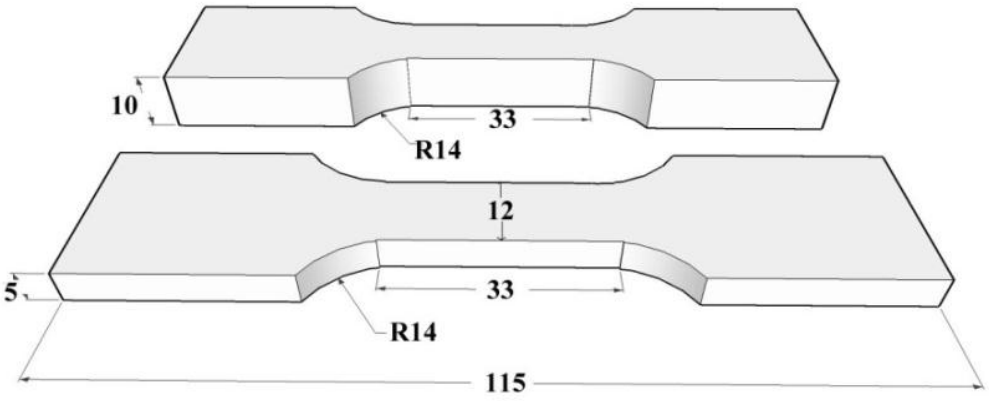

Figure 3-5. Test specimen geometry, where all dimensions are in millimeters.

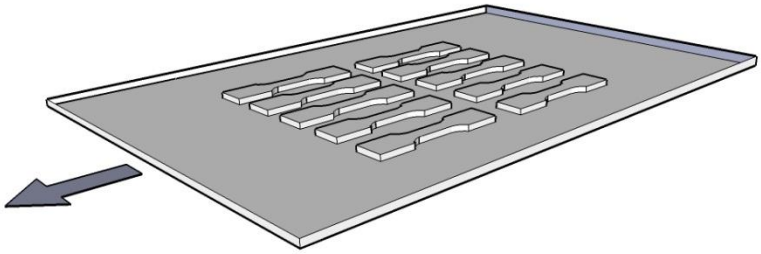

Figure 3-6. Test specimen geometry in relation to the extrusion direction, which is indicated by the arrow.

The tests were carried out at four different strain rates. The cross-head velocity v of the test machine was defined using Equation (3-1) [11], where L_0 is the initial length of the uniaxial area and $\dot{e}$ is the nominal strain rate. This strain rate corresponds approximately to the initial true strain rate. They are not exactly the same because there will be some deformation outside the parallel area in the test sample.

$$v = L_0 \dot{e} \tag{3-1}$$

An overview of the tests that were carried out, and their thickness, velocity and strain rate is shown in Table 3-2. The tests were named PP-T#, where PP means Polypropylene, T indicates Tensile test, and # is the number of the test. It was carried out two tests at each strain rate on the 5 mm thick samples to ensure repeatability. A third sample was ready to be tested as well, but it turned out to be not necessary since the data from the two first tests was similar.

Table 3-2. Survey of tension tests.

Test number	Strain rate [s^{-1}]	Velocity [mm/s]	Thickness [mm]
PP-T1	10^{-3}	0.033	5
PP-T2	10^{-3}	0.033	5
PP-T3	10^{-2}	0.33	5
PP-T4	10^{-2}	0.33	5
PP-T5	10^{-1}	3.3	5
PP-T6	10^{-1}	3.3	5
PP-T7	$10^{-2.5}$	0.104	10
PP-T8	$10^{-2.5}$	0.104	10
PP-T9	10^{-2}	0.33	10
PP-T10	10^{-1}	3.3	10
PP-T11	10^{-3}	0.033	10

3.4.1 Test method

The servo-hydraulic Dartec testing machine described in Section 3.2 was used in the tests. The tension test specimens were fastened to the machine by clamps, as shown in Figure 3-7. The bottom clamp was fixed, while the top clamp was moving at a constant velocity. This velocity is seen in Table 3-2.

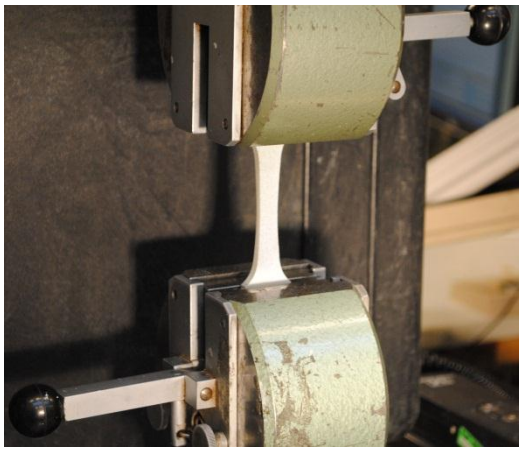

Figure 3-7. Test setup for tension tests.

3.4.2 Digital Image Correlation in the tension tests

The camera was placed right in front of the test specimen during the tests, as seen in Figure 3-8. A black background was used to obtain good contrast in the pictures. After the test, the pictures were processed in the computer software 7D, where the strain field in the longitudinal and transverse direction was found by using the DIC technique. Figure 3-9 shows the strain field in the longitudinal direction of test specimen PP-T2, obtained from 7D.

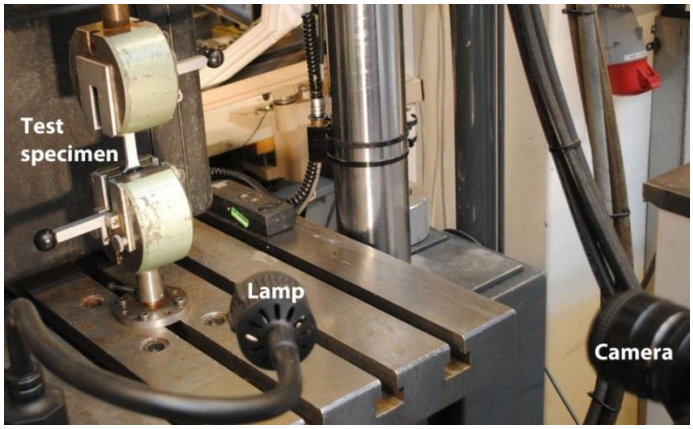

Figure 3-8. Test setup for tension tests.

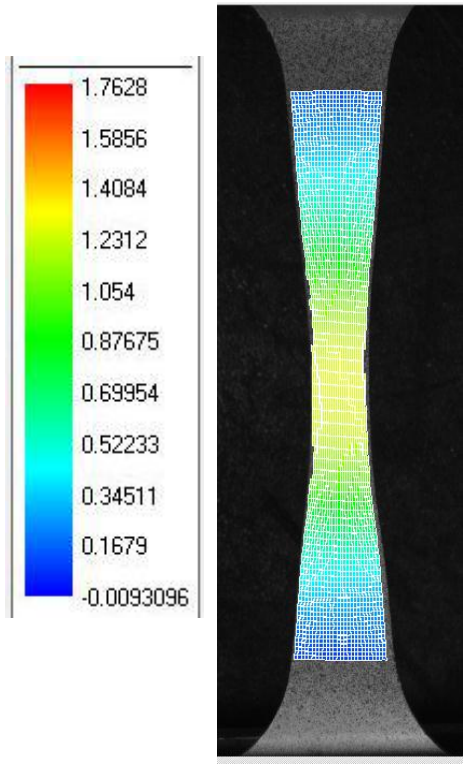

Figure 3-9. Longitudinal strain field of test specimen PP-T2 after a displacement of 34 mm.

The longitudinal strain at different cross sections of the sample was determined using MATLAB, and the section where the largest longitudinal strain occurred was located. The strain in the stress-strain curves from the tension tests was taken from this cross section. The MATLAB script that was made to determine the strain is seen in Appendix E.

3.4.3 True stress in the tension tests

When determining the true stress, it was assumed that the transverse strain ε_w was equal to the thickness strain ε_t, which means that the material was isotropic. To control that this assumption was valid for this specific material, the width and thicknesses of the test specimens were measured before and after the testing. Using Equation (3-2) and (3-3) [11],the nominal transverse strain e_w and the nominal thickness strain e_t was calculated for all of the test specimens that not experienced failure.

$$e_w = \frac{\Delta B}{B_0} \tag{3-2}$$

$$e_t = \frac{\Delta t}{t_0} \tag{3-3}$$

B_0 is the initial width, ΔB is the change in width, t_0 is the initial thickness and Δt the change in thickness. The results are gathered in Table 3-3.

Table 3-3. List of nominal transverse and thickness strains.

Test number	e_w [mm]	e_t [mm]
PP-T1	0.466	0.470
PP-T2	0.461	0.471
PP-T3	0.518	0.585
PP-T4	0.526	0.594
PP-T5	0.452	0.609
PP-T11	0.134	0.147

As shown in the table, the nominal transverse strains and thickness strains are approximately the same in most cases, and it seems to be a sound assumption that the transverse strain ε_w is equal to the thickness strain ε_t.

Once the transverse strain ε_w was known, the cross section area of the test specimen was calculated using Equation (3-4) [11] where A_0 is the initial cross section area. The true stress was obtained by Equation (3-5), where F is the force from the test.

$$A = A_0 e^{2\varepsilon_w} \tag{3-4}$$

$$\sigma = \frac{F}{A} \tag{3-5}$$

The Dartec machine provided measurements of the force and cross-head displacements. This data was synchronized with the DIC pictures, facilitating calculation of stresses and strains at a common time axis. Subsequently, these data were plotted as stress-strain curves.

3.4.4 Bridgeman corrector

When a circular test specimen is stretched, the stress state in the neck transition zone changes from uniaxial to triaxial tension, and Bridgeman developed a correction so that the triaxial behaviour was accounted for in the average stress. Le-Roy proposed an empirical approximation to the Bridgeman corrector [2]. The Bridgeman/Le Roy correction was investigated by Hovden [2], and based on the results found by Hovden, the Bridgeman effect is not included in this work.

3.4.5 The yield stress in the tension tests

The yield stress in polymers is assumed to occur at the maximum point on the nominal stress-strain curve, which coincides with the point where necking starts [6]. However, the tension tests did not have such a maximum point on the curve, so Considere's criterion, Equation (3-6) [11], was used to locate the yield stress. A graphical method was used, locating where the two lines $\frac{d\sigma}{d\varepsilon}$ and σ intersected.

$$\frac{d\sigma}{d\varepsilon} = \sigma \tag{3-6}$$

3.4.6 Results from the tension tests

All the results from the tension tests are presented in Appendix A. In this chapter, the most important results are explained and evaluated. As outlined in Table 3-2, a total number of 11 tension tests were carried out. 6 of the test samples were of thickness 5 mm, and 5 samples were of thickness 10 mm.

Figure 3-10 shows the true stress-strain relationship for all 11 tension tests carried out at 4 different strain rate levels and on two different test samples with thickness 5 mm or 10 mm.

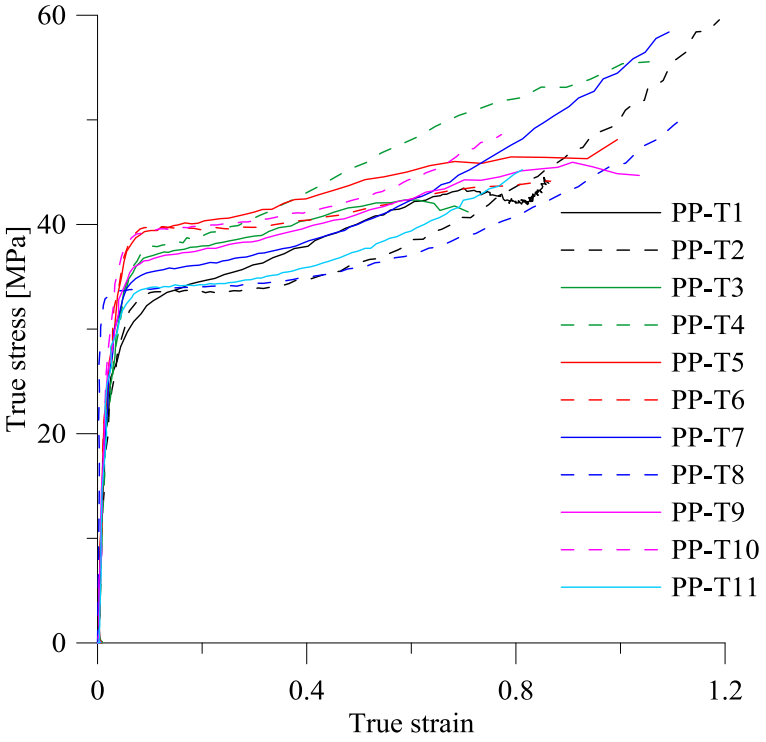

Figure 3-10. True stress-strain curves for all tension tests.

Only 2 of the 5 mm thick test specimens experienced failure, while 4 of the 10 mm thick samples fractured. Failure occurred in the tests carried out at highest strain rates, and none of the tests with a strain rate of 10^{-3} s^{-1} experienced failure. It is worth noting that the thickness of the test samples does not lead to a significant difference in the stress-strain curves.

The curves are, however, crossing each other when the strain gets large. They have a different strain hardening, and the trend seems to be that the tests of lowest strain rate have the highest strain hardening. The fact that the tests with highest strain rate have less hardening is likely to be caused by heating of the material, which makes the material softer.

The figure shows that a strain rate effect is present, but this is better observed in Figure 3-11 and Figure 3-12 where the true stress-strain relationship is shown for a representative test at each strain rate for the thin test specimens (Figure 3-11) and the thick test specimens (Figure 3-12).

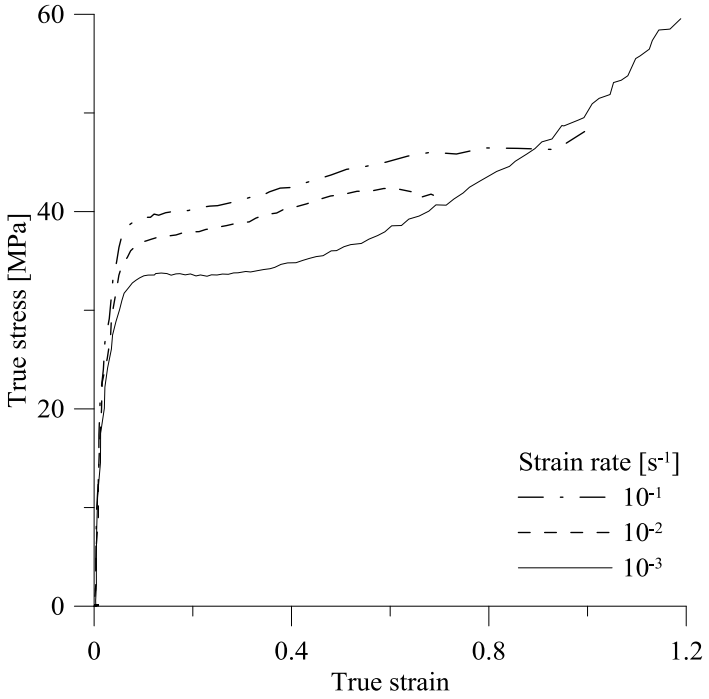

Figure 3-11. Representative true stress-strain curves for tension test samples made from 5 mm thick plate. Tests PP-T2, PP-T3 and PP-T5 are used.

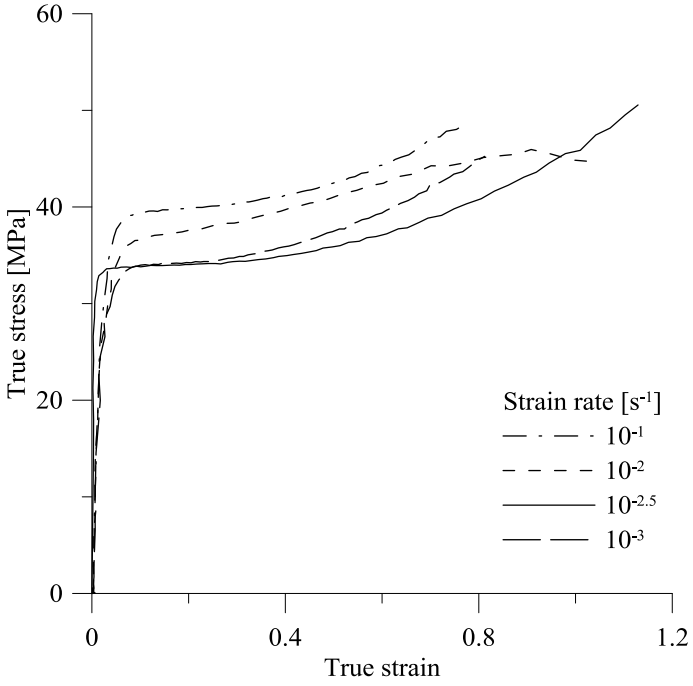

Figure 3-12. Representative true stress-strain curves for tension test samples made from 10 mm thick plate. Tests PP-T8, PP-T9, PP-T10 and PP-T11 are used.

As seen from the stress-strain relationship in Figure 3-11 and Figure 3-12 , PP experiences an increasing stress-strain curve, which means that there is hardening in the material. The yield stress increases with the strain rate, which indicates that the stress-strain curves are dependent on the

strain rate. This strain rate dependency is also seen in Figure 3-13, where the yield stress from the tension tests of thickness 5 mm is shown.

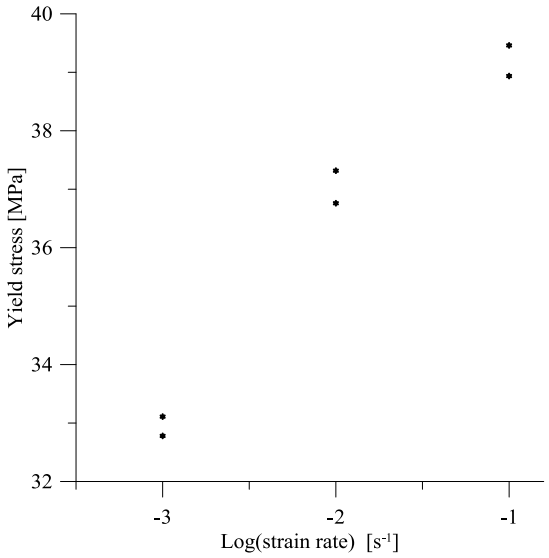

Figure 3-13. Yield stress in tension tests made from 5 mm thick plate.

The force-displacement relationship for the 5 mm test samples from representative tests at each strain rate is presented in Figure 3-14, and Figure 3-15 shows the same relationship for representative tests of thickness 10 mm. It is observed in the figures that the tension tests have softening in the force-displacement curves, while they have hardening in the true stress-strain curves in Figure 3-11 and Figure 3-12. A large reduction in the cross section area A in Equation (3-5) is likely to cause the different shape of the force-displacement and stress-strain curves.

It is also observed that the part of the curve after the peak force is reached in Figure 3-15 has a different shape than the curves in Figure 3-14.

The displacements in Figure 3-14 and Figure 3-15 are provided by the Dartec machine. It was desirable to measure the displacement only in the parallel area, but the displacement provided by the machine also included the displacement in the area of the test samples outside the parallel area. In addition, any suspensions or displacements inside the machine itself, and displacements in the clamp mechanisms will be included in the displacement measurements provided by the Dartec machine. Hence, the displacement in the parallel area is likely to be smaller than the displacement measured by the machine.

As mentioned, the true stress-strain curves were crossing each other, most likely due to heating in the material at high strain rates. This is also seen in the force-displacement curves, where the curves decrease faster after maximum force is reached in the tests at higher strain rates.

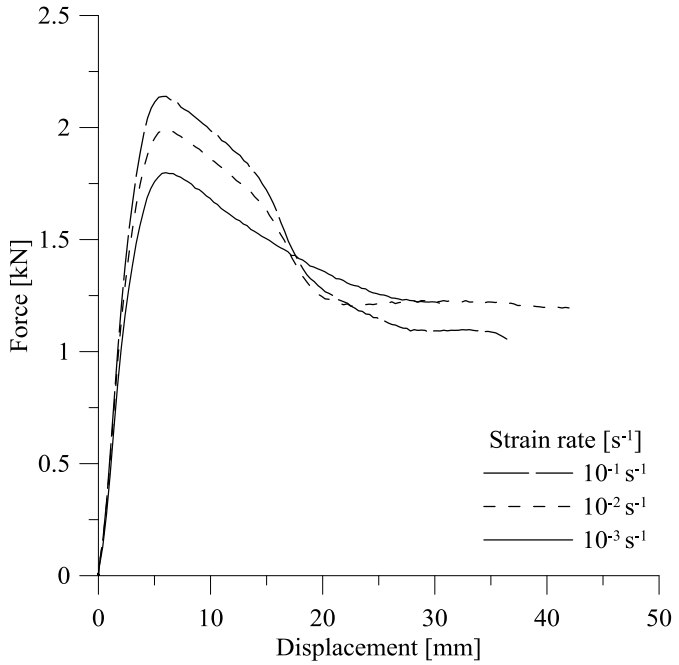

Figure 3-14. Representative force-displacement curves for tension test samples made from 5 mm thick plate. Tests PP-T2, PP-T3 and PP-T5 are used.

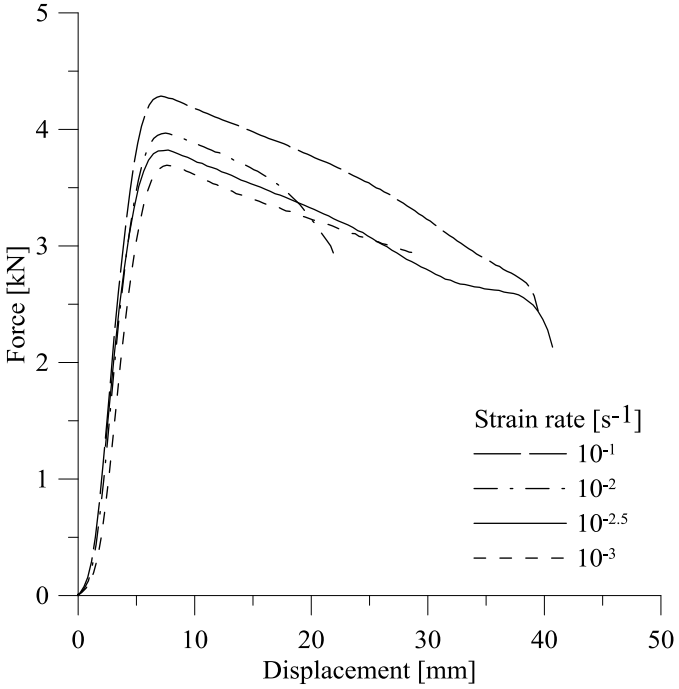

Figure 3-15. Representative force-displacement curves for tension test samples made from 10 mm thick plate. Tests PP-T8, PP-T9, PP-T10 and PP-T11 are used.

Tension test PP-T2

Figure 3-16 shows the tension test specimen PP-T2 after a deformation of 46 mm. It is likely that the specimen contacted a bit after being removed from the machine. As seen in the picture, the

test sample experienced a propagated necking, with stable dimensions in the necking area, but has a soft transition between the necking part and the part outside with small deformations.

Figure 3-16. Test specimen after a the testing, with a deformation of 46 mm.

Both test samples PP-T1 and PP-T2 were tested at the lowest strain rate, 10^{-3} s^{-1}. As seen in Figure 3-17, the two true stress-strain curves from test PP-T1 and PP-T2 deviate from each other. It was assumed that test PP-T1 had a deviating curve, while test PP-T2 had much of the same shape as the true stress-strain curves from the other tests carried out at higher strain rates. Therefore, test number PP-T2 was chosen to be the baseline test in the calibration. The longitudinal and transverse strain of test PP-T2 is seen in Figure 3-18.

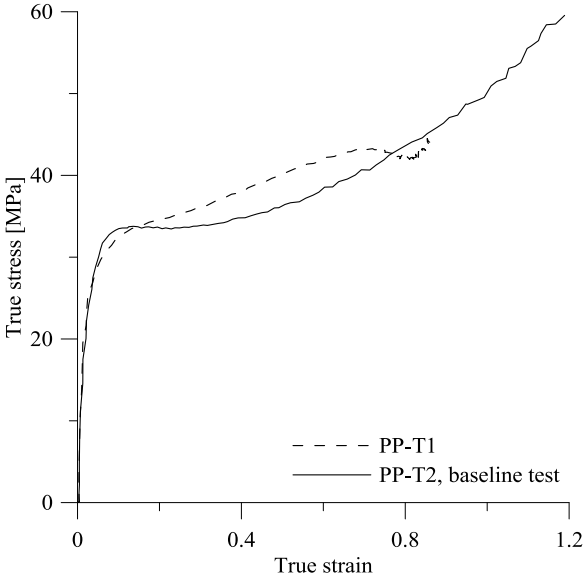

Figure 3-17. True stress-strain curves for tension tests PP-T1 and PP-T2, both tested at strain rate 10^{-3} s^{-1}.

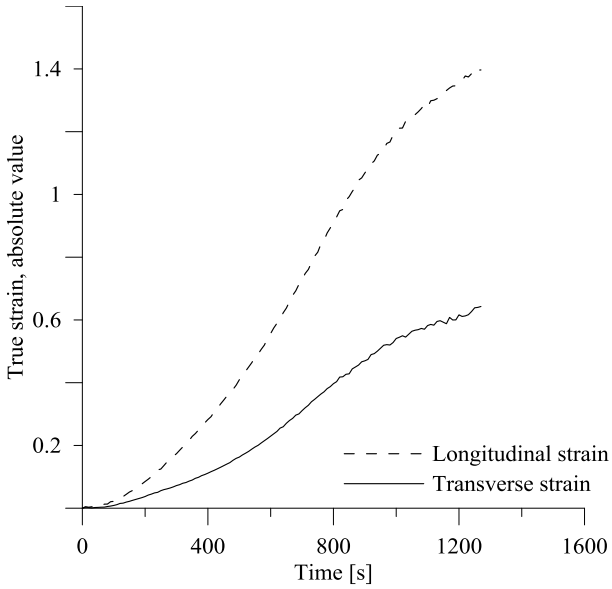

Figure 3-18. Strain curves in longitudinal and transverse direction in test PP-T2.

Equation (3-7) [11] gives the relationship between the volume strain ε_v, the longitudinal strain ε_l, the transverse strain ε_w and the thickness strain ε_t. The transverse strain is in Section 3.4.3 assumed to be equal to the thickness strain.

$$\varepsilon_v = \varepsilon_l + \varepsilon_t + \varepsilon_w \quad (3\text{-}7)$$

Figure 3-18 shows that the transverse strain in test PP-T2 is less than half the size of the longitudinal strain. According to Equation (3-7), this results in an increase of volume. Voids were observed in the test specimen during and after the tests, in addition to whitening. This is likely to be related to the volume increase.

3.5 Compression tests

A total of 5 compression tests were carried out on circular test specimens with different strain rates. The specimens had geometrical measures as shown in Figure 3-19 and Figure 3-20. An overview of the compressions tests is presented in Table 3-4, showing the test number, strain rate and geometry of the tests.

The test specimens were numbered PP-C#, where C means compression and # is the number of the test. The test samples of height 8 mm were cut from the plate with the longitudinal axis in the extrusion direction, while the test specimen of height 5 mm had the longitudinal axis perpendicular to the extrusion direction. Figure 3-21 and Figure 3-22 shows the angle that the samples were cut from the plate with respect to the extrusion direction, where the arrow indicates the extrusion direction.

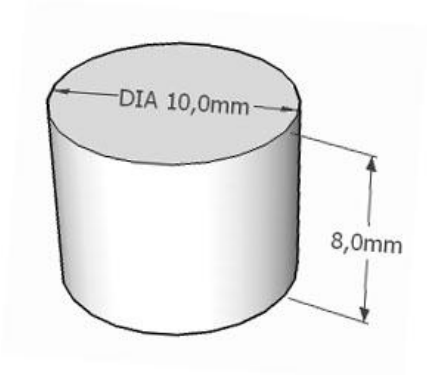

Figure 3-19. Geometry of samples with height 8 mm.

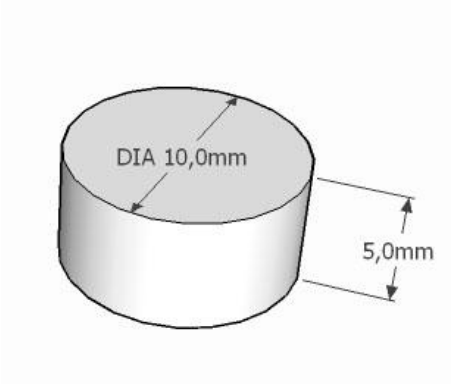

Figure 3-20. Geometry of sample with height 5 mm.

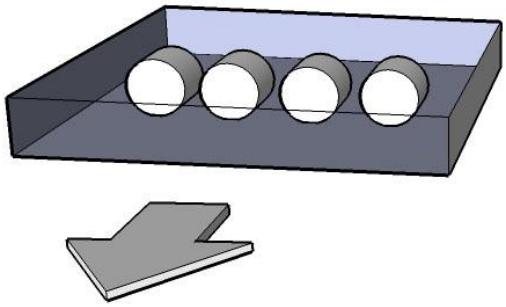

Figure 3-21. Extrusion direction of the test specimens with height 8 mm.

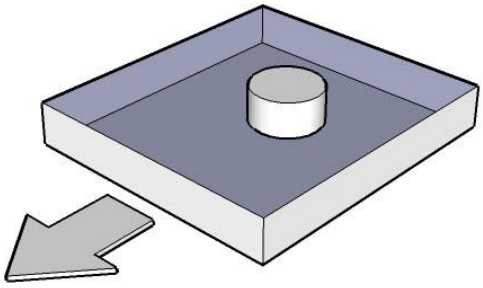

Figure 3-22. Extrusion direction of the test specimen with height 5 mm.

Tests were carried out at different strain rates. The velocity v of the cross heads of the test machine was defined using Equation (3-8) [11], where H_0 is the initial height of the test sample, and $\dot{e}$ is the nominal strain rate. This strain rate corresponds to the initial true strain rate.

$$v = H_0 \dot{e} \tag{3-8}$$

Table 3-4. List of compression tests.

Test number	Strain rate [s^{-1}]	Velocity [mm/s]	Initial height [mm]	Initial diameter [mm]
PP-C1	10^{-3}	0.008	8.04	9.55
PP-C2	10^{-3}	0.008	8.02	9.56
PP-C3	10^{-2}	0.08	8.02	9.56
PP-C4	10^{-1}	0.8	7.99	9.56
PP-C5	10^{-2}	0.05	4.89	9.99

The tests were done in the servo-hydraulic Dartec machine mentioned in Section 3.2. The circular test specimens were placed between two metal cylinders, as seen in Figure 3-23, and a lubricant was applied to make sure the surfaces were smooth and to avoid friction.

Figure 3-23. Test setup for compression tests.

3.5.1 Digital Image Correlation in the compression tests

The strains in the test specimens were determined using the series of pictures from the DIC camera taken during the tests. The pictures were imported into MATLAB, and converted to black and white pictures. The black and white pictures represented a matrix consisting of 0's and 1's, where 1 represent a white pixel and 0 a black pixel. With a white test specimen and a black background, MATLAB scripts was used to evaluate the height and diameter of the test specimens by counting the number of 1's in the correct cross section. The number of millimeters per pixel was calculated, and the diameter and height was converted into millimeters. The MATLAB script used to determine the diameter and height is seen in Appendix E.

Once the height was determined, the height strain ε_h was calculated using Equation (3-9), where *H* is the height of the test specimen and H_0 is the initial height. The diameter strain ε_d defined in Equation (3-9) was also calculated. The true stress was determined from Equation (3-5) [11], where the cross section area A was calculated using the diameter of the test specimen.

$$\varepsilon_h = \ln\left(\frac{H}{H_0}\right) \tag{3-9}$$

$$\varepsilon_d = \ln\left(\frac{D}{D_0}\right) \tag{3-10}$$

The yield stress in the compression tests was found at the maximum point on the curve [6], and this point coincides with the point where necking starts.

3.5.2 Results from the compression tests

All the results from the compression tests are presented in Appendix B. In this chapter, the most important results are explained. Figure 3-24 shows the true stress-strain curves of representative tests of the three different strain rates, on the samples of height 8 mm. The force-displacement relationship from the same tests is shown in Figure 3-25.

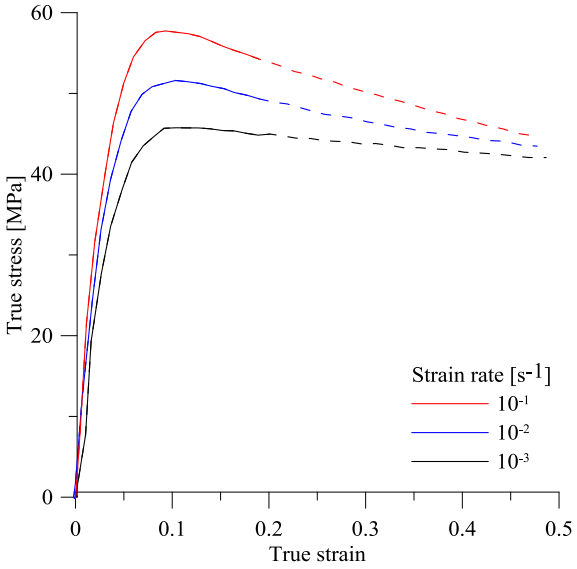

Figure 3-24. True stress-strain curves for compression tests with height of 8 mm. Tests PP-C1, PP-C3 and PP-C4 are used.

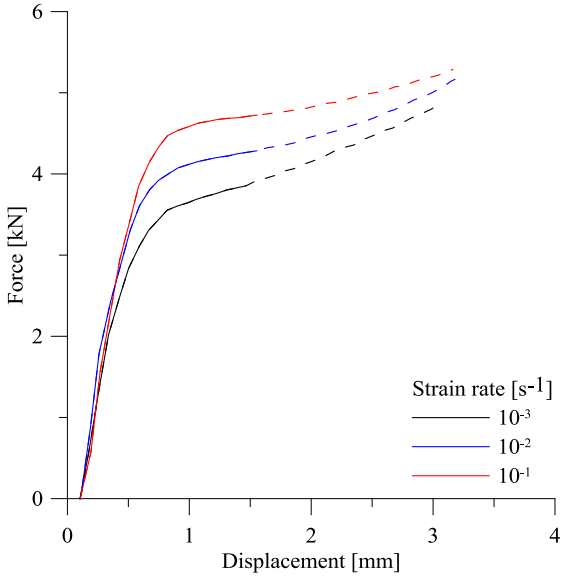

Figure 3-25. Force-displacement curves for compression tests with height of 8 mm. Tests PP-C1, PP-C3 and PP-C4 are used.

The DIC pictures taken during the testing show that a barreling effect occurs at around 0.2 on the true strain axis in Figure 3-24. It is likely that this barreling effect results in a too large area, A, in Equation (3-5), and therefore has lowered the true stress-strain curve in the area after a strain of 0.2. It may be assumed that the true stress-strain curve should have less softening. A true strain of 0.2 corresponds to a displacement of around 1.5 mm in Figure 3-25. The phase where the barreling effect occurs is indicated with dashed lines in both figures.

The true stress-strain curves from the compression tests in Figure 3-24 have a different shape than the true stress-strain curves of the tension tests in Figure 3-10. The compression curves have softening, while the tension curves have hardening, which indicates that the material is pressure dependent.

There are maximum points on the true stress-strain curves in Figure 3-24, which is where the yield stress occurs, and the figure indicates that the curves are dependent on the strain rate. Figure 3-26 shows the yield stress for the compression tests and the tension test. The compression and tension tests experience a different yield stress at the same strain rate, which indicates that the material is both strain rate dependent and pressure dependent.

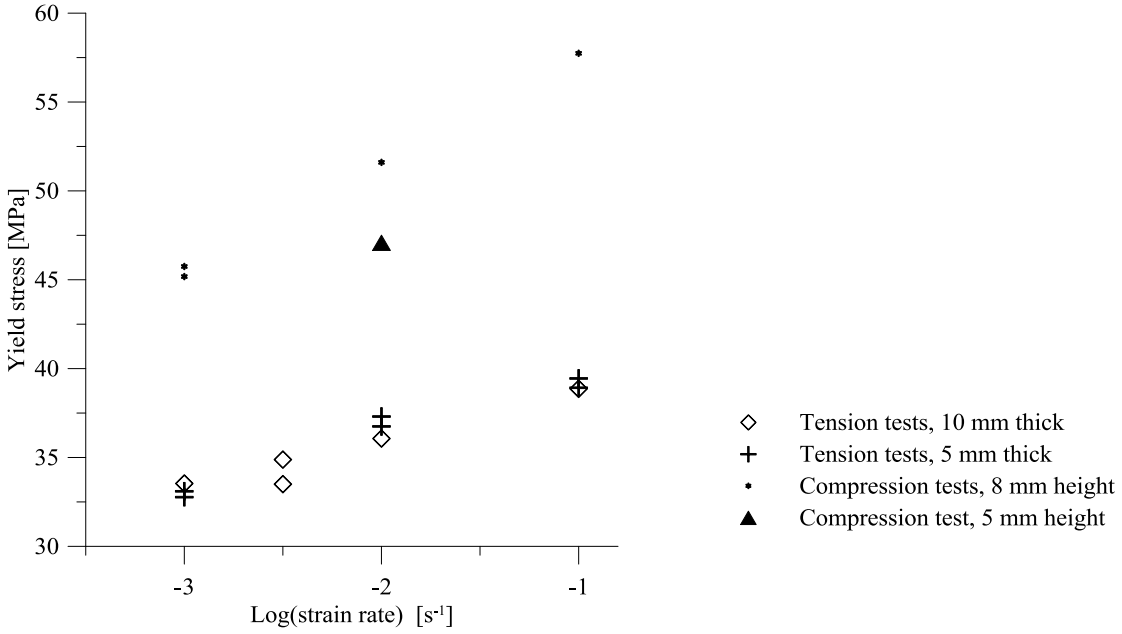

Figure 3-26. Yield stress for compression and tension tests.

Figure 3-27 shows the volume strain as a function of the longitudinal strain for one tension and one compression sample tested at a strain rate of 10^{-3} s^{-1}. The volume strains in tension and compression are determined from Equation (3-7). As seen in the figure, the material is expanding in tension and contracting in compression. In compression, the volume is decreasing until a

longitudinal strain of about 0.1, which is the elastic area. The volume strain is then increasing, and that is probably due to the barreling effect. This effect will give a larger diameter strain ε_d than it is in reality, resulting in a larger volume strain [15]. A barreling effect seems to occur in the pictures from the tests after a longitudinal strain of 0.2, and the volume strain after this point is indicated with a dashed line.

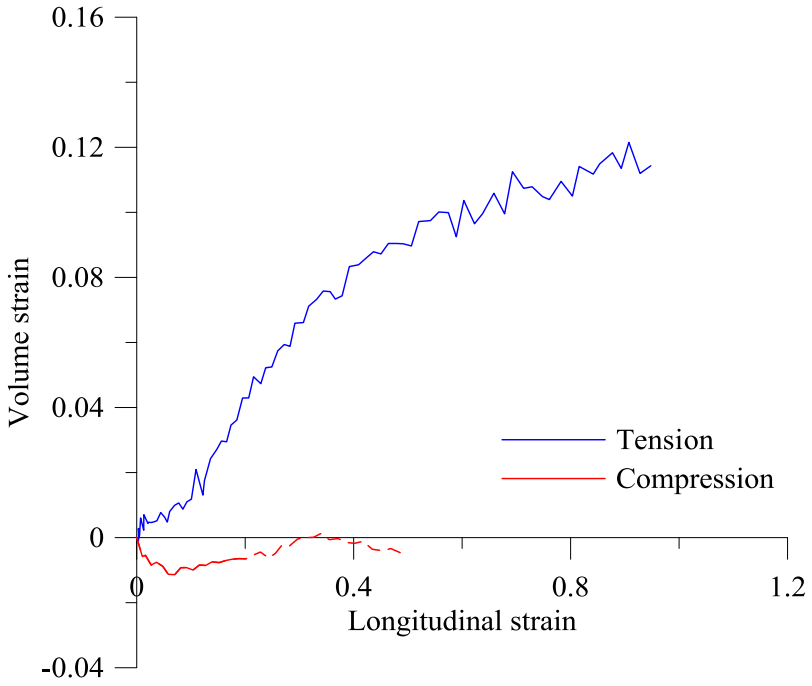

Figure 3-27. The volume strain as a function of the longitudinal strain for the two representative tests PP-T2 and PP-C1.

Figure 3-28 shows the true stress-strain curves for two compression tests with different loading directions. Test PP-C3 was loaded in the extrusion direction, while test PP-C5 was loaded in the thickness direction. It can be observed in the figure that PP experiences some direction dependency. The material is stronger in the extrusion direction than in the thickness direction. It is, however, worth noting that the diameter of the two samples are different, which affects the friction and thus the diameter change. The thicknesses are also different. While PP-C3 had a height of 8 mm and diameter of 9.56 mm, PP-C5 had a height of 5 mm and diameter of 9.99 mm.

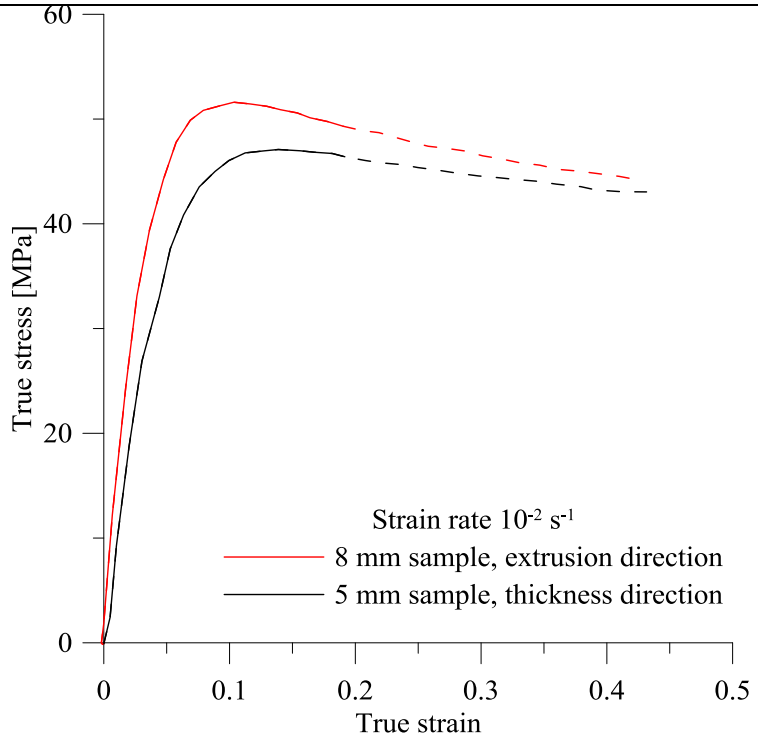

Figure 3-28. True stress-strain curves from compression tests in different loading directions at strain rate 10^{-2} s^{-1}. The dashed lines indicate the area where a barreling effect is present.

3.6 Sources of error in tension and compression tests

There are several sources of uncertainties in the experimental tests. MATLAB scripts were used to determine the strains in the compression tests based on the pictures taken during testing. The contrast in the pictures was essential for the determination of the dimensions. Bad contrast gave poor results, and it is also measuring uncertainties associated to where in the test specimens the diameter and height was measured.

The dimensions of the test samples were determined in pixels, and transferred into to millimeters. However, the definition of how many millimeters one pixel corresponded to was an approximate value, based on measurements done by a digital caliper.

4 Calibration of a material model for PP

A material model for PP was calibrated from the material tests described in Section 3, based on the hyperelastic-viscoplastic model described in Section 2.4. The analytical procedure described in detail by Hovden [2] and Clausen et al. [6] was followed to find the coefficients in this material model, and the equations used in this chapter are all obtained from Hovden [2] and Clausen et al. [6].

Microsoft Excel Solver was used for analytical determination of several coefficients. In addition, the software MATLAB was used for curve fitting.

The calibrated model was implemented as a user-defined material model in LS-DYNA. The required coefficients are gathered in Table 4-1, and the determination of these coefficients is explained in this chapter.

Table 4-1. Overview of coefficients required in the material model.

Part A coefficients	
Poisson's ratio	v
Parameter controlling the plastic dilatation	β
Pressure sensitivity coefficient	α
Reference strain rate	$\dot{\varepsilon}_{0A}$
Strain rate sensitivity coefficient	C
Yield stress in tension at strain rate 0 s^{-1}	σ_0
Young's modulus	E
Bulk modulus	K
Shear modulus	G
Saturation stress	σ_T
Hardening parameter	H
Part B coefficients	
Locking stretch	$\bar{\lambda}_L$
Initial elastic modulus of Part B	C_R

4.1 Baseline test

A baseline test was required when calibrating a material model, and this test is preferably a quasi-static tension test. Yield stresses from a representative compression test at the same strain rate, as well as additional tension and compression tests at higher strain rates are needed for the calibration.

As mentioned in Section 3.4.6, PP-T2 was chosen as a representative test, and became the baseline test of the calibration. Of the two compression tests carried out at strain rate 10^{-3} s^{-1}, the true stress-strain curves were approximately equal. Test PP-C1 was therefore chosen as a representative compression test. More details on the tests applied in the calibration are presented in Appendices A and B.

Some of the parameters in the material model were determined only from the baseline tension test, like Poisson's ratio v, the coefficient β and the reference strain rate $\dot{\varepsilon}_0^P$. Several of the parameters were determined based on the additional compression and tension tests as well, and a curve fit was used to determine the parameters H, C_R and $\bar{\lambda}_L$.

4.2 Part A parameters

The calibration of the parameters from Part A in the hypoelastic-viscoplastic material model described in Section 2.4 is presented here.

Poisson's ratio

Poisson's ratio was determined from the transverse and longitudinal strain in the elastic area, as seen in Equation (4-1).

$$v = -\frac{\varepsilon_t}{\varepsilon_l} \tag{4-1}$$

Figure 4-1 shows the transverse strain versus the longitudinal strain in the elastic part of test PP-T2, up to a longitudinal strain of approximately 0.1. Poisson's ratio, v, is the slope of the curve, and the number 0.45 was found using a curve fitting tool in MATLAB.

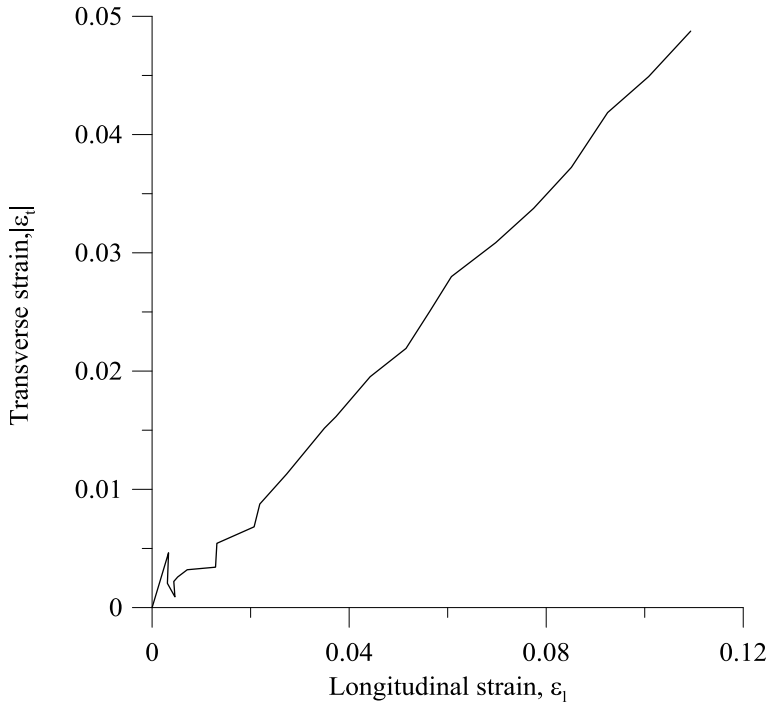

Figure 4-1. Transverse and longitudinal strain for test PP-T2.

Coefficient β

The coefficient β defined in Equation (4-2) describes the plastic volume change. When β=1, the volume is preserved.

$$\beta = \frac{2-\rho}{1+\rho} \tag{4-2}$$

The contraction ratio, ρ, is defined in Equation (4-3) and seen in Figure 4-2. For test PP-T2, the contraction ratio was close to 0.4.

$$\rho = -\frac{\varepsilon_t}{\varepsilon_l} \tag{4-3}$$

β has, according to Equation (4-2), a value of 1.14, which means that there is volume expansion in the material.

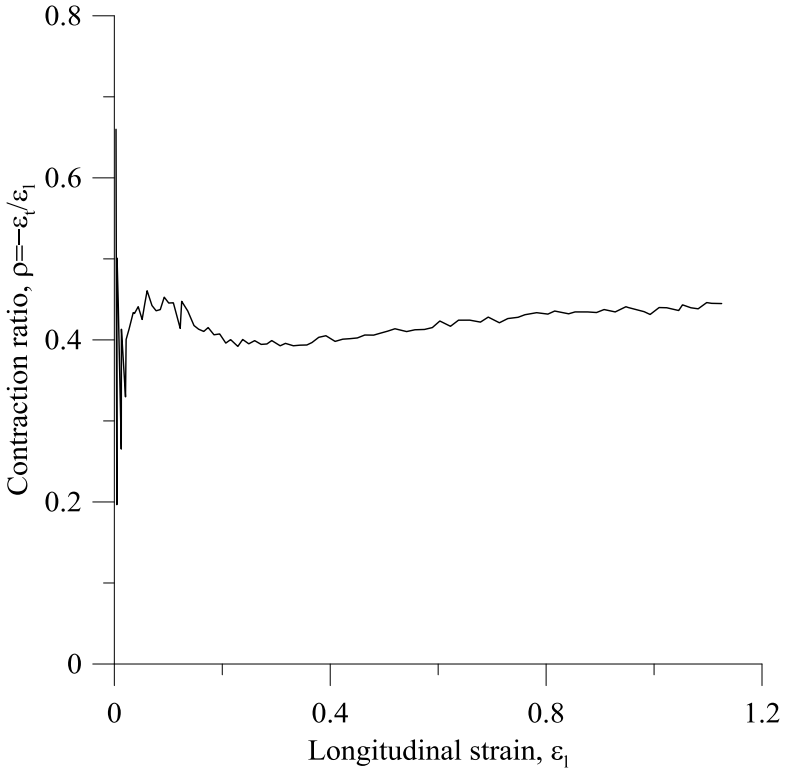

Figure 4-2. Contraction ratio for test PP-T2.

Pressure sensitivity coefficient α

The pressure sensitivity coefficient α is defined as the ratio between the yield stress in compression and tension. The baseline test PP-T2 and the representative compression test PP-C1 are seen in Figure 4-3. The compression test had a yield stress of 46.7 MPa and the tension test had a yield stress of 33.11 MPa. α was in Equation (4-4) calculated to be 1.38. Since the pressure sensitivity coefficient was higher than 1, PP was modeled as a pressure sensitive material.

$$\alpha = \frac{\sigma_C}{\sigma_T} = \frac{\sigma_{PP-C1}}{\sigma_{PP-T2}} = \frac{45.7\ MPa}{33.1\ MPa} = 1.38 \tag{4-4}$$

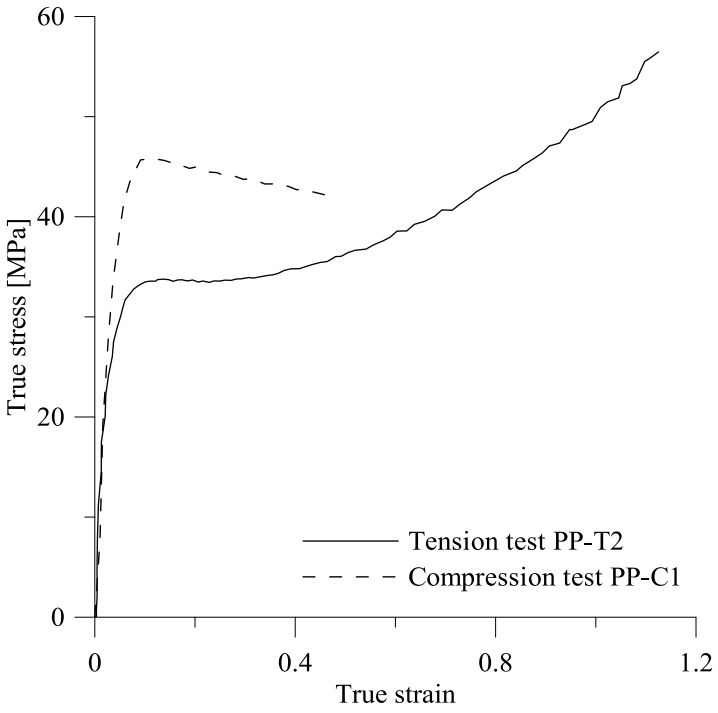

Figure 4-3. Representative tension and compression tests.

The relative strain rate and reference strain rate

The reference strain rate is seen in Equation (4-5) as $\dot{\varepsilon}_{0A}$, and $\dot{\varepsilon}_{rel}$ is the relative strain rate. $\dot{\varepsilon}_A^P$ is the observed logarithmic strain rate. The reference strain rate $\dot{\varepsilon}_{0A}$ is the local strain rate when necking occurs in test PP-T2, and was found to be 0.00075 s^{-1}.

$$\dot{\varepsilon}_{rel} = \frac{\dot{\varepsilon}_A^P}{\dot{\varepsilon}_{0A}} \tag{4-5}$$

The yield stress σ_0 at zero strain rate, and the coefficient C

The coefficients σ_0 and *C* were determined from the yield stresses in the 5 mm thick tension tests. Figure 4-4 shows these yield stresses and a linear curve fit. Along the x axis is $\ln(\dot{\varepsilon}_{rel} + 1)$, the natural logarithm of the relative strain rate plus 1.

Equation (4-6), which was introduced in Section 2.4, contains the parenthesis $(\dot{\varepsilon}_{rel} + 1)$, which will always be larger than 1 when $\dot{\varepsilon}_{rel}$ is a positive number. That happens when $\dot{\varepsilon}_0^P$ in Equation (4-5) is chosen as the lowest possible strain rate, which in this case is 10^{-3} s^{-1}. If the value of the yield stress at strain rate 10^{-3} s^{-1} is used as σ_T in Equation (4-6), the calculation of the equivalent stress $\bar{\sigma}_A$ at yielding will end up larger than it is in reality. To avoid this problem, σ_T should be

replaced by the yield stress at a fictitious strain rate of value 0, from here on named σ_0. This coefficient σ_0 is found by extrapolating the linear line in Figure 4-4 back to 0 on the x axis.

$$\bar{\sigma}_A = \sigma_T(1 + C \cdot \ln(\dot{\varepsilon}_{rel} + 1)) \tag{4-6}$$

However, the relative nominal strain rate $\dot{e}_{rel}$ was used instead of the relative strain rate $\dot{\varepsilon}_{rel}$ in Equation (4-6), because the fraction $\dot{e}/\dot{e}_0$ is approximately equal to $\dot{\varepsilon}_A^P/\dot{\varepsilon}_{0A}$. The nominal reference strain rate $\dot{e}_0$ was equal to the lowest nominal strain rate 10^{-3} s^{-1}, and $\dot{e}$ was the nominal strain rate in each tension test.

The equation of the linear line in Figure 4-4 is *32.38+1.564x*. Hence the value of the coefficient σ_0 is 32.4 MPa.

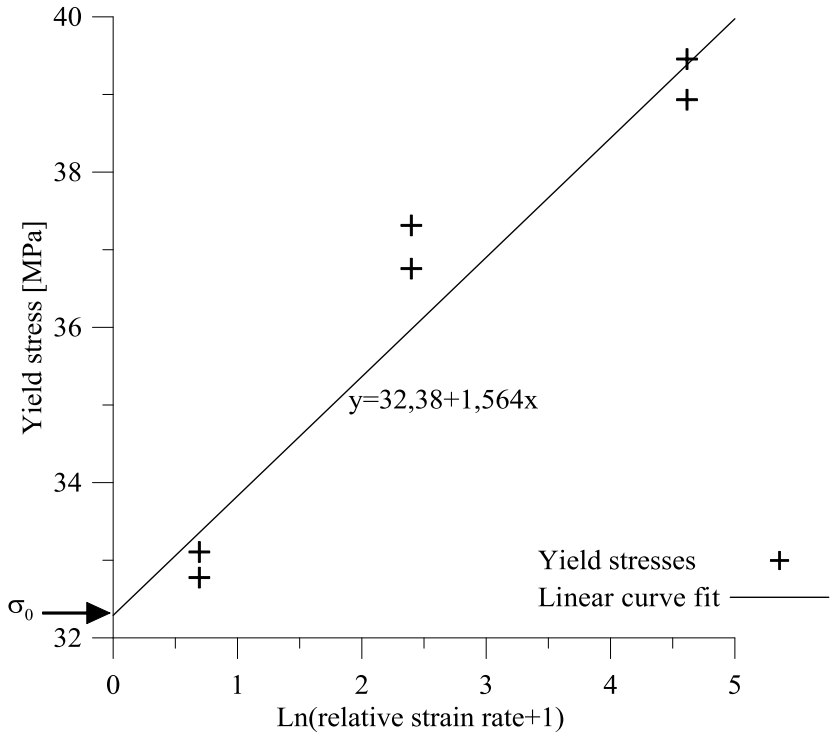

Figure 4-4. Yield stresses in the 5 mm thick tension tests.

As seen from Equation (4-6), $C \cdot \sigma_T$ represents the slope of the line, and the parameter C is found in Equation (4-7).

$$C = {}^{1.564}/_{32.38} = 0.0483 \tag{4-7}$$

Young's modulus, Bulk modulus and Shear modulus

Young's modulus was determined from the initial part of the true stress-strain curves from the 6 tension tests of thickness 5 mm. A curve fitting tool provided a linear fit to the true stress-strain curves.

Figure 4-5 shows Young's modulus from all 6 tension tests of thickness 5 mm. The baseline test PP-T2 had a Young's modulus of 1524 MPa, and the average value of all the Young's moduli was 1634 MPa. These were all rough estimates of Young's modulus, and the value 1600 MPa seemed therefore like a representative number. The curve with elastic stiffness of 1600 MPa had a good fit to the true stress-strain curve from test PP-T2 in Figure 4-6. Therefore it was chosen to use a Young's modulus of 1600 MPa, and not the value 1400 MPa provided by the supplier.

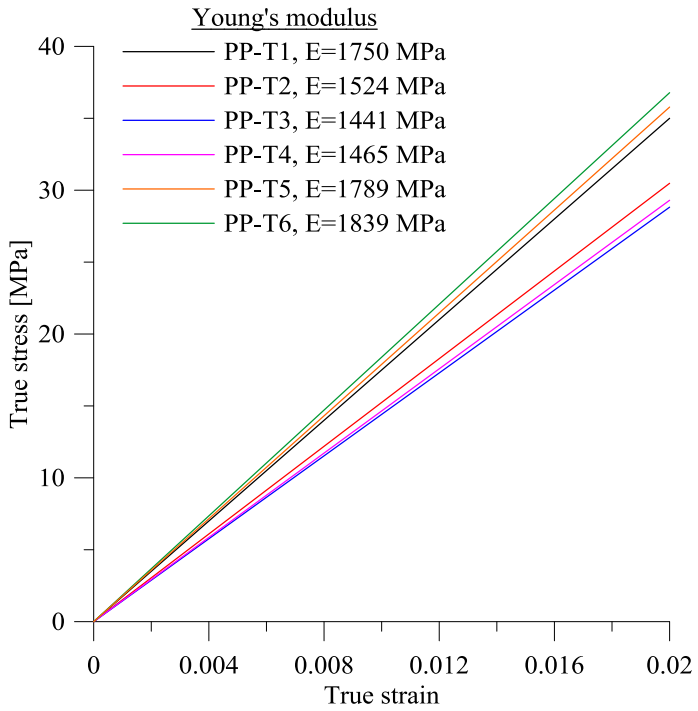

Figure 4-5. Young's modulus calculated for tension test specimens of thickness 5 mm.

The bulk modulus *K* and the shear modulus *G* were calculated using Equations (4-9) and (4-8), giving the values *K=4920 MPa* and *G=553 MPa*.

$$G = \frac{E}{2(1+\nu)} \tag{4-8}$$

$$K = \frac{E}{3(1-2v)} \tag{4-9}$$

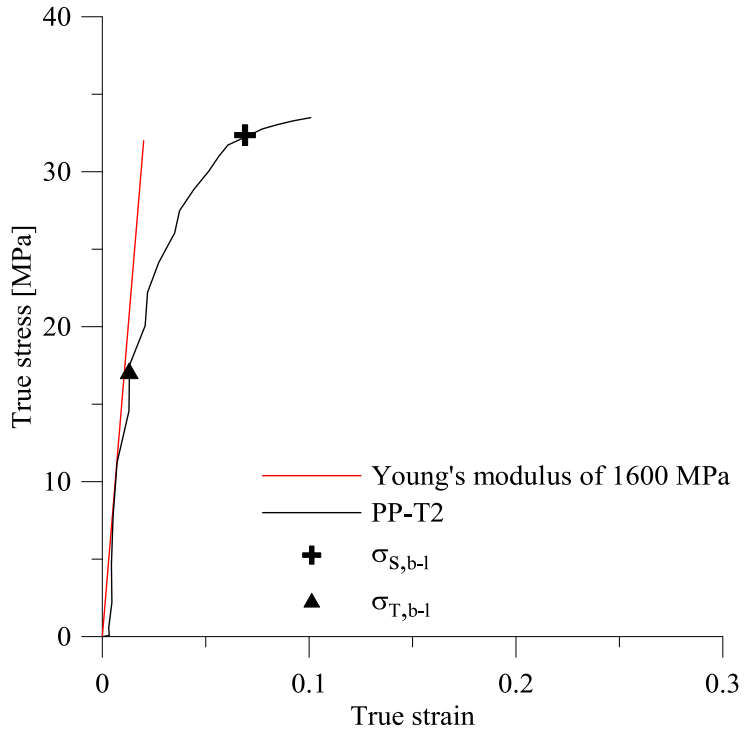

Figure 4-6. Young's modulus of 1600 MPa and the initial part of the true stress-strain curve from test PP-T2.

In Figure 4-6, the coefficient $\sigma_{S\,b-l}$ is the yield stress in tension test PP-T2. The subscript *b-l* refers to baseline, and the value of $\sigma_{S\,b-l}$ is 33.11 MPa.

Yield stress σ_T

In Equation (2-3) in Section 2.4 , *R* is a variable representing hardening or softening. The equation represents hardening when $\sigma_S > \sigma_T$, and softening when $\sigma_S < \sigma_T$. As seen in Figure 4-6, σ_S is larger than σ_T, and the hardening option is chosen for PP.

The coefficient σ_T seen in Equation (2-3) is required in the material model as well. This coefficient is equal to $\sigma_{T\,b-l}$, which is the baseline test yield stress, and is found from the interception point between the true stress-strain curve from PP-T2 and the straight line

representing Young's modulus. Figure 4-6 shows the interception point where $\sigma_{T\,b-l}$ is located, at approximately 17 MPa, which means that $\sigma_T = 17\ MPa$.

Hardening parameter H

The Solver function in Microsoft Excel was used to determine the parameters H, C_R and λ_L. A curve fit in the area between $\sigma_{T\,b-l}$ and $\sigma_{S\,b-l}$ seen in Figure 4-6 gave the hardening parameter H the value 48.9.

4.3 Part B parameters

Part B of the hypoelastic-viscoplastic material model consisted of the coefficients C_R and $\bar{\lambda}_L$.

Locking stretch, $\bar{\lambda}_L$, and initial elastic modulus of Part B, C_R

The coefficients C_R and $\bar{\lambda}_L$ were found from a curve fit of part B, using Microsoft Excel Solver, which gave the values $\bar{\lambda}_L = 1.94$ and $C_R = 1.30$ MPa.

4.4 The calibrated model

Figure 4-7 shows Parts A and B of the calibrated material model and Figure 4-8 shows the true stress-strain curve from test PP-T2 and the material model that is calibrated in this chapter. It is seen from Figure 4-8 that the model has good agreement with the test data up to the yield stress, before the model and test data deviate from each other. The predicted model is too high compared to the test data in the area just after yield stress, and the model has more hardening that the test here. In the area where the strain is between 0.6 and 1.0, the model is too low compared to the test data. Table 4-2 presents the values of the parameters found in the calibration.

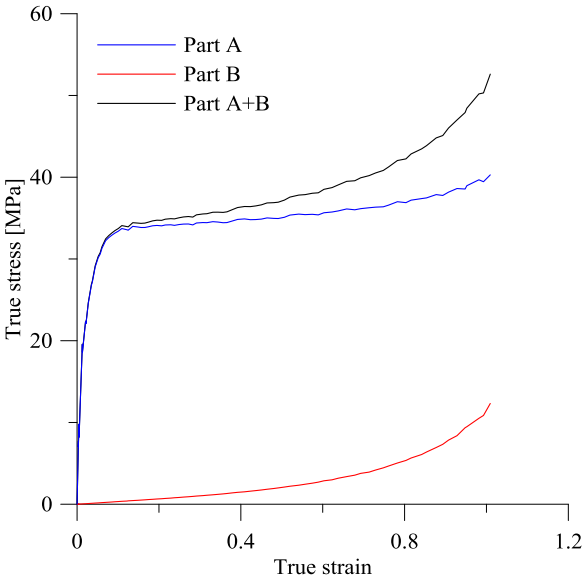

Figure 4-7. Part A and Part B in the calibrated material model.

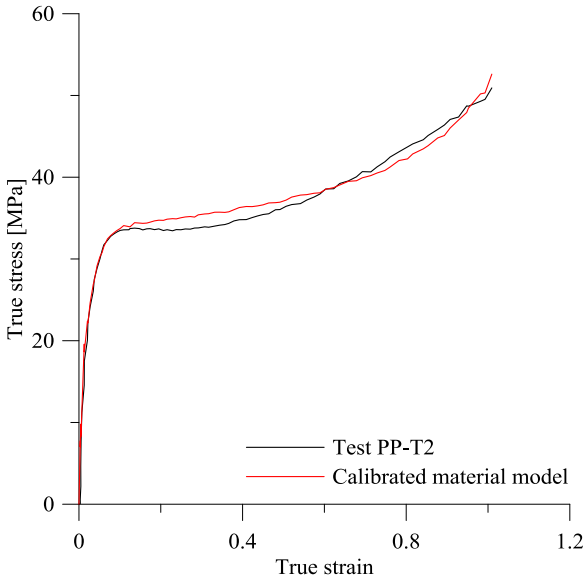

Figure 4-8. True stress-strain curves from test PP-T2 and calibrated material model.

Table 4-2. Coefficients in the material model for PP.

Part A coefficients			
Poisson's ratio	v_0	0.45	
Parameter controlling the plastic dilatation	β	1.14	
Pressure sensitivity coefficient	α	1.38	
Reference strain rate	$\dot{\varepsilon}_{0A}$	0.00075	s^{-1}
Strain rate sensitivity coefficient	C	0.0483	
Yield stress in tension at strain rate 0	σ_0	32.4	MPa
Young's modulus	E	1600	MPa
Bulk modulus	K	4920	MPa
Shear modulus	G	553	MPa
Yield stress	σ_T	17	MPa
Hardening parameter	H	48.9	
Part B coefficients			
Locking stretch	$\bar{\lambda}_L$	1.94	
Initial elastic modulus of Part B	C_R	1.30	MPa

4.4.1 Discussion

The elastic stiffness E was determined from the stress-strain curve. Since the accuracy is poor for small strains, it could be difficult to determine this value correctly, and it might would have been more correct to use the value of Young's modulus provided by the supplier, and not the one calculated.

The material model is calibrated from test PP-T2 carried out at a strain rate of 10^{-3} s^{-1}. When comparing the true stress-strain curve from this test with tests at higher strain rates, as in Figure 3-10, it is clear that the curves are crossing each other when the true strain is large. The material model is calibrated from the curve with the most hardening, and that could result in a model with too much hardening at strain rates larger than 10^{-3} s^{-1}.

Figure 3-27 shows that there is a volume expansion in tension and volume contraction in compression. The coefficient $\beta = 1.14$ describes the plastic volume change, and is determined from the volume increase in the baseline tension test. When $\beta > 1$, the material model will predict much volume increase in tension and some volume increase in compression, and $\beta < 1$ gives much volume decrease in compression and some in tension. The model is thus not able to predict both volume expansion in tension and volume contraction in compression, and this is a drawback in the model.

In addition, Figure 3-28 indicate some direction dependency in the material. The material seems to be stronger in the extrusion direction than in the thickness direction, while the material model does not include any direction dependency.

It is also worth mentioning that the material model is calibrated from tests carried out at strain rates in the range 10^{-3} to $10^{-1}s^{-1}$. The linear line in Figure 4-4 is assumed to be extrapolated log-linearly, but that is a rough assumption because what really happens when we have very high strain rates of magnitude 10^{2} or 10^{3} s^{-1} is difficult to predict. Tensile testing for calibration of strain rates in this area is not possible, and assumptions have to be made. Whether the model is correct for very high strain rates could be a source of error. The value of the parameter C is directly influenced by the slope of the line, and a parameter study regarding this is presented later on in the thesis, where inverse modeling is applied.

The material behaviour is assumed to be elastic-viscoplastic. Viscoelasticity is not included in the material model, and a constant Young's modulus is used. However, in reality Young's modulus will increase at high strain rates. This is further discussed later, and different Young's moduli are tested.

4.5 Alternative material model for PP

The material model seen in Figure 4-8 does not have a perfect agreement in the phase of the curve after yield stress, and it was therefore desirable to also calibrate a material model based on softening in Equation (2-3), which means that $\sigma_S < \sigma_T$.

Several of the parameters in Table 4-2 got a new value, including σ_T, σ_0, H, C_R and λ_L. Since σ_S in this case is smaller than σ_T, the value 32.28 MPa was now chosen as σ_T. A curve fit gave the value of the coefficients σ_0, H, C_R and λ_L, and the results are seen in Table 4-3. Figure 4-9 shows the true stress-strain curve of the alternative material model.

Table 4-3. New parameters in the alternative material model for PP.

σ_T	32.380	MPa
σ_0	30.256	MPa
H	1093.8	
C_R	2.426	MPa
λ_L	2.34	

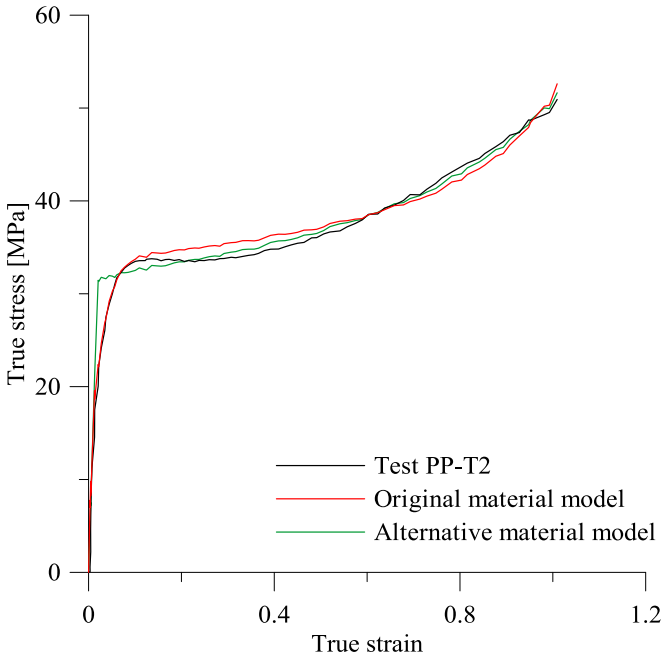

Figure 4-9. True stress-strain curves from tension test PP-T2, the original material model from Section 4.4, and the alternative material model determined in Section 4.5.

As seen in Figure 4-9, the alternative material model has a better agreement to the test data in the part after yield stress occurs than the original material model has. However, the alternative model is not a good prediction in the phase before yield stress. This is due to the fact that the alternative material model is increasing linearly up to the yield stress of 32.38 MPa, while the original model has a gradual transition from the elastic to plastic area. Numerical simulations were carried out with both material models, and are presented later on.

5 Numerical simulations of material tests

Numerical simulations of the tension and compression tests were carried out to verify the parameters in the calibrated material model from Section 4.4. The simulations were done in the finite element code LS-DYNA, using explicit non-linear finite element analysis. A LS-DYNA keyword file for a representative test is seen in Appendix F. The model does not include fracture, and the simulations were therefore stopped at a chosen displacement.

The numerical results are compared to the experimental results in true stress-strain and force-displacement curves. The maximum force, the shape of the curve and the constant force are comparable factors. The constant force is the value of the force when it is stabilized.

Numerical simulations of the tension tests are first presented and evaluated, before the numerical simulations of compression tests are explained.

5.1 Tension tests

It was decided to do numerical simulations of tension tests PP-T2, PP-T3 and PP-T5. They were all 5 mm thick, and were carried out at strain rates 10^{-3}, 10^{-2} and 10^{-1} s^{-1} respectively. Additionally, one of the 10 mm thick tension test samples was numerically simulated and evaluated.

Tension test PP-T2 was the baseline test of the calibration. A numerical simulation of this test was of high interest because it gave an indication of whether the calibration parameters were correct. The true stress-strain curves from the simulations were compared with the calibrated model. Numerical simulations of tests at higher strain rates gave a good indication of the strain rate dependency of the material model.

The results from the numerical simulations are in this section presented and evaluated, and furthermore the strain rate dependency of the model is discussed.

5.1.1 Model

The tension tests were numerically simulated with the geometry seen in Figure 5-1. As discussed in Section 3.4.6, the displacements provided by the Dartec machine included the displacements in the entire test coupon between the two clamps. To get comparable results, the visible part of the test sample located between the two clamps of the Dartec machine was therefore modeled.

To simulate the fixed ends, the nodes on the left surface of the model in Figure 5-1 were fixed in x, y and z directions, while the nodes on the right surface were given a constant velocity.

The specimen was modeled with solid elements, and with an element size of 1.5 x 1.5 mm in the parallel area. Simulations with element size 1 x 1 mm were tried as well, giving the same results as simulations with element size 1.5 x 1.5 mm.

The specimen had 4 elements in the thickness direction, resulting in a thickness of 1.23 mm per element. In total there were 1472 elements and 2115 nodes in the model. Both 8 node elements with reduced integration, and selectively reduced integration were tried. The simulations with selectively reduced integration gave the best results. A structured mesh was applied. Different factors of mass scaling were tried in the simulations, and it was always controlled that the kinetic energy was very small compared to the total energy of the simulation.

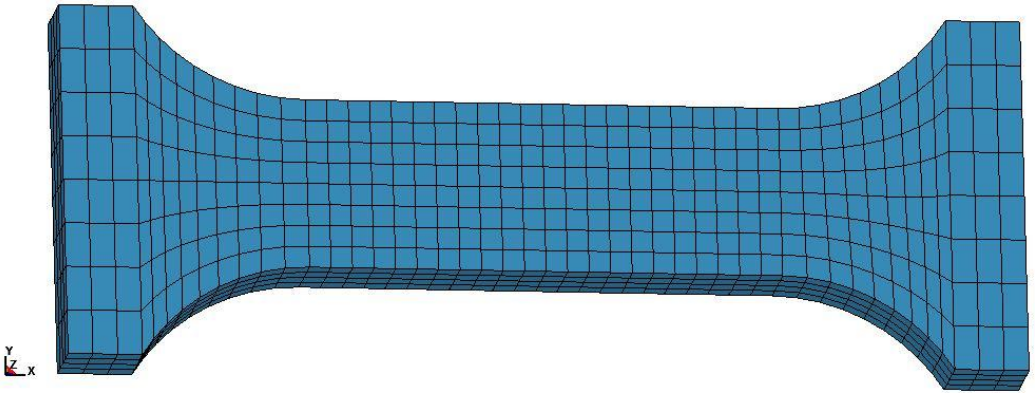

Figure 5-1. Geometry and mesh of the tension test sample.

The displacement of the test sample was obtained from the right side of the specimen, which was the same side as where the boundary condition with constant velocity was located. The force was obtained from a cross section of the test sample, while the stresses and strains were obtained as the average from all elements over the width in the middle of the parallel area.

5.1.2 Numerical simulations of tension test PP-T2

Tension test PP-T2 was the baseline test in the calibration, and was carried out at a strain rate of 10^{-3} s^{-1}. The model was given a constant velocity of 0.033 mm/s. A mass scaling of 10^{9} turned out to be the best alternative. A smaller mass scaling factor gave equal results, but had a many times larger computational time.

Results

Figure 5-2 shows a combined image of the numerical simulation and the test specimen after the testing. A diffuse necking is seen in both the numerical prediction and in the picture. The necking has propagated, but there is no distinct localized necking present, neither in the simulation nor in

the picture. The sample has a soft transition between the part of the specimen with necking and the part with small deformations.

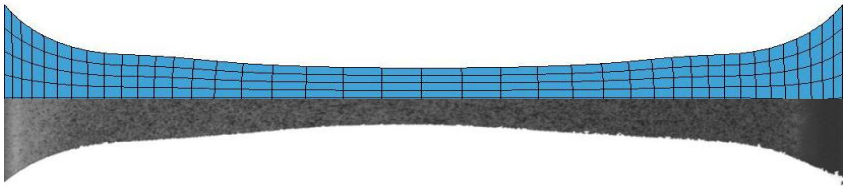

Figure 5-2. Test specimen after 30 mm displacement.

Figure 5-3 shows the true stress-strain curves from the numerical simulation, the experimental data and the calibrated material model. The numerical simulation seems to be a good fit to the calibration curve in the area before yield stress occurs. After the yield stress is reached, the simulation curve is quite similar to the calibration curve until the strain reaches about 0.6, where the calibration curve is stronger than the simulation. This might be associated with a triaxial stress state in the simulation.

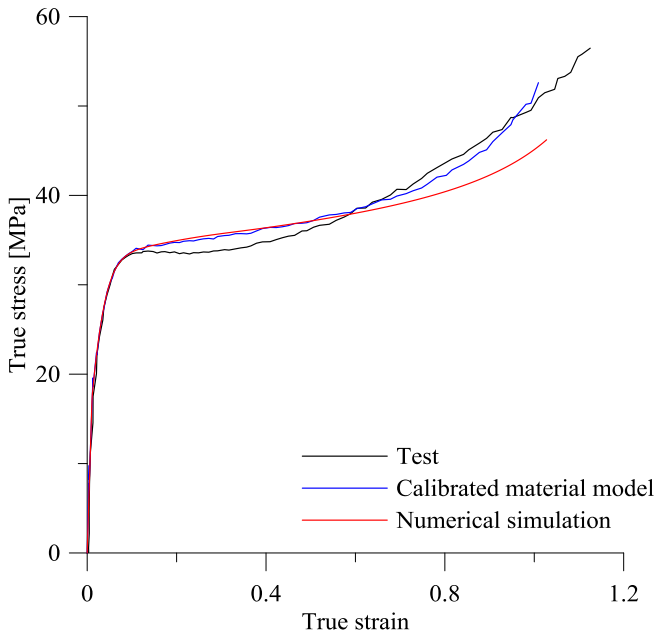

Figure 5-3. True stress-strain relationship for the tension test PP-T2, the calibrated material model and the numerical simulation.

The force-displacement curves from the experimental data and numerical simulation of tension test PP-T2 is seen in Figure 5-4. The displacement measurements in the simulation were obtained

from the right side of the model in Figure 5-1, and the displacements in the experimental test are provided by the Dartec machine.

The shape of the force-displacement curve from the simulation is similar to the curve from the test. The maximum force of the simulation is located about 20 N above the test curve. This might be because of a too small Poisson's ratio, resulting in a too large area.

In addition, the stable force is not captured perfectly by the simulation. It is likely to be caused by the calibrated material model. As seen from Figure 5-3, the test curve in the part after yield stress is flat. The calibrated model on the other hand is not able to represent this flat level, and it has an increasing curve, which is likely to be the reason why the constant force in Figure 5-4 is not captured by the model.

The simulated model is from the starting point located on the left side of the test curve. This may indicate that Young's modulus is too high, but it is also likely to be caused by the displacements measurements provided by the Dartec machine. These measurements include any displacements or suspensions that occur inside the machine, as well as displacements in the parts of the test sample located in the clamps.

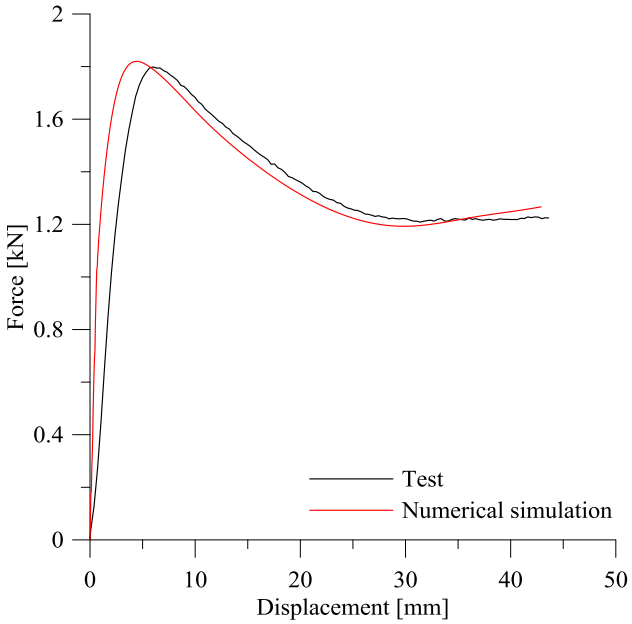

Figure 5-4. Force-displacement curves from test and numerical simulation.

5.1.3 Volume strain

Volume increase was included in the material model through the coefficients β and v. When β equals 1, the model predicts no volume change in the plastic phase, and when v equals 0.5, there

will be no volume change in the elastic area. However, in the material model for PP, $\beta = 1.14$ and $v = 0.45$, and thus the volume in the experimental tests increased.

Figure 5-5 shows the volume strain from the experimental test and numerical simulation of PP-T2. The volume strains were determined from Equation (3-7), and the longitudinal and transverse strains were determined from the cross section with highest strains both in the numerical simulation and the experimental test.

The numerical simulation predicts a rather linear relationship between the volume strain and longitudinal strain, and captures the volume strain fairly good up to a longitudinal strain of 0.4. After that, the experimental curve levels off and the simulation overestimates the volume strain. However, this bend in the experimental curve is not a trend that is general for all the thin tension tests, as seen from Figure 5-6, where the volume strain from the experimental tests of 5 mm thickness is seen.

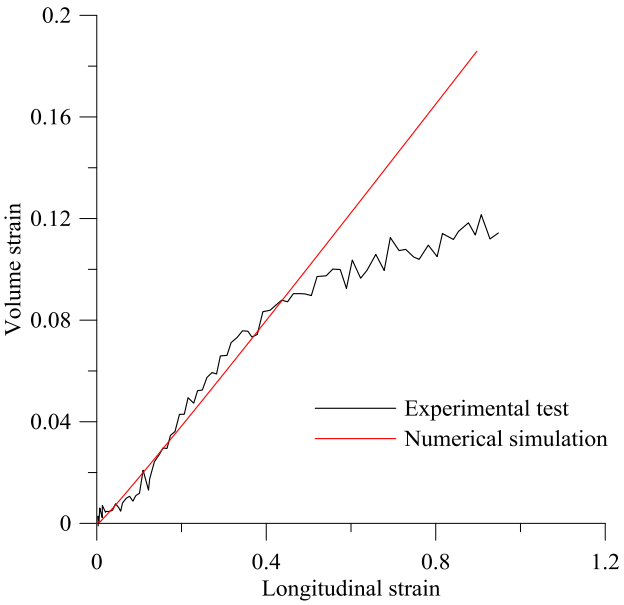

Figure 5-5. Volume strain for experimental test PP-T2 and numerical simulation.

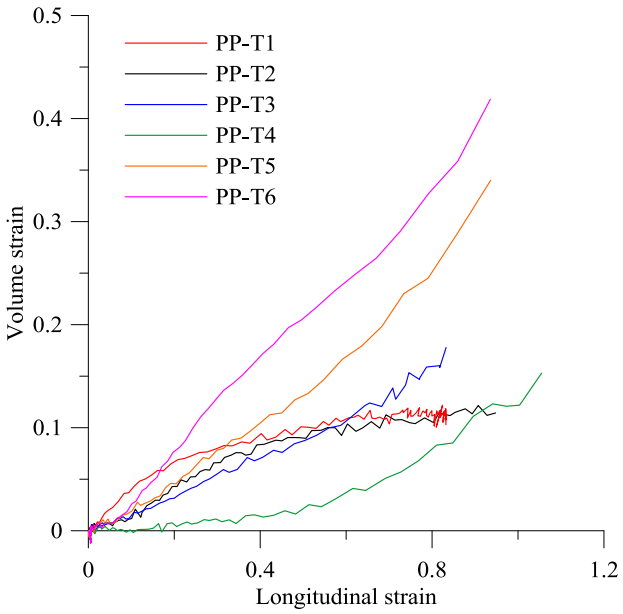

Figure 5-6. Volume strain from the experimental tension tests of 5 mm thickness.

5.1.4 Numerical simulation of tension test at strain rate $10^{-2}s^{-1}$

Test PP-T3 had a velocity of 0.33 mm/s, and a mass scaling of 10^7 was applied. Figure 5-7 shows the force-displacement curves from the test and the numerical simulation. As seen in the figure, the shape of the curve is quite well captured until a displacement of about 15 millimeters. After

this point, the test curve bends down and gets steeper than the simulation curve, which is probably because of heating in the material, resulting in a softer material. The material model will not capture this heating effect because the baseline test did not have the same bend in the curve due to heating in the material.

The simulation has a maximum force that is smaller than in the test, which is opposite of what was observed in the curves from tension test PP-T2. It might be due to the fact that the Poisson's ratio observed for test PP-T3 was slightly smaller than the one in the calibrated model, resulting in a too small area and force.

Like in test PP-T2, the model is not able to correctly predict the stable force level of the test. The experimental data ends up on a force level of around 1.2 kN, but the simulation curve does not flatten out. Instead, the force reaches a minimum point around a displacement of 27 mm before it increases.

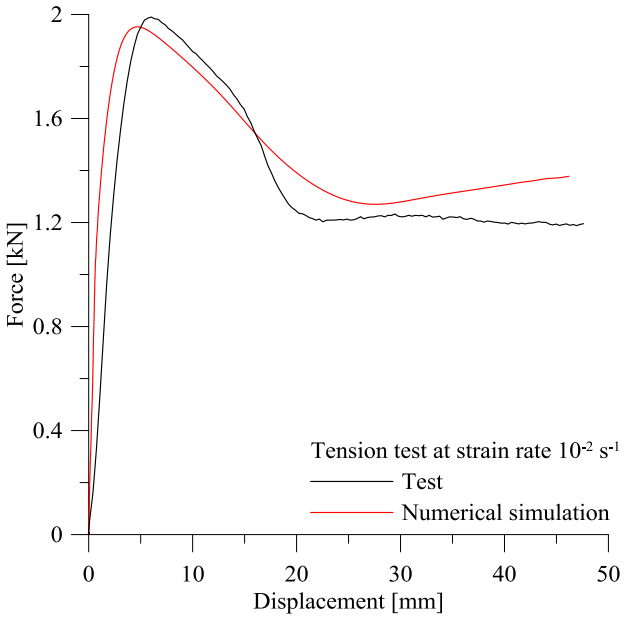

Figure 5-7. Force-displacement curves from numerical simulation and test, from test PP-T3.

5.1.5 Numerical simulation of tension test at strain rate 10^{-1} s^{-1}

Test PP-T5 was carried out at a strain rate of 10^{-1} s^{-1}, and had a velocity of 3.3 mm/s. A mass scaling of 10^6 was used. The test specimen experienced failure, but the material model does not include fracture and the simulation was stopped at a chosen displacement.

In Figure 5-8 the force-displacement curves from the experimental data and the numerical simulation are seen. The same trend is seen in this figure as in Figure 5-7, where the test and simulation curves have a similar shape until the displacement reaches 15 mm, before they deviate from each other. In this case, the test curve is even steeper than in Figure 5-7. It is likely that a test at a higher strain rate will produce more heat, and then again influence the material so that the curve is softer.

The maximum force of the simulation curve is quite similar to the test data, but as observed in the two previous tension test simulations, the stable force is not captured by the material model.

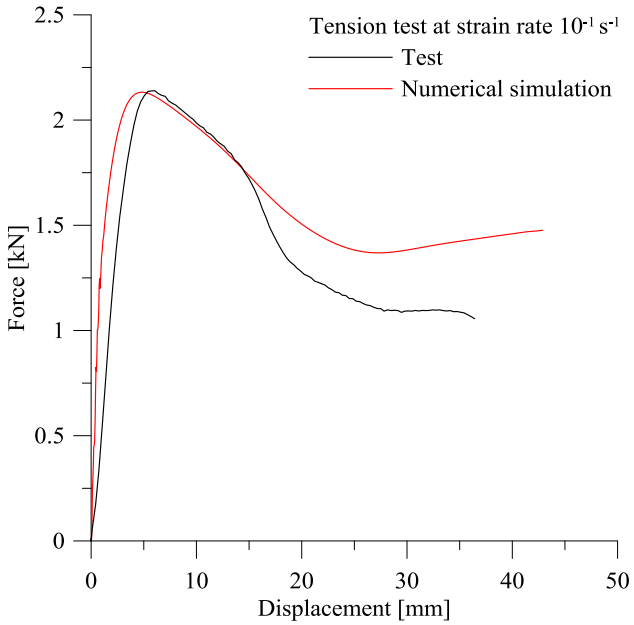

Figure 5-8. Force-displacement curves from test PP-T5 and numerical simulation.

5.1.6 Strain rate sensitivity in the tension tests

The tension tests at higher strain rates were numerically simulated in order to control the strain rate sensitivity of the material model. Figure 5-9 shows force-displacement curves from the numerical simulations of three representative tests at each strain rate. The same representative tests from the experimental data are seen in Figure 5-10. It is seen that the material model is able to show strain rate sensitivity because of the increase in force with the strain rate.

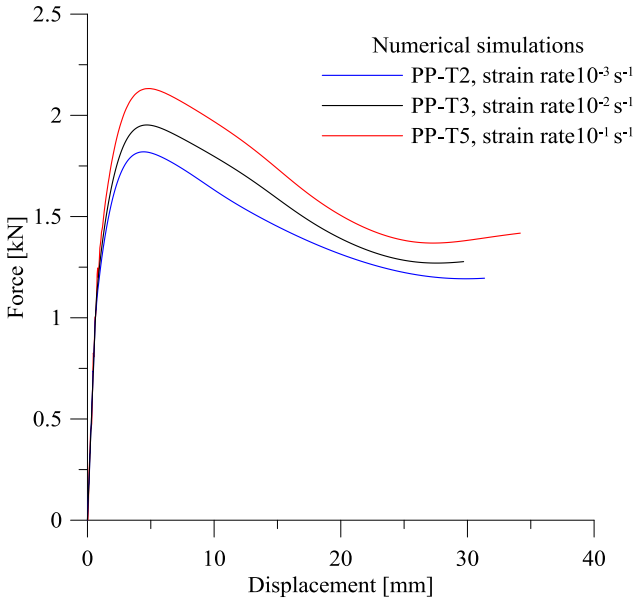

Figure 5-9. Force-displacement curves from numerical simulations of representative tests at three different strain rates.

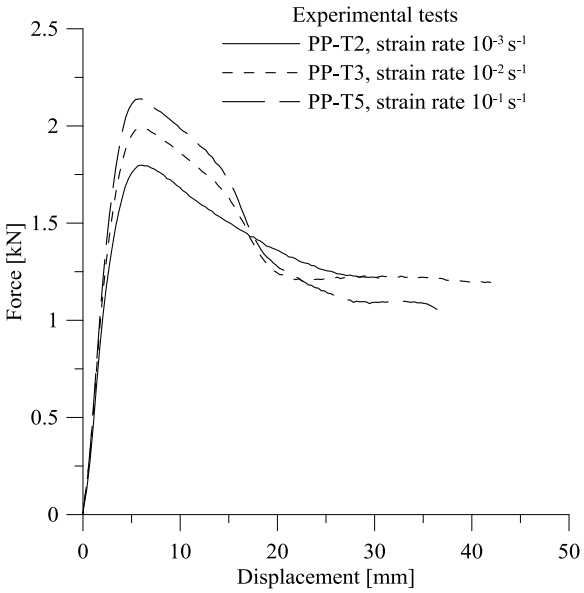

Figure 5-10. Force-displacement curves from experimental tests of representative tests at three different strain rates.

5.1.7 Discussion

In hindsight, symmetry planes could have been applied in the numerical simulations to reduce the computational time. On the other hand, the computational time of the simulations was maximum 4 hours, and it was therefore decided not to change the model to include symmetry planes. Another improvement would have been to use a different mesh in the parallel area, with long and thin elements, so that when the parallel area was stretched, the aspect ratio of the elements improved.

As mentioned in Section 5.1.2, it is possible that a Young's modulus of 1600 MPa was too large since the numerical simulation was located to the left of the experimental test curve in all the tension test simulations. Therefore it was of interest to see the result from simulations with lower Young's moduli. The values 500 and 1000 MPa were chosen.

The results are seen in Figure 5-11. As seen from the figure, a material model with Young's modulus of 1000 MPa and 500 MPa gives a better representation of the experimental test curve in the elastic area. However, the overall shape of the curve from the simulation with 1600 MPa is still the best one, which may indicate that the calibrated Young's modulus of 1600 MPa is the best alternative. Hence, the difference between the deformation in the experimental test and the numerical simulations is most likely caused by the measurements provided by the Dartec machine.

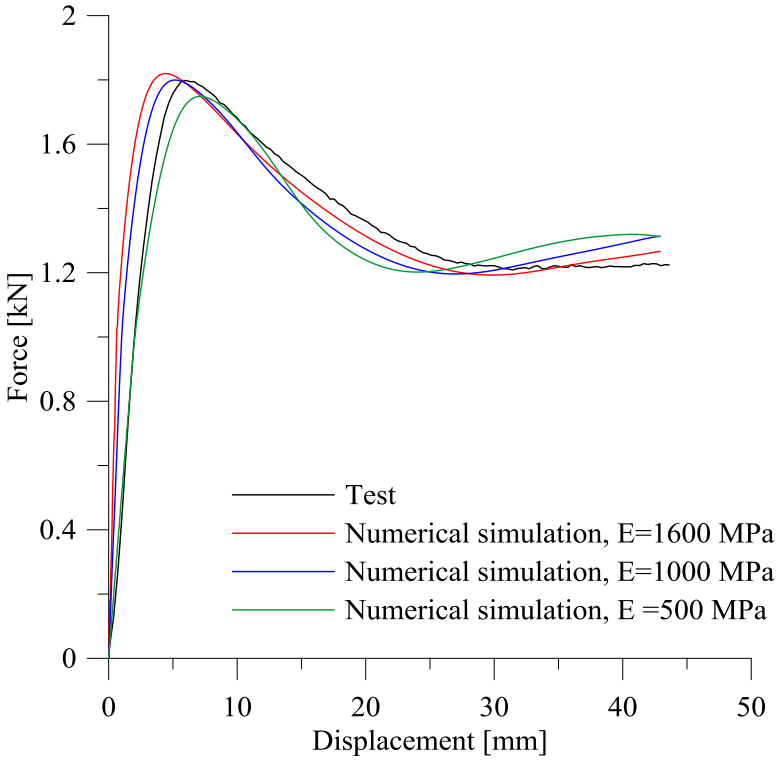

Figure 5-11. Experimental data and numerical simulations of tension test PP-T2 with different Young's modulus.

5.1.8 Numerical simulation of tension test PP-T10

It was decided to do a numerical simulation of one of the 10 mm thick test specimens, and tension test sample PP-T10 was chosen. Test PP-T10 was carried out at a strain rate of 10^{-1} s^{-1}, and the model had 9 elements in the thickness direction. A mass scaling of 10^{6} was applied.

Figure 5-12 shows the force-displacement curves from the test and the numerical simulation of test PP-T10. As seen from the figure, the force-displacement curves from the numerical simulation did not capture the experimental curve as well as in the 5 mm thick tension tests PP-T2, PP-T3 and PP-T5 described in Section 5.1. It is observed that the experimental curve from test PP-T10 had a different shape than the curve from the experimental tests PP-T2, PP-T3 and PP-T5 seen in Figure 5-10, while the numerical simulation curve from test PP-T10 is rather similar to the numerical simulation curves from the same tests. Hence, the difference in the numerical simulation and experimental test from PP-T10 seen in Figure 5-12 seems to occur because the experimental curve from PP-T10 has a different shape than the baseline test.

The reason why the model is not able to predict the behaviour correctly might be because of the parameter β, describing the plastic dilatation. β is larger in test PP-T10 than in the baseline test. Test PP-T10 has $\beta = 1.27$ and the baseline test has $\beta = 1.14$, which results in a larger volume

expansion in the plastic area in test PP-T10 than in the baseline test. The stress-strain curves from test PP-T10 and baseline test PP-T2 are seen in Figure 3-10, and they have a similar shape. However, the cross section area of test PP-T10 evolves different than in the baseline test, giving the force-displacement curves a different shape.

The model predicts a volume expansion like in the baseline test, and is therefore not able to represent the behaviour of test PP-T10 as well as it did with the 5 mm thick tests.

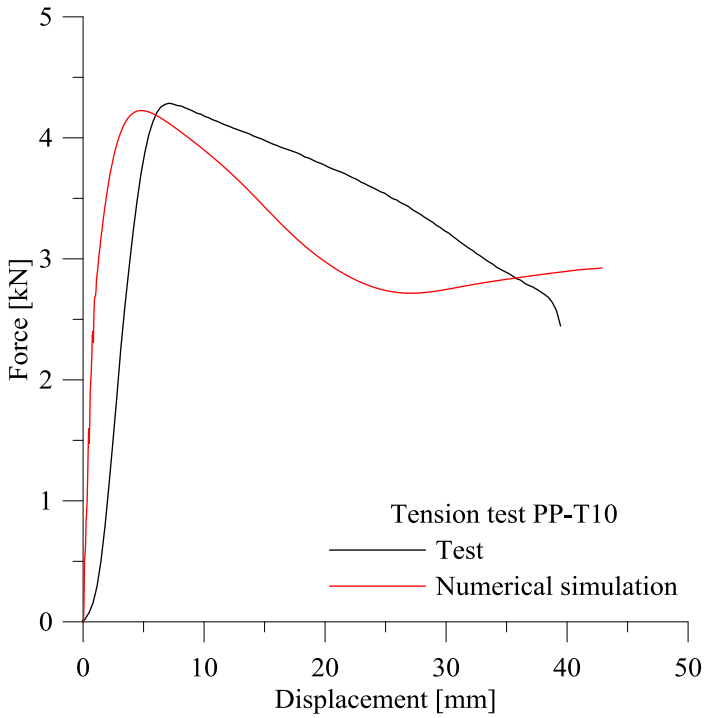

Figure 5-12. Force-displacement curves from experimental test PP-T10 and numerical simulation.

5.2 Compression tests

Numerical simulations of the compression tests were of interest because they would give an indication of whether the pressure sensitivity coefficient, α, was correct. The numerical simulations of the compression tests were based on the true stress-strain curve from the baseline tension test used in the calibration, but the parameter α scaled the curve. It was therefore expected that the numerical simulations of the compression tests would give pretty good predictions of the yield stress, but it was not expected that the model would predict correctly in the phase after the yield stress.

It was decided to do a numerical simulation of compression tests PP-C1, PP-C3 and PP-C4, and they were carried out at strain rates 10^{-3}, 10^{-2} and 10^{-1} s^{-1} respectively. The results from the simulation of the test at strain rate 10^{-1} s^{-1}, PP-C4, are described in detail in this section, and further the results from the tests at lower strain rates are briefly described. Finally, all the tests are compared and the strain rate sensitivity discussed.

5.2.1 Model

Figure 5-13 shows the geometry of test specimen PP-C4, having height 8 mm and diameter 10 mm. The strain rate of this test was 10^{-1} s^{-1}, and the velocity was 0.8 mm/s.

A mass scaling of 10^6 turned out to be the best alternative, and element sizes of 1 x 1 mm and 0.5 x 0.5 mm were tested, giving exactly the same results. Figure 5-13 shows the test sample with element size 1 x 1 mm, and with 8 elements in the thickness direction. The model had a number of 837 nodes and 616 elements.

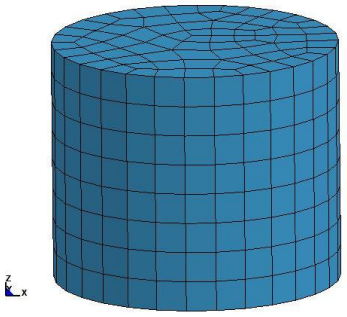

Figure 5-13. Geometry of compression test.

As mentioned in Section 3.5, a lubricant was applied during testing to avoid friction between the test samples and the cylinders. Even though this did not remove all friction, the LS-DYNA model was simplified and therefore modeled frictionless. This was done by fixing all the nodes on the bottom surface of the sample only in the z-direction, so that the test sample was able to expand in x and y directions. The nodes on the top surface of the specimen were given a constant negative velocity in the z direction.

Reduced and selectively reduced integration were tested, giving exactly the same results. Hence, reduced integration was the best option because of a shorter computational time.

5.2.2 Results from numerical simulation of compression test PP-C4

Figure 5-14 and Figure 5-15 show the force-displacement curves and true stress-strain curves respectively, from the test and numerical simulation of compression test PP-C4.

As seen from the figures, the simulation curves are differing from the test curves. The true stress-strain curve from the numerical simulation has a pretty good fit until the yield stress is reached, and the same is seen in the numerical predicted force-displacement curve.

The yield stress in the numerical simulation was found from Considere's criterion, see Equation (3-6), giving a value of 56 MPa. The yield stress in the experimental test was 57.7 MPa. The yield stresses are marked in Figure 5-15, and they are quite similar. Hence, it seems like the parameter α was predicted fairly well.

After the yield stress occur, the curves deviate from each other. The difference in the curves is likely to be caused by the fact that the numerical predictions of the compression tests are based on the true stress-strain curve from the baseline tension test used in the calibration. This curve was completely different from the stress-strain curves determined from the compression test.

The difference could also be caused by the difference in the calibration curve and the curve from the experimental data, seen in Figure 5-3, where the calibration and test curves are quite similar until yielding. After the yield stress is reached, the calibration curve lies higher than the test curve, which means that the calibration curve is stronger than the test curve in this area. This seems to happen in Figure 5-14 and Figure 5-15 as well, where the numerical simulation is stronger than the test curve after yield stress is reached.

In the last part of the calibration and test curves in Figure 5-3, after the true strain reaches 0.6, the test curve is again stronger than the calibration curve. However, it is likely to believe that the compression test samples not were compressed so much that they reached this part of the calibration curve.

In addition, some of the difference in the true stress-strain curves is likely to be caused by a barreling effect. The part of the curve where a barreling effect was present is indicated with a dashed line. As mentioned in Section 3.5.2, a barreling effect occurs in the compression tests after a true strain of around 0.2 is reached. This effect will influence the stress-strain curve and result in more softening than it originally should have.

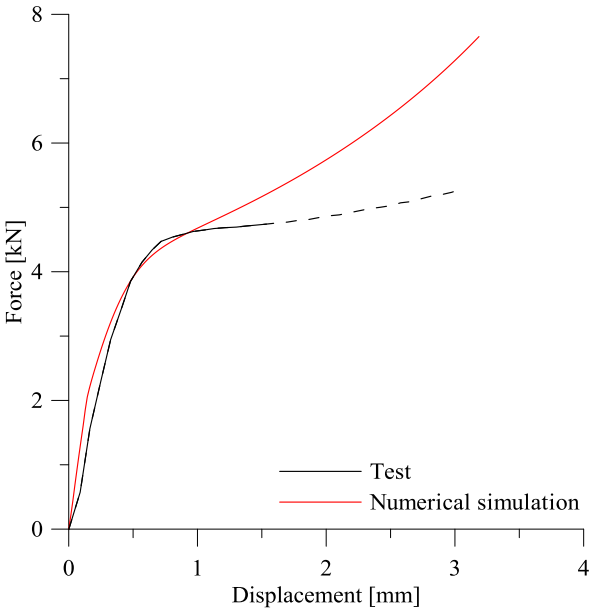

Figure 5-14. Force-displacement curves from test and numerical simulation, from test PP-C4. The dashed line indicates the part of the curve where a barreling effect is present.

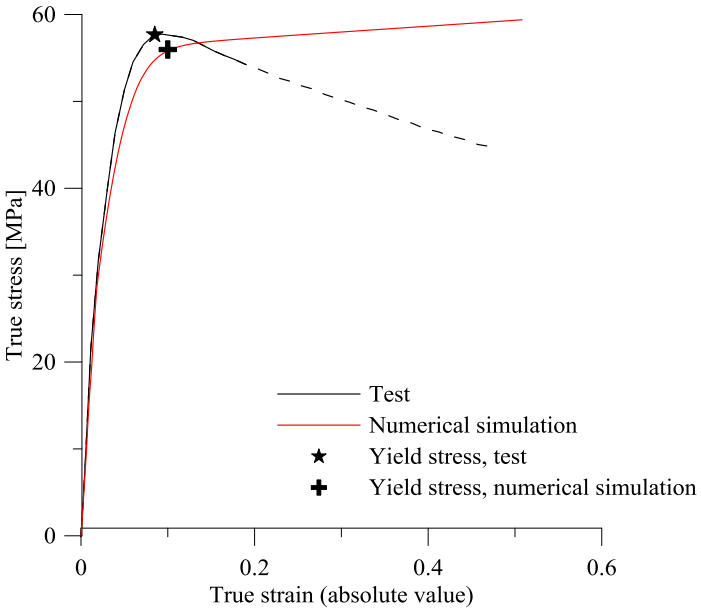

Figure 5-15. True stress-strain curves from test and numerical simulation, from test PP-C4. The dashed line indicates the part of the curve where a barreling effect is present.

5.2.3 Strain rate dependency in compression tests

In Figure 5-16, the numerical simulation and experimental data from compression tests PP-C1, PP-C3 and PP-C4 are seen. They all have a fairly good fit until the yield stress is reached. It is also observed in the figure that the numerical simulation of the test at strain rate 10^{-1} s^{-1} has a lower yield stress than the experimental data, but the numerical simulation of the test at strain rate 10^{-3} s^{-1} has a higher yield stress than the experimental data. The simulations underestimate yield stress at high strain rates and overestimates at low strain rates.

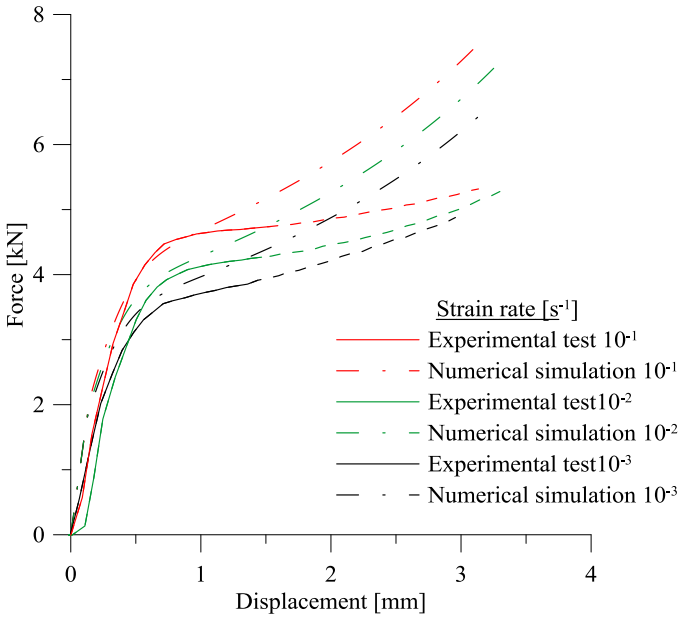

Figure 5-16. Force-displacement curves from tests PP-C1, PP-C3 and PP-C4.

5.2.4 Volume strain

Figure 5-17 shows the volume strain for the numerical simulation and experimental test PP-C4. Both the experimental test and the numerical simulation indicate a volume increase. This was expected for the numerical simulation, since the material model is not able to predict volume decrease in compression and expansion in tension, as discussed in Section 4.4.1. The numerical simulation shows a small contraction in the elastic area, before the volume increases.

It is, however, strange that the experimental test PP-C4 in Figure 5-17 indicates volume expansion, because compression test PP-C1 in Figure 3-27 experiences contraction. The only difference between the tests PP-C1 and PP-C4 was the strain rate, as test PP-C1 was carried out at a strain rate of 10^{-3} s^{-1} and test PP-C4 was carried out at strain rate 10^{-1} s^{-1}. The difference in the volume strain is probably due to uncertainty of measuring results and experimental diversification, considering that the volume strain is sensitive to where in the test sample the diameter was measured.

Additionally, there was a barreling effect seen in the DIC pictures from the tests after a longitudinal strain of around 0.2, which means that the data after this point was uncertain.

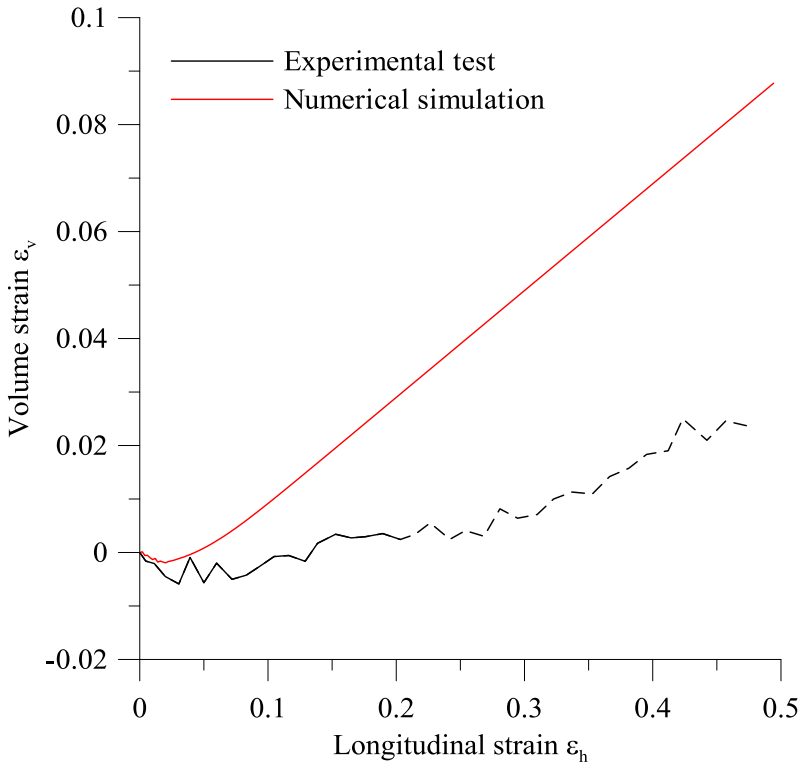

Figure 5-17. Volume strain of numerical simulation and experimental test PP-C4.

6 Validation tests

The material model calibrated in Section 4 was implemented as a user-defined material model in LS-DYNA. In order to evaluate the material model, two different component tests were carried out.

The first part of the validation tests were tension tests carried out on a plate with a hole. A plate with a hole was a desirable component to use in validation of the material model because it had simple, clearly defined geometry and boundary conditions, with a complex stress and strain state in the area around the hole. Stretching of a plate with a hole will control the properties of the material model at low strain rates.

The second round of the validation tests was plate impact tests in an Instron CEAST 9350 Drop Tower machine. These tests were of interest because they tested the properties of the material model at high strain rates.

This chapter will first present and evaluate the validation tests on the plate with a hole, before the plate impact tests are given an account of. The sensitivity of some of the parameters in the model was investigated of as well. All simulations were carried out as explicit non-linear finite element analysis in the finite element code LS-DYNA.

6.1 Stretching of plates with a hole

This section will first present the experimental tests on a plate with a hole, before the numerical simulations are explained. Force-displacement curves are used to compare the results from the experimental tests and numerical simulations. In addition, various dimensions of the test specimen are evaluated, and the differences between the experimental data and the simulations are discussed.

The transverse strains in the necking area of the plate were evaluated as well. However, the software 7D was not able to determine the strains further than half of the testing time since the paint pattern on the test specimen in the necking area became unclear at large strains. This made it difficult to compare the transverse strains from the simulation and experimental test, and the evaluation was therefore excluded from the report.

6.1.1 Material testing

A total of 4 tests were carried out on a plate with a hole. The test specimens consisted of two different diameters of the hole, 20 mm and 30 mm. The geometry of the plates is seen in Figure 6-1. The test samples were cut from the 5 mm thick PP plate in the extrusion direction, as seen in Figure 3-1 in Section 3.2.

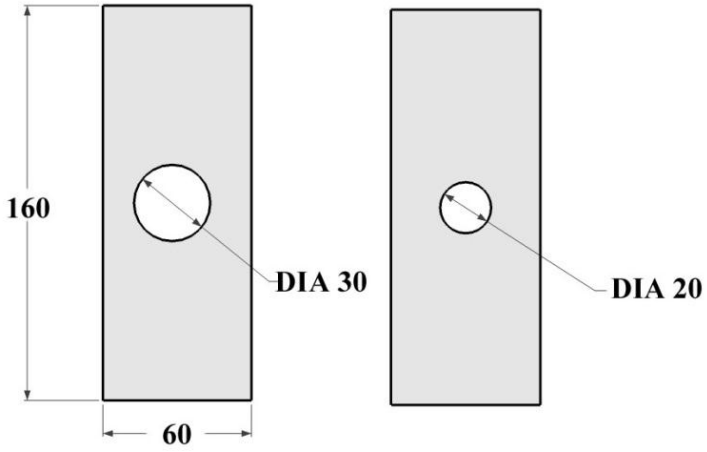

Figure 6-1. Geometry of test specimens. All dimensions are in millimeters.

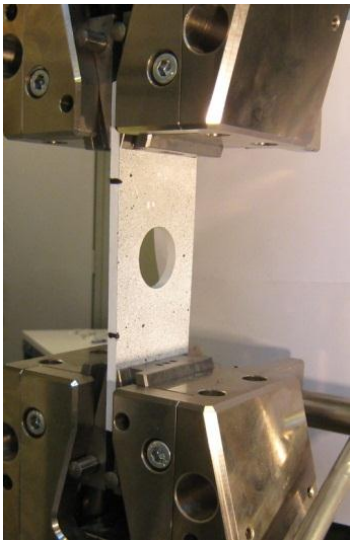

Figure 6-2. Setup of tension tests on a plate with a hole.

The servo-hydraulic Dartec testing machine described in Section 3.2 was used in these tests as well. The test specimens were fastened to the machine by clamps, as shown in Figure 6-2. The bottom clamp was fixed, while the top clamp was moving at a constant velocity.

An overview of the tests carried out is presented in Table 6-1. The tests were named PP-H#, where H indicates "hole", and # is the number of the test. The table also shows the initial diameter of the hole and the cross-head velocity.

The machine had a cross head velocity of 0.05 mm/s or 0.5 mm/s during the tests. The strain rate was not used like in the tension and compression tests, because it would vary throughout the test sample. The strain rate around the hole was decided to be of magnitude in the range 10^{-3} to 10^{-2} s^{-1}, and the cross head velocities were estimated based on that.

Table 6-1. Tests on a plate with a hole.

Test number	Cross-head velocity [mm/s]	Initial diameter of hole [mm]
PP-H1	0.05	29.85
PP-H2	0.05	19.71
PP-H3	0.5	29.87
PP-H4	0.5	19.58

Two cameras were used during the testing for later to use the DIC technique to determine displacements. Camera 1 was placed right in front of the test specimen, taking pictures of the front of the test sample like in Figure 6-3. Camera 2 was placed on the side of the specimen, taking pictures of the thickness of the test sample like Figure 6-4 shows.

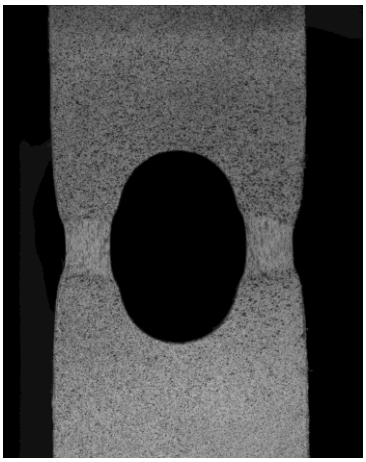

Figure 6-3. Picture taken with Camera 1.

Figure 6-4. Picture taken with Camera 2.

The force was measured by the Dartec machine, and this data was synchronized with the DIC pictures, ensuring stresses and strains at the same time axis.

It was desirable to know the displacement 40 mm above the center of the hole for later to use when comparing the test results with the numerical simulation results. The software 7D and the DIC technique described in Section 3.3 was used to find the mean displacement of the cross section 40 mm above the center of the hole in the plate. The strain field in the area around the hole was found by the same technique.

Figure 6-5 shows the dimensions *w1*, *w2*, *dx* and *dy*. These were all determined for test PP-H1 from the pictures taken with Camera 1. In addition, the thickness *t* of the plate in the same cross

section as *w1* and *w2*, was determined from the pictures taken with Camera 2. The dimensions were obtained by processing the pictures from the digital cameras in MATLAB, where they were converted into black and white pictures. The same method that was used to find the diameter and height of the compression tests, described in Section 3.5.1, was used. Once the pictures were transformed into black and white, the dimensions were determined. The MATLAB scripts that were used in these calculations are seen in Appendix E.

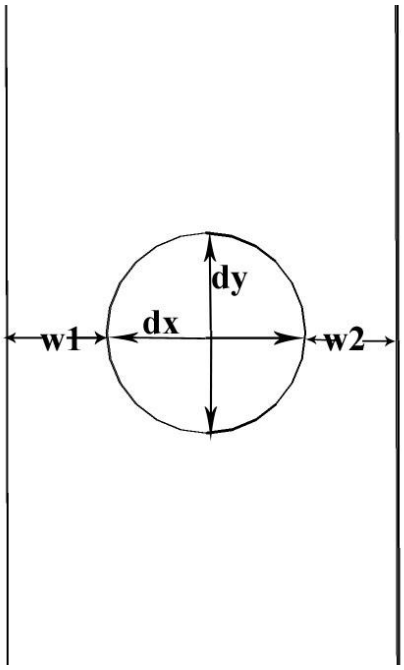

Figure 6-5. A section of the plate, with several of the dimensions that were found in MATLAB.

6.1.2 Results

All the results from the tests on plates with a hole are presented in Appendix C. In this section, the most important results are reported.

As seen from Figure 6-3 and Figure 6-4, test PP-H1 experienced a propagated neck, with stable cross section dimensions.

Figure 6-6 shows the force and displacement curves for the tests. As seen in the figure, two of the tests, PP-H3 and PP-H4 experienced failure. They were both carried out at a cross head velocity of 0.5 mm/s.

The test samples with the 30 mm diameter of the hole, PP-H1 and PP-H3, withstand significantly less forces than test samples PP-H2 and PP-H4 with the 20 mm diameter hole. It is also worth noting that the curves are dependent on the velocity. Higher velocity gives a higher force-displacement curve.

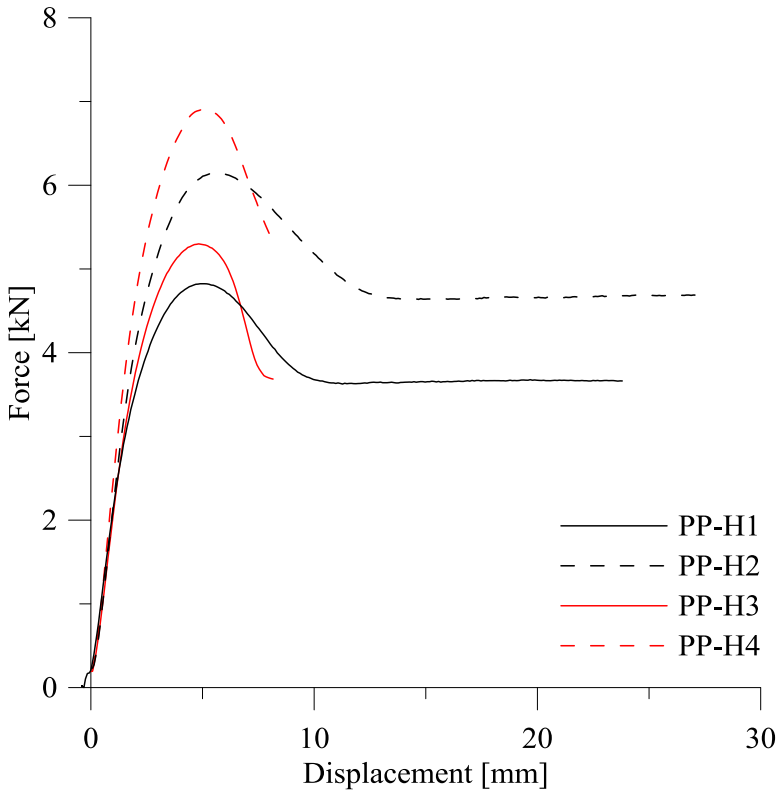

Figure 6-6. Force and displacement curves for the four tests on a plate with a hole.

6.1.3 Numerical simulations of the stretching of a plate with a hole

Numerical simulations in LS-DYNA were carried out on the four tests on the plate with a hole, and they are compared to the experimental data in this chapter. The numerical model is firstly described, before the results from the numerical simulation of test PP-H1 are explained in detail. A parameter study was done on this model, also presented here. In addition, the dimensions shown in Figure 6-5 are compared for PP-H1. Furthermore, tests PP-H2, PP-H3 and PP-H4 are briefly explained and evaluated.

Model

The geometry of the plate with the hole of diameter 20 mm is seen in Figure 6-7. Several different meshes were tried, giving minor changes in the global response. A mesh made of long and thin elements in the analysis area was chosen as the final mesh. The elements had this shape because the aspect ratio of the elements would improve when the plate was stretched. The elements were of size 1.5 x 0.5 mm. The upper part of the model had an element size of 1.5 x 1.5 mm, and in the thickness direction there were 4 elements. Simulations with 5 elements in the thickness direction were tried as well, but since it resulted in only minor changes, 5 elements were not used. The model had 5830 nodes and 4264 elements.

The plate with a hole was modeled with one symmetry plane. The reason why only one symmetry plane was used was that the hole was not located perfectly in the center of the plate. To model the symmetry, the nodes on the bottom surfaces in the model were fixed in y-direction, and in the rotational degrees of freedom in x and z directions. The nodes on the top surface of the model were given a constant velocity.

The original length of the test specimen between the clamps in the machine was 100 mm, meaning that when half the plate was modeled, it should be 50 mm high. However, to reduce the computational time, only 40 mm of the plate was modeled. It was checked that the displacement in the experimental test at 40 mm above the center was nearly exactly the same as at 50 mm, and it was assumed uniform over the width of the plate. Thus, a constant velocity was applied 40 mm above the symmetry plane in the numerical model.

The forces from the simulation were taken from a cross section of the plate, and the displacement was obtained as the mean displacement of a cross section located 40 mm above the center of the hole. The average of the displacements was used in case there was a non-uniform displacement over the cross section, and because it was the average displacement that was measured from the experimental tests. That way the displacement from the experimental data and the simulations were comparable.

Various factors of mass scaling were tested, and a value of 10^8 for the tests at velocity 0.05 mm/s turned out to be the best compromise between computational time and result, combined with a low kinetic energy relative to the total energy. The tests at velocity 0.5 mm/s had a lower mass scaling, of size 10^6, to ensure small time steps.

Two of the experimental tests fractured. As mentioned, the material model did not include fracture, and the simulations were ended at an adequate displacement.

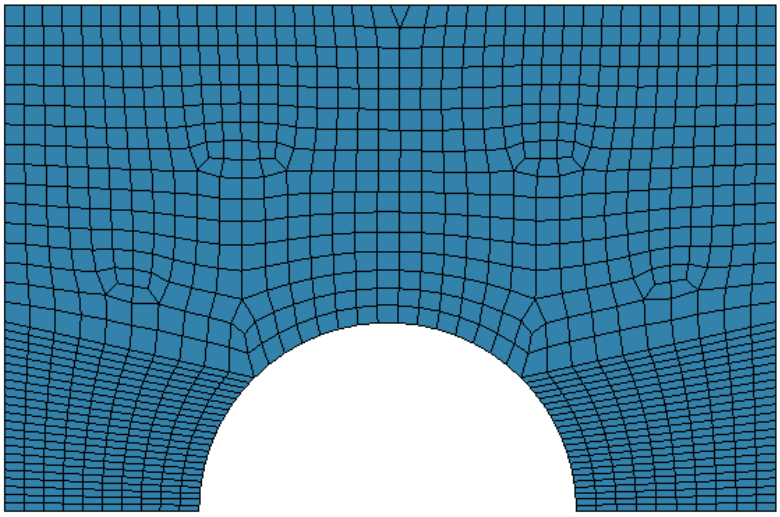

Figure 6-7. The geometry of the plate with a hole with one symmetry plane.

6.1.4 PP-H1

Test PP-H1 had a velocity of 0.05 mm/s. Mass scaling was necessary to reduce the computational time, and a factor of 10^8 was applied. The kinetic energy was checked to be very small compared to the total energy of the simulation.

Several element formulations were tested, and fully integrated quadratic 8 node elements with nodal rotations gave the best results. Other element formulations that were tried were constant stress solid elements with reduced integration, fully integrated selectively reduced solid elements, and fully integrated selectively reduced solid elements intended for elements with poor aspect ratio. In LS-DYNA, the element formulation for fully integrated quadratic 8 node elements with nodal rotations is given the number 3, and from here on this is called element formulation 3 [16].

Figure 6-8 shows the global response from the numerical simulation and experimental test. As seen in the figure, the shape of the curves is quite similar. However, Young's modulus seems a bit too high in the simulation, which cannot be caused by displacements and suspensions in the machine like it was in the tension tests, because the displacement in this case was found 40 mm above the center of the hole using the DIC technique.

The maximum force seems to be a little overestimated, but it is in the constant force that the curves differ the most. There, the numerical simulation experiences hardening although the experimental curve flattens out. The hardening in the simulation curve is likely to be caused by the difference between the calibrated material model and the experimental test, explained in Section 5.1.2.

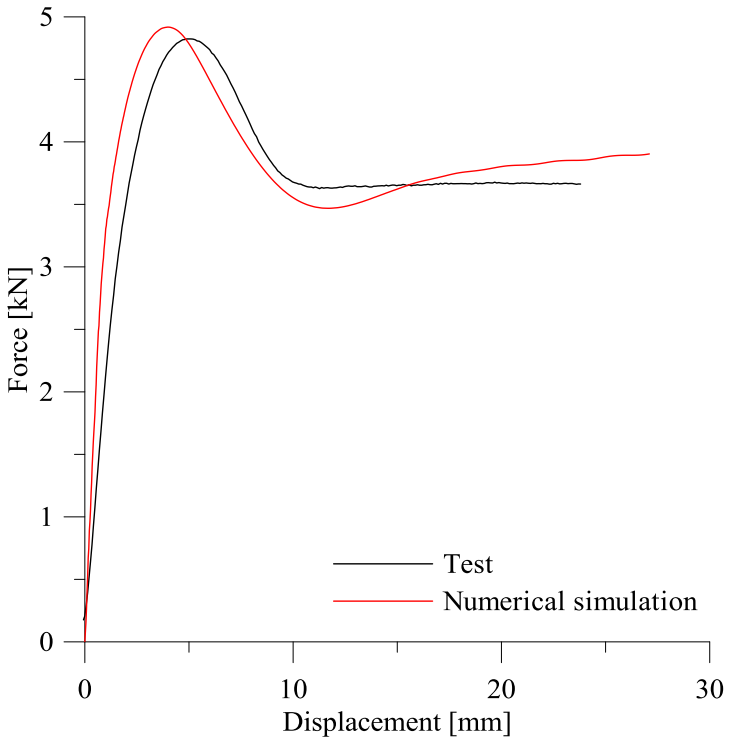

Figure 6-8. Force-displacement curves from test PP-H1 and numerical simulation.

Comparing the dimensions

Figure 6-9 shows a picture of half of the test sample and half of the numerical simulation. The simulation gives a shape of the test sample that is quite similar to the experimental test, but it is observed that the experimental test has a more localized neck than the numerical simulation. The more localized neck in the experimental test results in a smaller thickness in the necking area. Figure 6-10 shows the thickness of the simulation and experimental test after a deformation of 25mm, where the differences in the thickness are visible.

The material model does not capture the localization of deformation, which is likely to be due to the fact that in Figure 4-8, the test curve is flattening out in the phase of the curve after yield stress is reached. In this part of the experimental testing, the deformations in the plate will increase a lot with just a small rise in the force. The material model does, however, not have this flat level, and will experience a hardening after the yield stress occurs. This hardening gives a more uniform distributed deformation over the analysis area of the plate, and the deformation is not localized as much as in the test, which results in a larger thickness in the numerical simulation.

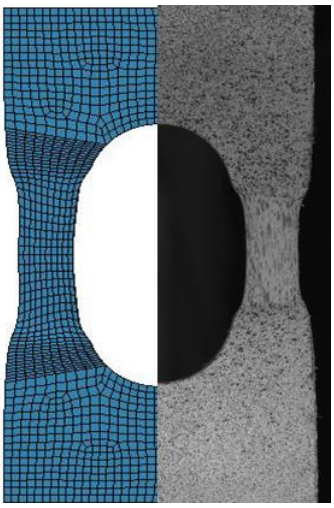

Figure 6-9. Numerical simulation and experimental test of PP-H1 after a displacement of 25 mm.

Figure 6-10. Numerical simulation and experimental test of PP-H1 seen from the side after a displacement of 25 mm.

Since the numerical simulation gives a varying geometry of the area around the hole relative to the test, it was of interest to compare a variety of the dimensions on the plate. The dimensions described in Section 6.1.1, and seen in Figure 6-5 were determined from the numerical simulation of test PP-H1 as well as the experimental data.

Figure 6-11 to Figure 6-13 show the results. The displacement *u* on the x axis is the displacement of the plate 40 mm above the center of the hole. The y axis represents the change in the dimensions *w1, w2, dx, dy* and *t*.

The dimension *dy* in Figure 6-11 is constantly increasing, while *dx* is slowly decreasing before increasing. It makes sense that *dx* decreases in the beginning, considering that the plate is stretched. After a displacement of about 5 mm, *dx* starts to increase, which is due to the fact that the entire upper and lower end of the plate is fixed. This result in a process where the two necking areas are forced apart, leading to a larger *dx*. The numerical simulation provides a good representation of both *dx* and *dy*.

Figure 6-12 shows that *w1* and *w2* from the experimental data have a different starting point, but they are parallel. This can be explained by the fact that *w1* and *w2* initially had different sizes. The geometry in the numerical simulation was based on measurements carried out on the test samples with a digital caliper before the testing. *w1* and *w2* in the numerical simulations do not have the exact same starting point as the experimental tests, which indicate inaccurate measurements of

the test specimen before the testing. Still, the shape of the curves is fairly well captured by the numerical simulation. However, *w1* and *w2* are stabilized at a higher displacement in the simulation than in the experimental test. In the experimental test *w1* and *w2* stabilize in the very last phase of the curves, at a displacement of around 10 mm. This makes sense since the experimental tests had a more localized neck and thus became thinner.

The thickness *t* of the plate in Figure 6-13 is slowly decreasing. However, the last part of the *thickness* curve from the numerical simulation is overestimated, and it stabilizes on a thickness of around 3 mm. In the experimental test, a small area experiences a large necking, resulting in a smaller thickness than in the numerical simulation. The thickness curve from the experimental test has a lot of noise, which is due to low contrasts in the pictures taken from Camera 2, complicating the determination of the thickness.

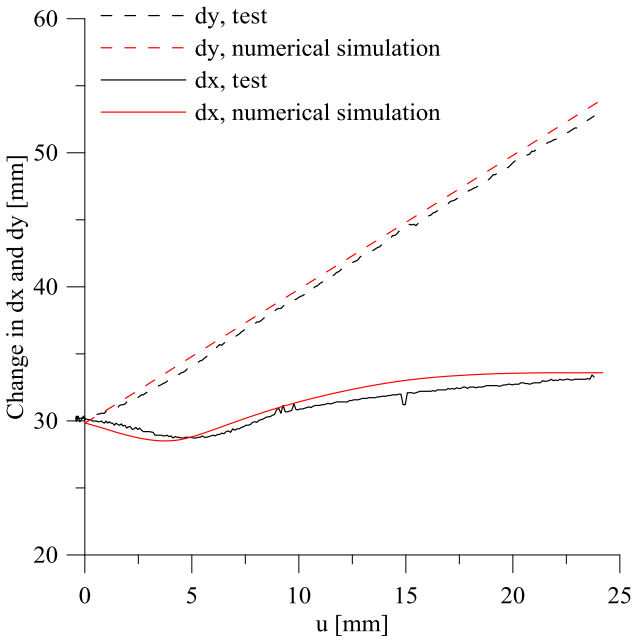

Figure 6-11. Dimensions *dx* and *dy* plotted versus the total displacement *u* of the plate 40 mm above the center of the plate for test PP-H1.

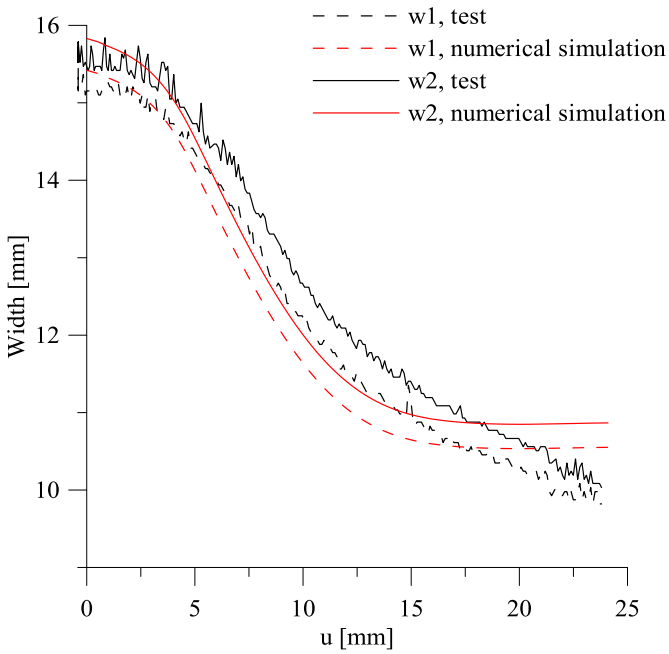

Figure 6-12. w1 and w2 from test and numerical simulation.

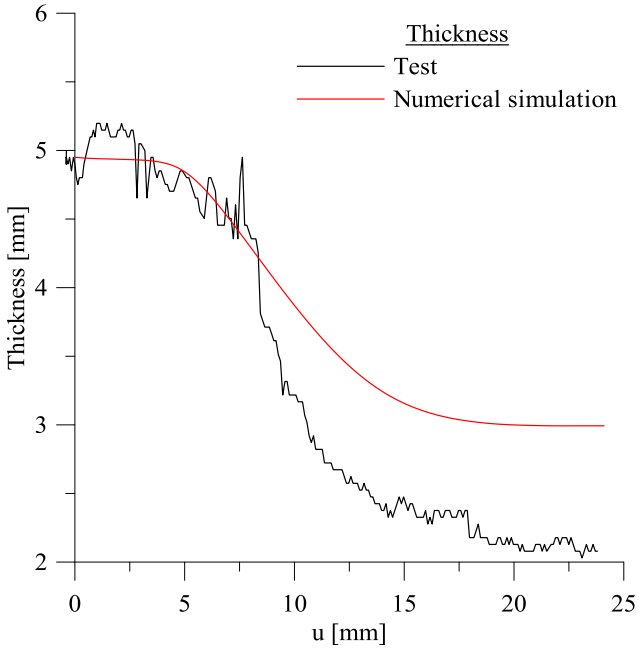

Figure 6-13. Thickness of plate.

6.1.5 PP-H2, PP-H3 and PP-H4

Test PP-H3 had the same diameter of the hole as PP-H1, and was modeled with the same geometry as in Figure 6-7 . A new geometry was made for tests PP-H2 and PP-H4 with a hole of diameter 20 mm.

Test PP-H2 was carried out at velocity 0.05 mm/s, and tests PP-H3 and PP-H4 had a velocity of 0.5 mm/s. The differences in testing time resulted in a different necessary mass scaling to reduce the computational time. The test at 0.05 mm/s had a mass scaling of 10^8, and the tests at velocity 0.5 mm/s had a mass scaling of 10^6. It was controlled that the kinetic energy was very small compared to the total energy in the simulations.

It turned out that fully integrated selectively reduced solid elements, intended for elements with poor aspect ratio gave the best results for the tests PP-H3 and PP-H4 of velocity 0.5 mm/s. In LS-DYNA, this element formulation is called -1. Element formulation 3 was used in simulation of test PP-H2.

The reason why different element formulations gave best results in the tests of velocity 0.05 mm/s and 0.5 mm/s is probably because tests PP-H3 and PP-H4 both fractured before the stable force was reached. Element formulation -1 gave a good representation also in tests PP-H1

and PP-H2 in the first part of the test, until the stable force was reached. However, element formulation 3 gave a better prediction of the stable force, and thus a better global response.

On the other hand, the reason why different element formulations gave optimal results in the simulations when they have the same mesh and only the velocity is changed could be that stiffer or softer elements correct the deficiencies in the material model [11].

Figure 6-14 and Figure 6-15 show the overall response of the experimental tests and the numerical simulations from tests PP-H2, PP-H3 and PP-H4. The shape of the curves from the numerical simulations is pretty similar to the experimental tests. Since fracture is not included in the material model, the simulations of test PP-H3 and PP-H4 were ended at a convenient displacement.

However, it seems like Young's modulus in the numerical simulations is too high, which was also observed in test PP-H1. A parameter study where different Young's moduli were tested is presented later in this section. The maximum force is pretty well captured in all the simulations, though it is a bit overestimated in PP-H2 and a bit underestimated in PP-H4.

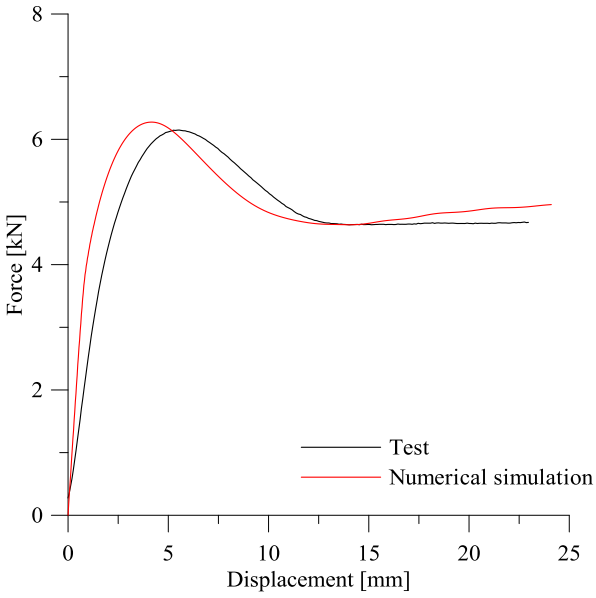

Figure 6-14. Force-displacement curves from test PP-H2, carried out at velocity 0.05 mm/s.

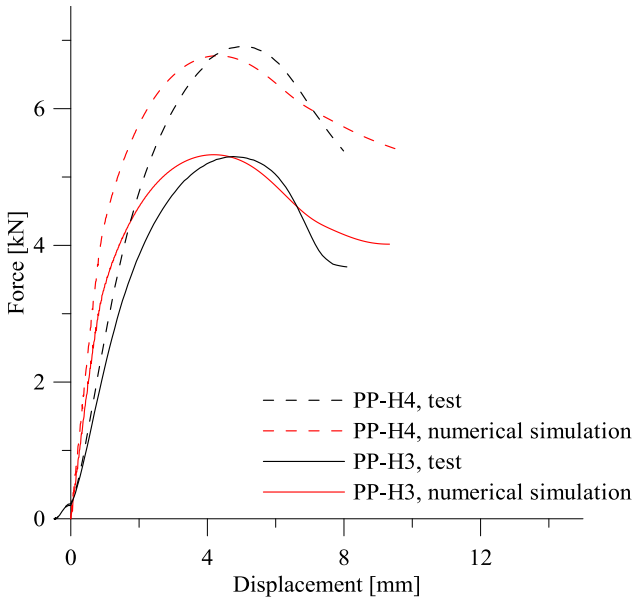

Figure 6-15. Force-displacement curves from tests PP-H3 and PP-H4, both carried out at velocity 0.5 mm/s.

6.1.6 Parameter study

As mentioned, the elastic stiffness was probably too large in the tests carried out on the plates with a hole. Therefore, inverse modeling was applied on test PP-H1, testing a lower value of Young's modulus. The calibrated material model had a Young's modulus of 1600 MPa, and the value 1000 MPa was tried in this parameter study.

The results are seen in Figure 6-16, and it is clear that a lower value of Young's modulus gives a better representation of the first part of the curve before the peak force is reached. However, the simulation with Young's modulus of 1600 MPa gives a better representation of the overall shape of the curve than the simulation with E=1000 MPa does.

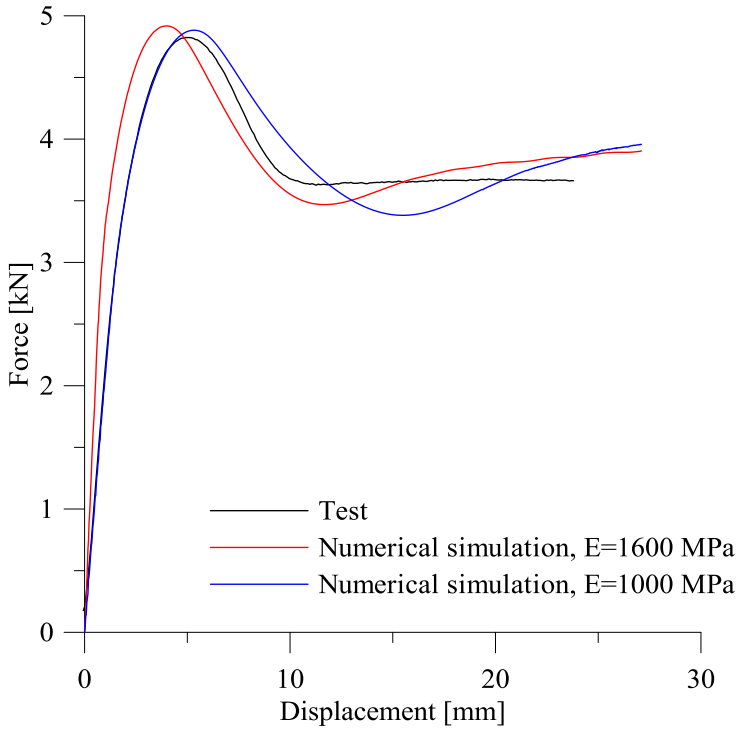

Figure 6-16. Experimental test and numerical simulations with different values of Young's modulus.

A simulation with the alternative material model presented in Section 4.5 was tried as well, giving poor results. Neither the shape of the curve nor the stable force was captured by the alternative material model.

6.2 Plate impact tests

Plate impact tests were carried out in order to control the properties of the material model at high strain rates. In this section, the material testing is firstly presented, before numerical simulations are explained and evaluated. In the end of the chapter, a parameter study of several parameters is given an account of.

6.2.1 Material testing

A number of 6 impact tests were carried out on plates with dimensions 100 x 100 x 4.94 mm in the Instron CEAST 9350 Drop Tower machine, where a free falling weight impacted the center of the test specimens. The striker had a hemispherical shape with a diameter of 20 mm. The test setup in the Drop Tower machine is shown in Figure 6-17 and Figure 6-18. The test sample was fixed between two rings with inner diameter 70 mm like seen in the pictures.

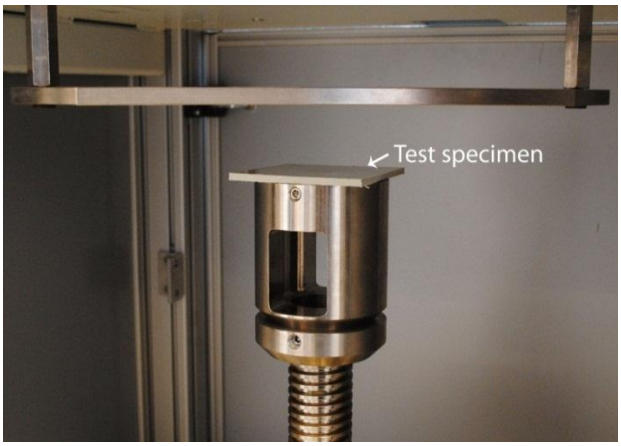

Figure 6-17. Test setup in the Drop Tower machine.

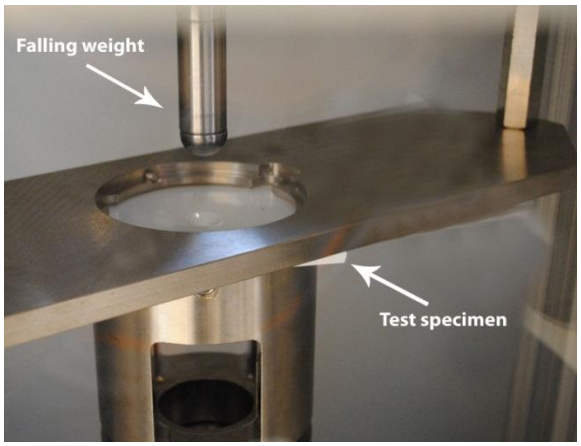

Figure 6-18. Test setup in the Drop Tower machine, with the falling weight.

Table 6-2 gives an overview of the tests that were carried out, as well as the mass and velocity of the free-falling impactor and total kinetic energy. The test samples were cut from the 5 mm thick PP plate, and they were named PP-D#, where D means Drop Tower, and # is the number of the test. The falling weight had a mass of 5.045 kg, and an addition of 5 kg was added for the four last tests. The velocity was estimated based on a decision of the magnitude of the energy and mass, using Equation (6-1).

$$E_k = \frac{1}{2}mv^2 \tag{6-1}$$

Table 6-2. Tests carried out in the Drop Tower machine.

	Mass [kg]	Velocity [mm/s]	Energy [kJ]
PP-D1	5.045	4430	50
PP-D2	5.045	6263	100
PP-D3	10.045	4430	100
PP-D4	10.045	6263	200
PP-D5	10.045	5424	150
PP-D6	10.045	5774	170

A strain gauge was located inside the falling weight, and force, displacement and energy data from the tests were provided. The recording began when the striker hit the plate. Use of Digital Image Correlation was not necessary for these tests.

6.2.2 Results

All of the results from the tests in the Drop Tower machine are presented in Appendix D, together with pictures of the test specimens after the testing. In this chapter the force-displacement curves from the tests are evaluated. Figure 6-21 shows the force-displacement curves from tests PP-D1, PP-D2 and PP-D3. Figure 6-22 shows the curves from tests PP-D4, PP-D5 and PP-D6.

In all of the tests shown in Figure 6-21, the falling mass bounced back after hitting the test specimen. However, the curve from test PP-D3 had a decreasing displacement when the force is decreasing, which is hard to explain. It is strange that the maximum displacement in test PP-D1 and PP-D3 are approximately equal, considering the pictures of tests PP-D1 and PP-D3 in Figure 6-19, where a big difference in the plastic deformation is seen. In addition, the velocity curve seen in Figure 6-20 indicates that the velocity at the end of the test after 20 milliseconds is higher than the initial velocity, which is impossible since energy has been dissipated. It seems like the displacement measurements provided by the machine are wrong.

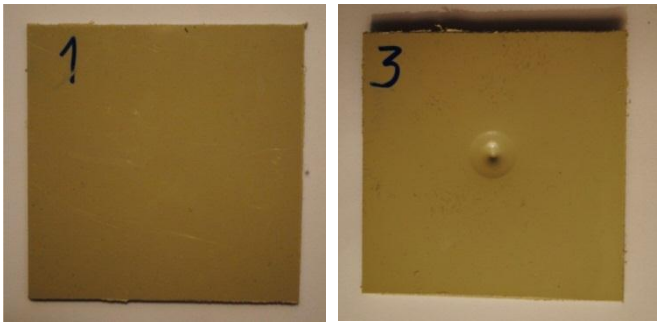

Figure 6-19. Pictures of test specimens PP-D1 and PP-D3 after the impact testing.

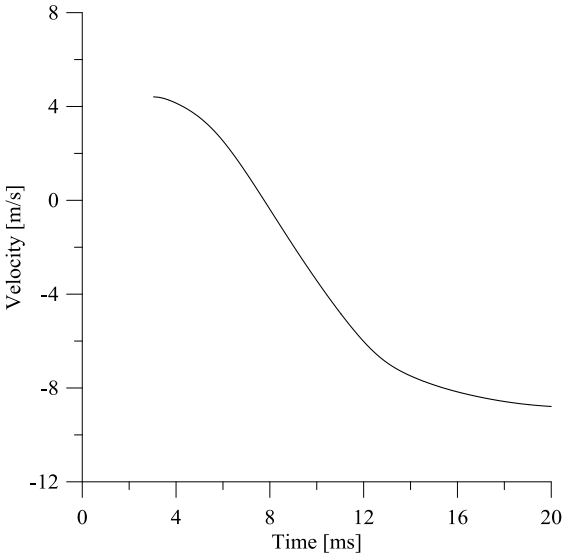

Figure 6-20. Velocity in test PP-D3.

The velocities in tests PP-D5 and PP-D6 had the same defects as in test PP-D3, where the velocity at the end of the test was larger than the initial velocity. Additionally, the curves PP-D5 and PP-D6 experienced high frequency noise after reaching the maximum force, which is due to the fact that the striker got stuck inside the plate when it was bouncing back. Test PP-D5 and PP-D6 did not experience fracture, but they had a visible plastic deformation. Figure 6-23 shows test sample PP-T5 after testing.

It is likely that some of the differences between the loading and unloading phase in curves PP-D1, PP-D2 and PP-D4, in Figure 6-21 and Figure 6-22 are caused by a viscoplastic effect. The strain rate in unloading is most likely smaller than the strain rate in loading. Additionally, a viscoelastic effect might be present in the material as well, due to the high strain rates in the plate impact tests.

In the last phase of the unloading, the slope of the curves decreases. This could probably be caused by kinematic hardening in the material. During the impact by the free-falling mass, the plate first experiences mostly bending, before the plate is stretched and experience tension stresses. The tension stresses leads to higher stiffness in the plate, called geometrical stiffness. This is a membrane effect, and it is assumed that there is no sliding of the fixed boundary of the plate. In the unloading phase, compression in the plate occurs. Kinematic hardening gives a smaller value of the yield stress in compression than in tension, as well as a lower elastic stiffness.

Curve PP-D4 shows fracture at the peak force. The plate fractured because of shear forces, leading to a failure where a plug separated from the plate.

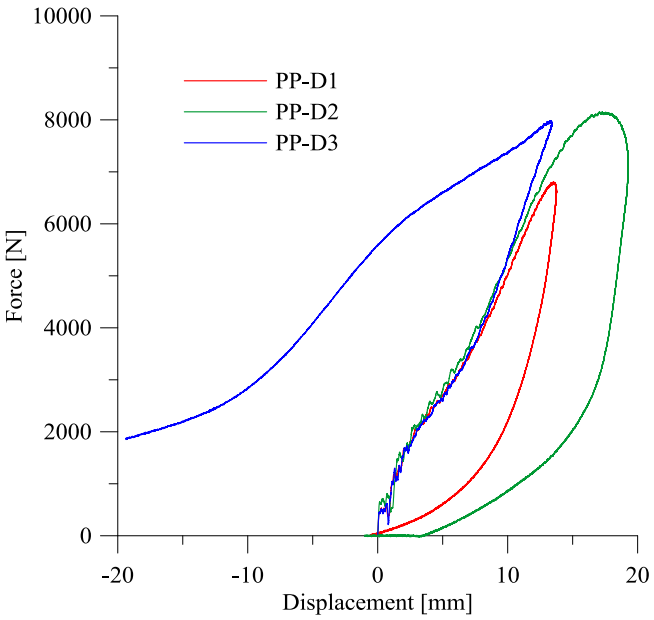

Figure 6-21. Force-displacement curves for tests PP-D1, PP-D2 and PP-D3.

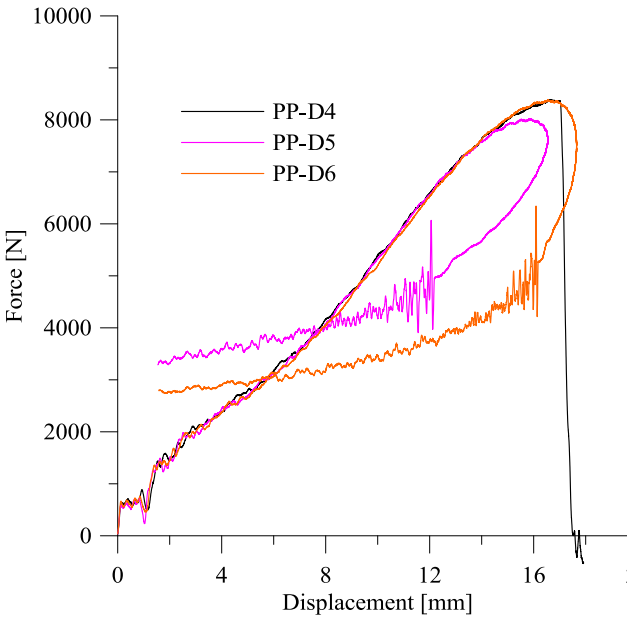

Figure 6-22. Force-displacement curves for tests PP-D3, PP-D4 and PP-D5.

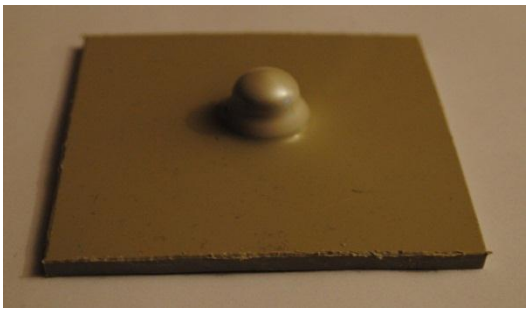

Figure 6-23. Test specimen PP-D5 after testing.

6.2.3 Discussion

There are several sources of error in these tests. The boundary conditions might be unclear, because the plate probably slides a bit between the two rings where it was fixed. In addition, the friction between the striker and the plate is a source of uncertainty.

Another source of error is that the plate impact tests were the first tests ever to be carried out in that Drop Tower machine, and the laboratory staff was not familiar with the machine and its

settings. The same strange displacement measurements seen in tests PP-D3, PP-D5 and PP-D6 were also observed in the results from tests carried out on other polymers, and may indicate wrong use of the machine, or an error in the measuring device in the machine.

6.2.4 Numerical simulations of the plate impact tests

It was decided to do a numerical simulation of two of the tests carried out in the Drop Tower machine. It was desirable to do a simulation of one of the tests where the weight had the mass 5.045 kg and one with the mass 10.045 kg. In addition, it was interesting to see if the model was able to capture the behaviour of the material in one of the tests were the falling weight bounced back. Therefore, tests PP-D2 and PP-D4 were modeled.

Model

The plate and falling weight was modeled with axisymmetric shell elements, and symmetry around the y axis was applied. The elements had a thickness of $1/2\pi$ mm. Figure 6-24 shows the geometry of the model.

The plate was divided in three parts, each with a different element size, running from 0.2 x 0.2 mm on the left side of the plate in Figure 6-24, to 0.4 x 0.4 mm in the middle of the plate, and to 0.6 x 0.4 mm on the right side. The falling weight was modeled with elements of 1 x 1 mm size, and the entire model had 2440 nodes and 2281 elements. 4 integration points over the thickness were applied.

The clamped end of the plate was modeled by fixing the nodes in the right end of the plate in Figure 6-24 in x, y and z directions. A contact definition including a friction coefficient was applied. In addition, the falling weight was given an initial velocity in negative y direction. Gravity was neglected, and mass scaling was not applied as it would result in high kinetic energy.

Force measurements were taken from the y-component of the forces in a section on the lower part of the falling weight in the area that was in contact with the plate. The deformation was measured from the bottom of the falling weight, and the initial distance between the plate and falling weight was later subtracted, so that the recording began when the striker hit the plate. The data from the simulation was therefore comparable to the experimental data.

The falling weight was modeled as an isotropic elastic plastic material with the material parameters of steel. The mass of the weight was given the correct value by adjusting the density parameter of the material.

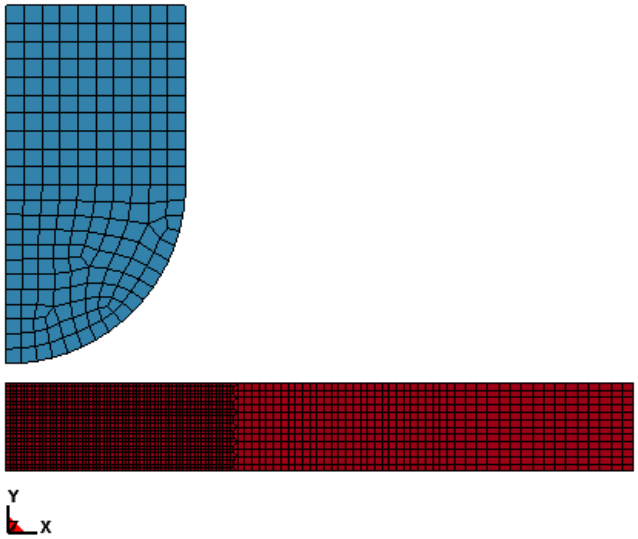

Figure 6-24. The geometry of the plate and free-falling impactor.

6.2.5 Numerical simulation of tests PP-D2 and PP-D4

Tests PP-D2 and PP-D4, both with impact velocity of 6263 mm/s, were simulated using the model described above. They had an impact mass of 5.045 kg and 10.045 kg respectively. Mass and velocity of the free-falling striker were taken from Table 6-2. The friction coefficient in the test was difficult to predict, and a static friction coefficient of 0.2 was assumed [17]. The applied dynamic friction coefficient was 10% smaller than the static friction coefficient [11].

It was not expected that the numerical simulation would capture the unloading phase, but it was desirable with a good representation of the curve until after passing the peak force. Test PP-D4 experienced failure, which was not included in the material model.

The force-displacement curves from the numerical simulations and the experimental tests are seen in Figure 6-25 and Figure 6-26. The numerical simulation underestimates the force in both cases, but the shape of the curves is quite good captured.

The simulation of PP-D2 is, however, not able to capture the unloading phase. The material model follows approximately the same Young's modulus in unloading as in loading. Part B in the material model will modify the stiffness in unloading, but this modification is minimal in tests of strain rates in the range of the plate impact tests described here.

Additionally, viscoelasticity is not included in the model, but as mentioned in Section 6.2.2 it is likely that some viscoelastic effects are present in the material.

Also, the displacement at the start of unloading was not captured by the model. It was desirable to do a recalibration of some of the parameters in the material model. The simulations seen in Figure 6-25 and Figure 6-26 were used as baseline tests in a parameter study of several parameters.

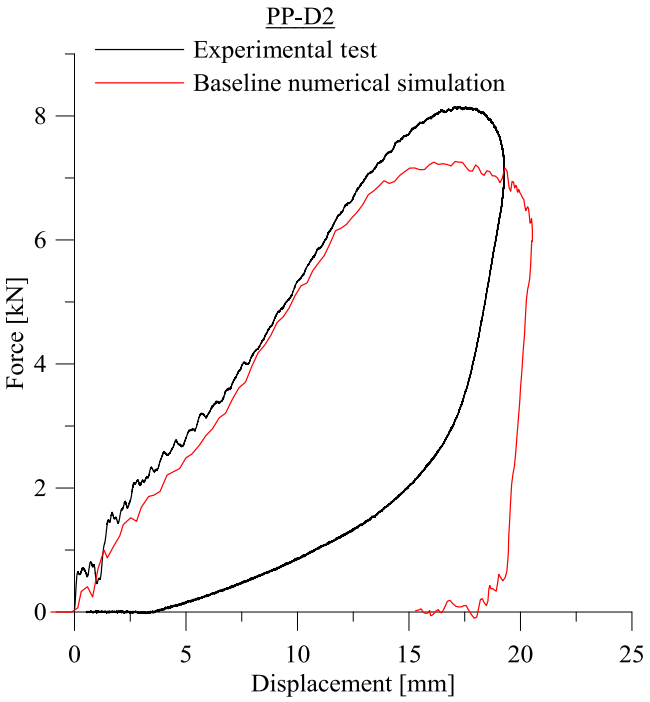

Figure 6-25. Experimental test PP-D2 and baseline numerical simulation.

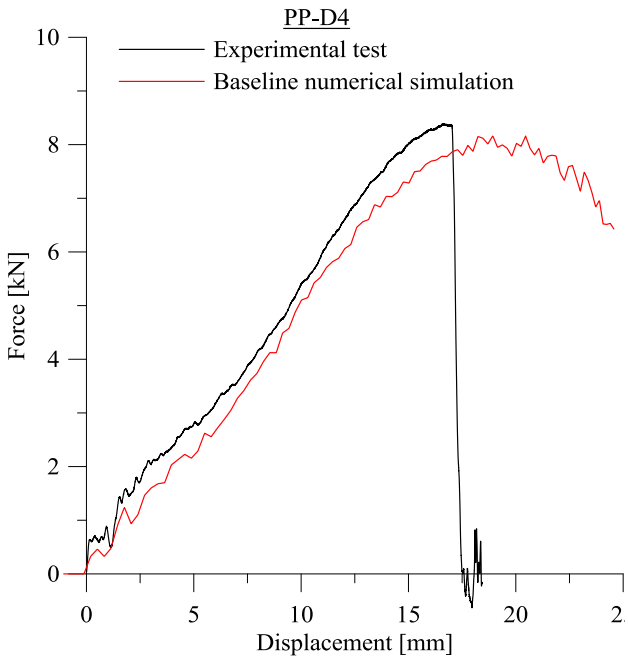

Figure 6-26. Experimental test PP-D4 and baseline numerical simulation.

6.2.6 Parameter study

To improve the numerical simulations of PP-D2 and PP-D4, a parameter study was carried out on the baseline tests seen in Figure 6-25 and Figure 6-26. The parameters that were investigated were the friction coefficient, Young's modulus and the parameter C.

Young's modulus

Viscoelasticity was not included in the material model, and Young's modulus was assumed constant for all strain rates. However, Young's modulus will, for many materials, increase with the strain rate. Since Young's modulus was calibrated from tests at strain rates in the range 10^{-3} to 10^{-1} s^{-1}, it is possible that the elastic stiffness in the plate impact tests was higher, considering that

the strain rates were located in the range 100 to 500 s^{-1}. This is significantly larger than the strain rates in the calibration tests. Hence, it was of interest to carry out simulations with larger values for Young's modulus to support this theory. Figure 6-27 and Figure 6-28 show the global response from the baseline tests and the simulations with varying values of Young's modulus.

The simulations with higher values of Young's modulus give better representations of the experimental test in the first phase of the loading. The figures support the assumption that Young's modulus increase with the strain rate. A value of 2200 MPa seems like the best choice for the simulation of both tests.

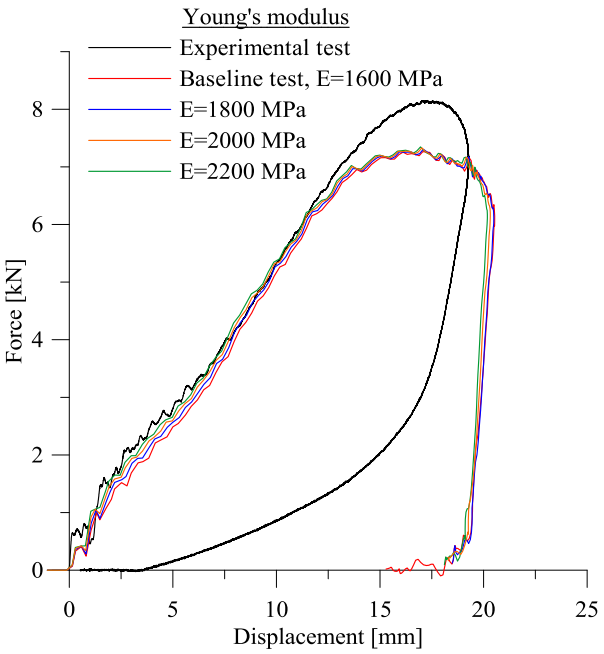

Figure 6-27. Different Young's moduli in the numerical simulations of test PP-D2.

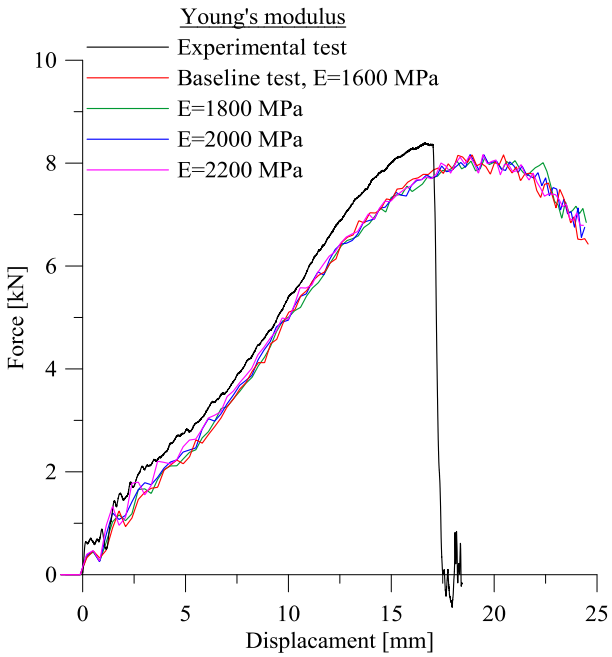

Figure 6-28. Different Young's moduli in numerical simulations of test PP-D4.

Friction coefficient μ

Several values of the friction coefficient μ were tried in order to get a better representation of the peak force. Four different values of the friction coefficient were tested for PP-D2 and PP-D4. The global response of the simulations is seen in Figure 6-29 and Figure 6-30.

PP-D2 was tested with static friction coefficients of 0.2, 0.25, 0.3 and 0.4. The dynamic friction coefficient was 10% smaller than the static friction coefficient in all cases. The friction coefficient referred to in this section is the static friction coefficient. Simulations with friction coefficients of 0.3 and 0.4 resulted in an increased peak force, but at the same time displacement at the onset of

the unloading phase was not captured. A friction coefficient of 0.25 seems like the best choice for test PP-D2.

Simulations of PP-D4 with friction coefficients of 0.2, 0.3, 0.4 and 0.5 were carried out. A value of 0.5 gives the best representation of the peak force. However, when considering the shape of the curve, a friction coefficient of 0.4 is likely to be a better choice. The curve with friction coefficient 0.5 seems to have peak force occurring at a too large displacement.

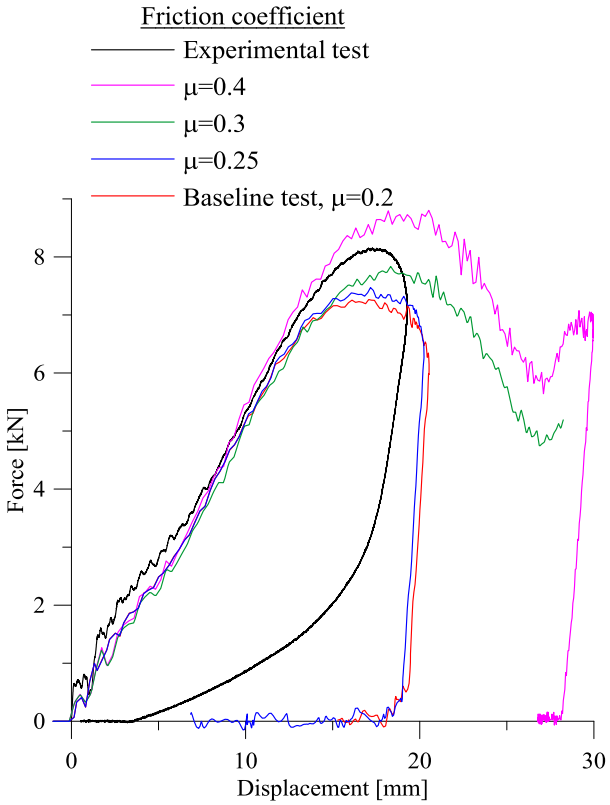

Figure 6-29. Different friction coefficients tested on the baseline test for PP-D2.

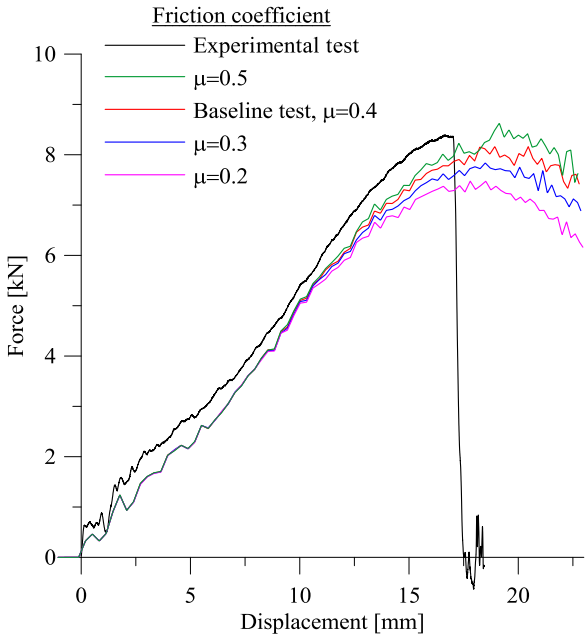

Figure 6-30. Different friction coefficients tested on the baseline test for PP-D4.

It is observed that the friction coefficient giving the best representation of the peak force is higher in test PP-D4 than in test PP-D2. It is probably because the mass of the striker was larger in test PP-D4, resulting in larger plastic deformations. It is likely that larger plastic deformations lead to higher friction because as the voids in the material grows the surface become rougher [11].

Parameter C

The parameter C, describing the strain rate sensitivity of the material, was in Section 4.2 calibrated from tension tests at strain rates in the range 10^{-3} to 10^{-1} s^{-1} to be 0.4482. The linear line in Figure 4-4 was assumed to be extrapolated log-linearly. However, this is a rough assumption when it comes to relatively high strain rates, and it is likely that the line is not log-linear in the area of strain rates 100 to 500 s^{-1}. To support this theory, numerical simulations with higher values of the parameter C were tried.

For test PP-D2, the values 0.055, 0.06 and 0.067 were tested, in addition to the baseline test of 0.0483. Figure 6-31 shows the results. It is clear that the peak force increases with C, and the deformation on the onset of unloading decreases. When considering the peak force and the deformation at the onset of unloading, C=0.06 seems like the optimal value for PP-D2.

The values 0.05, 0.06 and 0.075 were tried in the numerical simulations of PP-D4, and the results are seen in Figure 6-32, where the peak force increases with C. It seems from the figure that C=0.06 is a good assumption for PP-D4 as well.

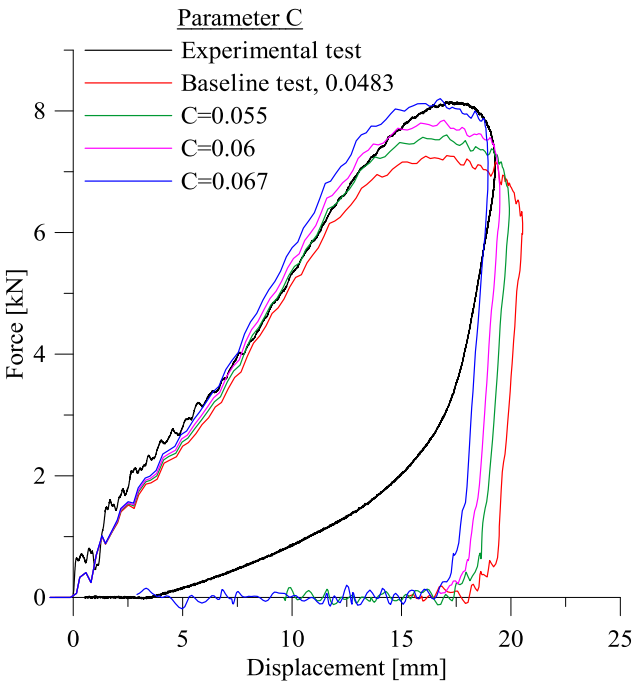

Figure 6-31. Different values of the parameter C for test PP-D2.

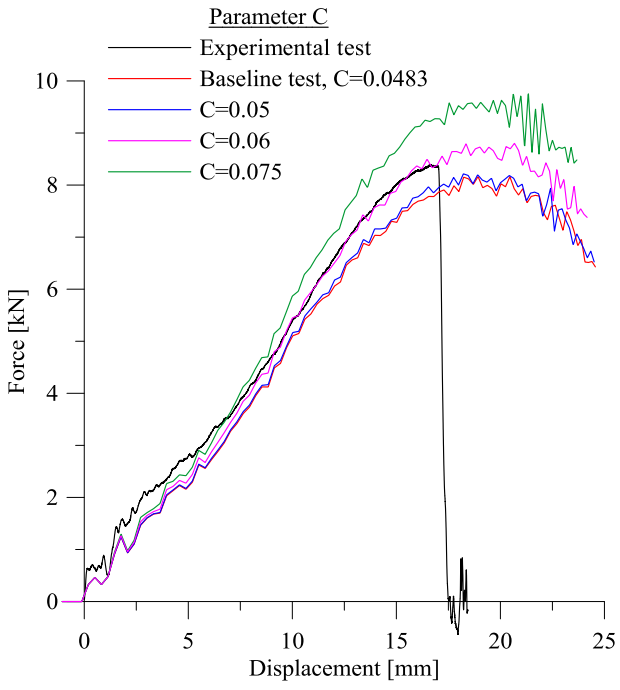

Figure 6-32. Different values of the parameter C for test PP-D4.

6.2.7 Test PP-D2 and PP-D4 simulated with a recalibrated material model

A simulation combining the improved values of the parameters E, C and μ was carried out for test PP-D2 and PP-D4. The recalibrated material model from test PP-D2 had a Young's modulus of 2200 MPa, a friction coefficient of 0.25 and the value of the parameter C was 0.06. The only difference to the material model for test PP-D4 was the friction coefficient, as test PP-D4 had a friction coefficient of 0.4.

In Figure 6-33 the global response from the baseline simulation is compared to the improved simulation of test PP-D2. The improved curve gives a good representation in the first phase of loading, up to a displacement of 5 mm, before the simulation is overestimating the curve. The peak force is however fairly good captured, but the simulation is not able to capture the displacement at the onset of the unloading phase.

Figure 6-34 shows the results from the simulations of test PP-D4. The improved numerical simulation is able to predict the behaviour of the experimental curve quite good. However, it is likely that the peak force of the simulation occur at a larger displacement than in the experimental test.

Consequently, the improved numerical simulations give a better overall representation of the experimental test than the baseline numerical simulations did, which indicate that modifying some parameters in the material model gives better results for tests at higher strain rates. Yet, putting all the best parameters together doesn't necessarily give a perfect result, since changing one parameter will influence the other parameters. This is seen in the displacement at the onset of the unloading phase in PP-D2. This displacement was correct or overestimated in Figure 6-27, Figure 6-29 and Figure 6-31, but in numerical simulation with the improved material model in Figure 6-33 it is underestimated.

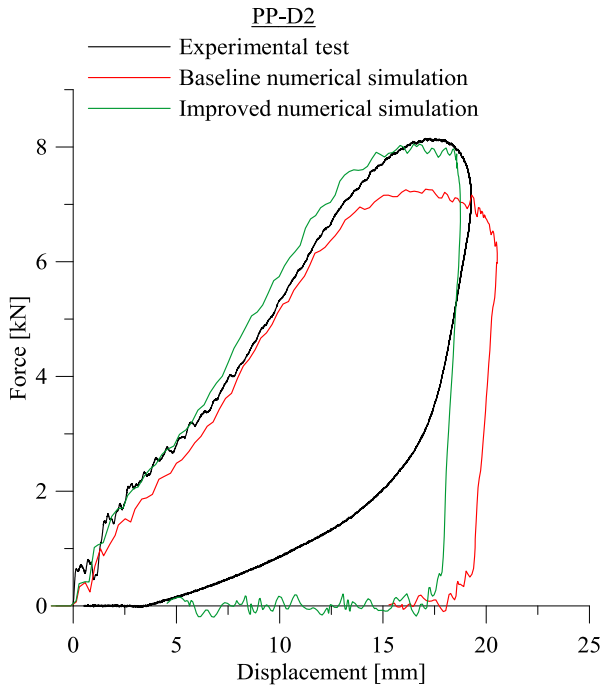

Figure 6-33. Numerical simulations and experimental test curve for PP-D2. The improved curve has E=2200 MPa, C=0.06 and μ=0.25.

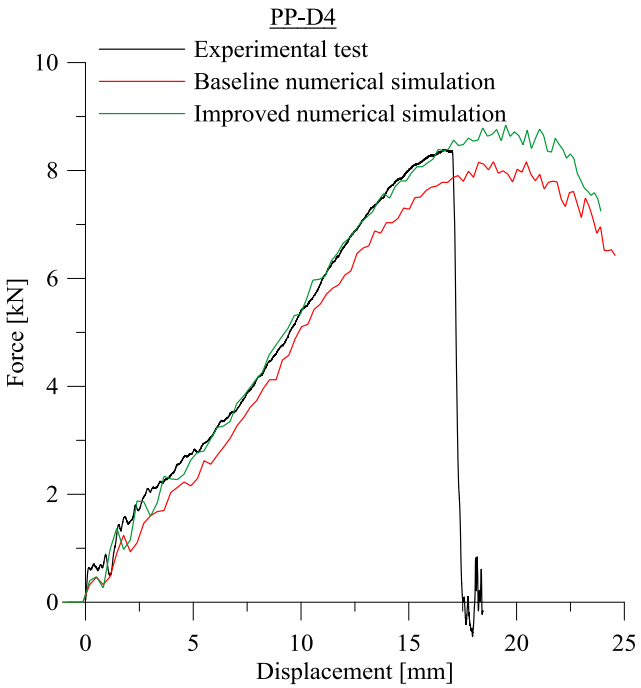

Figure 6-34. Numerical simulations and experimental test curve for PP-D4. The improved curve has E=2200 MPa, C=0.06 and μ=0.4.

6.2.8 Numerical simulations of tests PP-D1, PP-D5 and PP-D6

Tests PP-D1, PP-D5 and PP-D6 were numerically simulated using the recalibrated material models. It was chosen not to do a numerical simulation of test PP-D3, because of the abnormal curve. However, numerical simulations of tests PP-D5 and PP-D6 were carried out, and the force-time curve was used as a basis for comparison instead of the force-displacement curve, since there seemed to be errors in the displacement data from these tests.

A Young's modulus of 2200 MPa was applied, together with a value 0.06 of the parameter C. Both friction coefficients of 0.25 and 0.4 were tried for all the tests.

The result of the simulation of test PP-D1 is seen in Figure 6-35. The variation in the friction coefficient gives small impact on the peak force, which is fairly good captured in both simulations. The shape of the loading curves is similar, and the unloading phase is, as expected, not captured by the material model.

Results from simulations of tests PP-D5 and PP-D6 are seen in Figure 6-36 and Figure 6-37 respectively. The simulation with friction coefficient 0.25 gives a fairly good representation of the

shape of the curves until after the peak force is reached in both tests, and the peak force is pretty well captured. This may indicate that a friction coefficient of 0.4 in test PP-D4 was a bit too high.

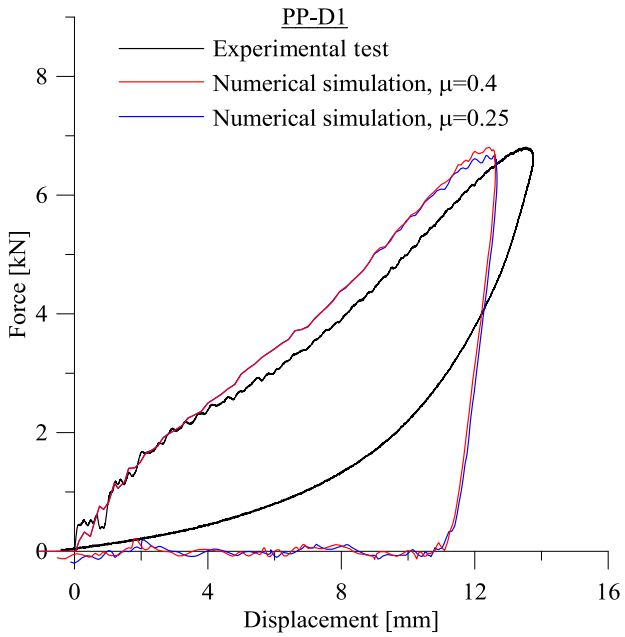

Figure 6-35. Numerical simulations and experimental test, PP-D1.

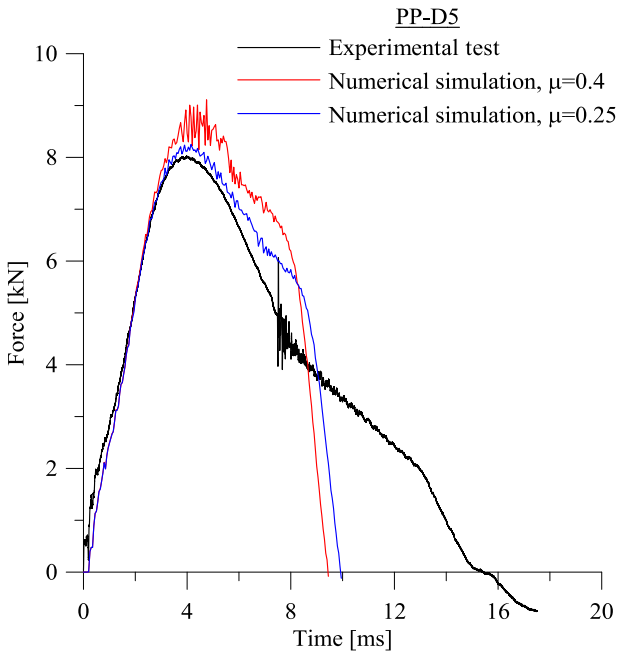

Figure 6-36. Numerical simulations and experimental test, PP-D5.

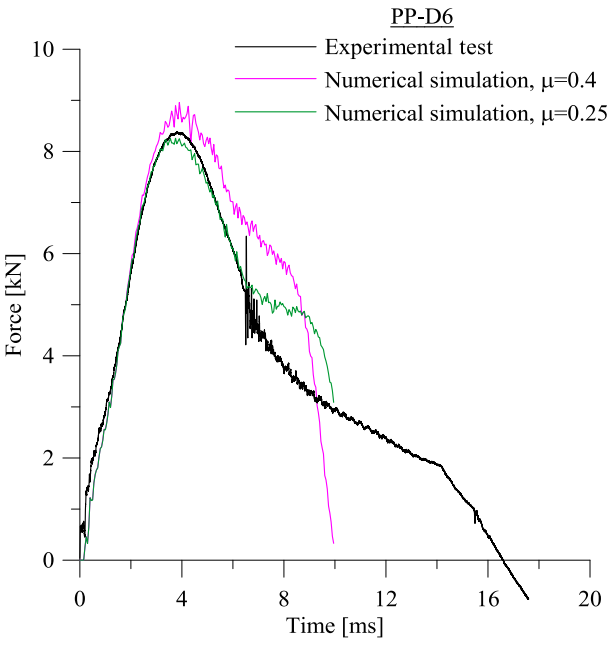

Figure 6-37. Numerical simulations and experimental test, PP-D6.

7 Conclusions

In this thesis a hyperelastic-viscoplastic material model for polypropylene has been calibrated and validated through material and component tests.

Several rounds of material tests were carried out in the laboratory. Tension and compression tests at different strain rates, as well as tension tests on a plate with a hole and plate impact tests were done.

A material model was calibrated based on the experimental data from the tension and compression tests. It was observed that the material experienced hardening in the tension tests, as well as strain rate dependency. The tension and compression tests were numerically simulated in order to validate the parameters in the material model.

The tests on the plates with a hole and plate impact tests were used as validation tests because they covered different situations. Stretching of a plate with a hole is a tension dominated, quasi static test with a simple, clearly defined geometry. Plate impact tests were dynamic tests with a fixed boundary, controlling the properties of the material model at high strain rates.

The calibrated material model was able to capture the main characteristics of the material polypropylene. However, the model had limitations, as it was not able to correctly predict the behaviour of the material at high strain rates. The material model was partly recalibrated in the numerical simulations of the plate impact tests due to the high strain rate in these tests, compared to the strain rate in the tests that the calibration was based on. Viscoelastic behaviour in the material was observed, and the model did not capture the elastic stiffness at high strain rates. The parameter C, describing the strain rate sensitivity of the material, was recalibrated for high strain rates as well.

Additionally, the experimental tension tests gave true stress-strain curves with a flat level before hardening occurred. The calibrated material model was not able to capture this level, resulting in numerical simulations not able to correctly predict the constant force level of the experimental tests.

Recommendations for further work

The hyperelastic-viscoplastic material model did not include viscoelasticity, and it was necessary to change the value of Young's modulus in the material model at high strain rates. Hence, it would be of interest to have a material model including viscoelasticity.

In addition, the strain rate sensitivity parameter C was recalibrated for the tests at high strain rates, and a model predicting correct values of C should be looked into. Another improvement could be to involve volume expansion in tension and contraction in compression in the material model.

The flat level in the stress-strain curves from the experimental tension tests in the area after yield stress was difficult to adapt in the material model, and this should be looked into as well.

8 References

1 RT Moura, AH Clausen, E Fagerholt, M Alves, M Langseth: "*Impact on HDPE and PVC plates-Experimental tests and numerical simulations*", International Journal of Impact Engineering 2010;37:580-598.

2 M Hovden. "*Tests and numerical simulations of polymer components*", Master thesis, NTNU, 2010.

3 H Daiyan. "*Experimental and Numerical Investigation of the Mechanical Resopnse of Injection Moulded Polypropylede Materials"*, Doctoral Dissertation, University of Oslo, 2011.

4 M Polanco-Loria, AH Clausen, T Berstad, OS Hopperstad. "*Constitutive model for thermoplastics with structural applications*", International Journal of Impact Engineering, 2010;37:1207-1219.

5. J Rösler, H Harders, M Bäker. "*Mechanical Behaviour of Engineering Materials*, Springer", 2007.

6 AH Clausen, M Polanco-Loria, MT Hovden, M Haugen, OS Hopperstad: "*Experimental and numerical study of HDPE and PVC at different loading conditions*", In preparation for possible journal publication (2012).

7 A Ram. "*Fundamentals of POLYMER ENGINEERING"*, Plenum Press, 1997.

8 OS Hopperstad, T Børvik. *Lecture Notes, TKT4135 Mechanics of materials*, NTNU, 2012.

9 OU Colak. "*Modeling deformation behavior of polymers with viscoplasticity theory based on overstress*", International Journal of Plasticity 2005;21:145-160.

10 PA Du Bois, S Kolling, M Koesters, T Frank. "*Material behaviour of polymers under impact loading*". International Journal of Impact Engineering, 2006;32:725-740.

11 Meetings with supervisors.

12 R Raghava, RM Caddell, GSY Yeh. "*The macroscopic yield behavior of polymers*", Journal of Materials Science 1973;8:225-232.

13. SIMONA, Product Information 08/95, http://www.simona.de/static/sites/default/de/assets/Informationsmaterial/englisch/PI_e/PP-DWU-DWST-C_e.pdf, 30.05.12

14 AS Ognedal, T Seelig, M Helbig, P Hempel, T Berstad, OS Hopperstad, AH Clausen: *"Experimental and micromechanical study of void growth in a mineral filled PVC*",15th International Conference on Deformation, Yield and Fracture of Polymers, 2012.

15 V Delhaye, AH Clausen, F Moussy, R Othman, OS Hopperstad. *"Influence of stress state and strain rate on the behaviour of a rubber-particle reinforced polypropylene",* International Journal of Impact Engineering, 2011; 38:208-218.

16 "*LS-DYNA Keyword User's Manual Volume I"*, Livermore Software Technology Corporation (LSTC), version 971, 2007.

17 H Dayian, E Andreassen, F Grytten, H Onsnes, RH Gaarder. "*Shear Testing of Polypropylene Materials Analysed by Digital Image Correlation and Numerical Simulations"*, Experimental Mechanics, DOI 10.1007/s11340-012-9591-7, 2012.

Appendix A

Tension tests

Tension tests

11 tension tests were carried out in a servo-hydraulic Dartec M1000/RK testing machine with a capacity of 20 kN. The geometry of the test specimens are seen in Figure 1. Table 1 shows all the tests that were carried out, and that are presented in this appendix. The appendix presents force-displacement curves and stress-strain curves for all tests, in addition to a plot of the contraction ratio and information about the test, like maximum force and yield stress. The force and displacement were obtained from the Dartec machine. The strains were obtained by use of the DIC technique.

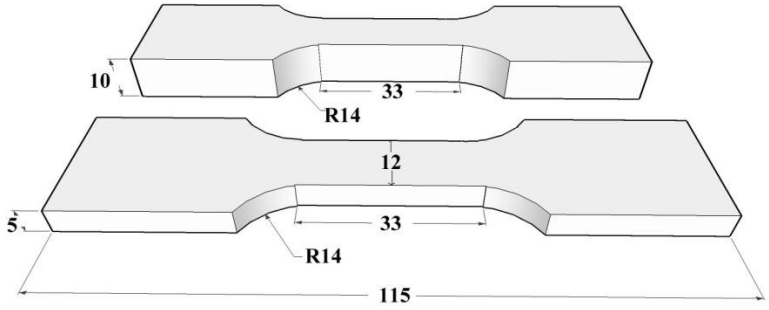

Figure 1. Dimensions of tension test samples, where all numbers are in millimeters.

Table 1. Overview of tension tests carried out.

Test	Strain rate [s^{-1}]	Velocity [mm/s]
PP-T1	10^{-3}	0.033
PP-T2	10^{-3}	0.033
PP-T3	10^{-2}	0.33
PP-T4	10^{-2}	0.33
PP-T5	10^{-1}	3.3
PP-T6	10^{-1}	3.3
PP-T7	$10^{-2.5}$	0.1044
PP-T8	$10^{-2.5}$	0.1044
PP-T9	10^{-2}	0.33
PP-T10	10^{-1}	3.3
PP-T11	10^{-3}	0.033

PP-T1

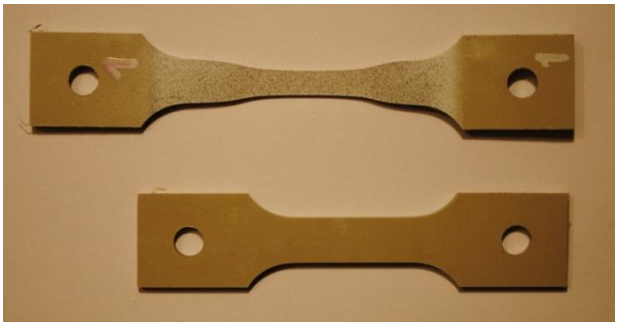

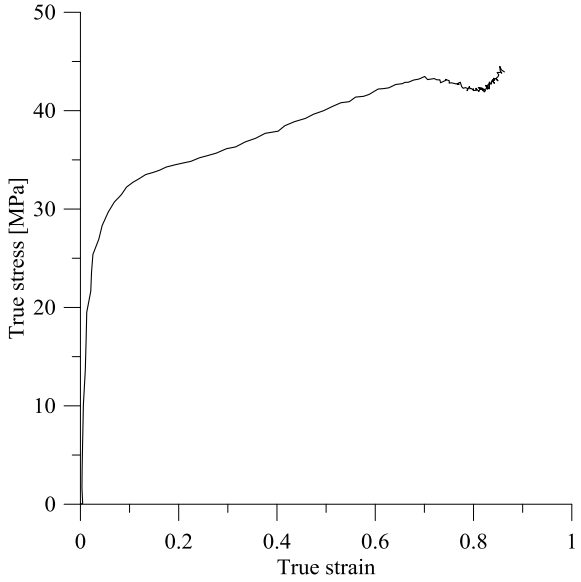

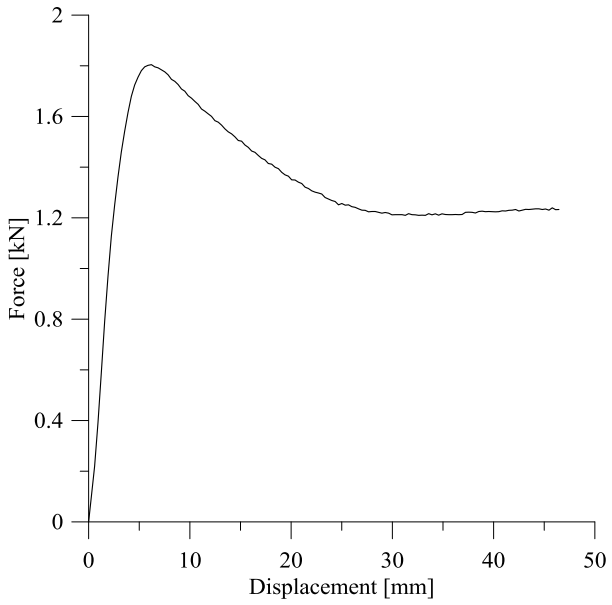

Initial thickness	4.89	mm
Thickness after testing	2.59	mm
Initial width	11.96	mm
Width after testing	6.37	mm
Velocity	0.033	mm/s
Strain rate	0.001	s^{-1}
Yield stress	32.8	MPa
Maximum force	1.80	kN
Poissons ratio ν	0.44	
Contraction ratio ρ	0.4	
Young's modulus	1750	MPa

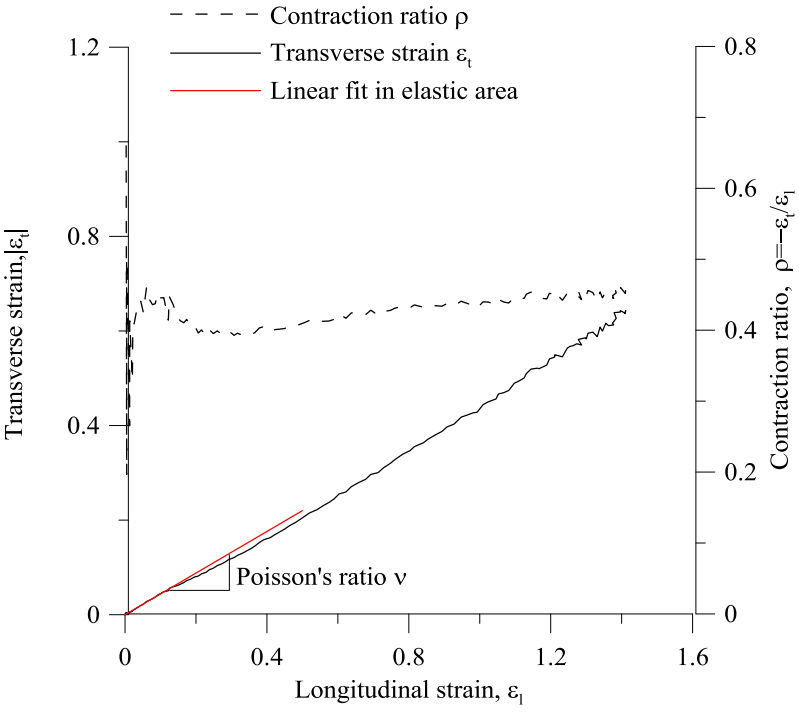

PP-T2

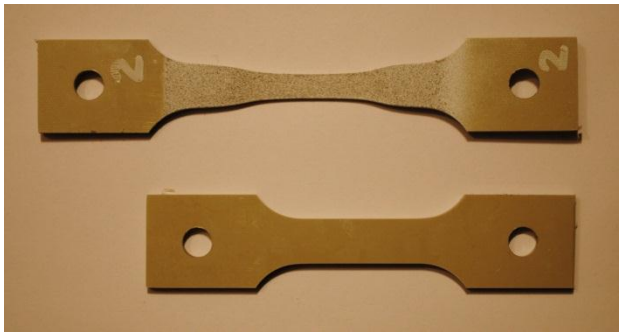

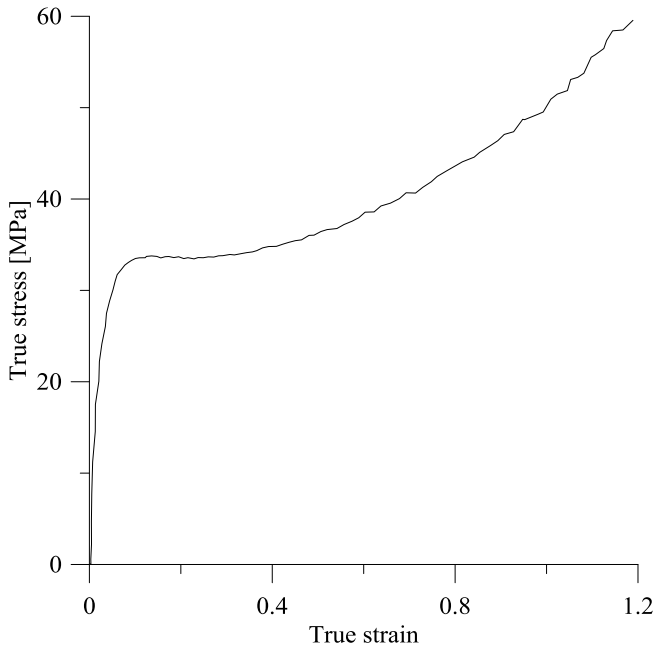

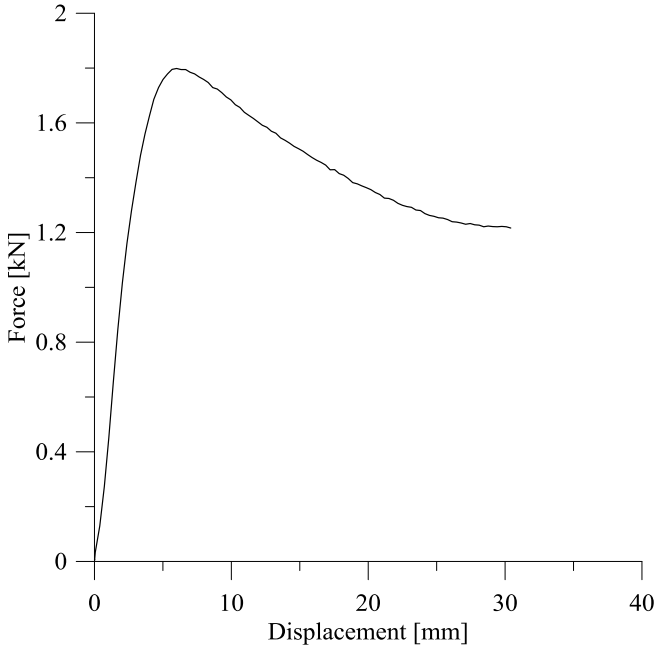

Initial thickness	4.91	mm
Thickness after testing	5.59	mm
Initial width	11.95	mm
Width after testing	6.43	mm
Velocity	0.033	mm/s
Strain rate	0.001	s^{-1}
Yield stress	33.1	MPa
Maximum force	1.80	kN
Poissons ratio ν	0.45	
Contraction ratio ρ	0.4	
Young's modulus	1524	MPa

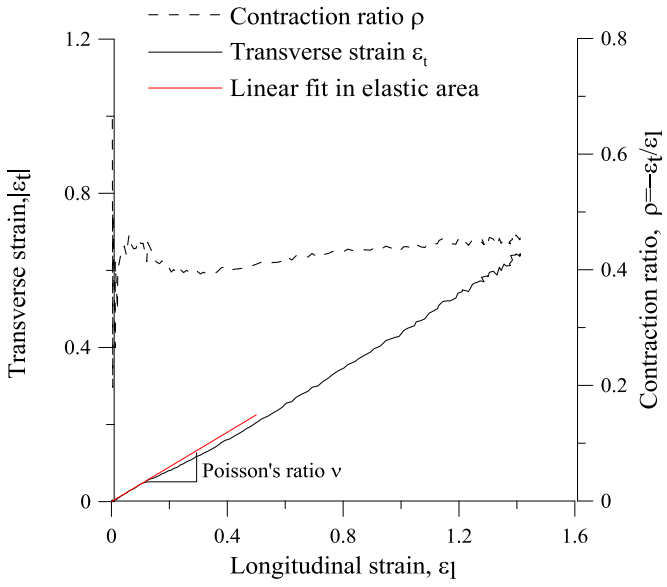

PP-T3

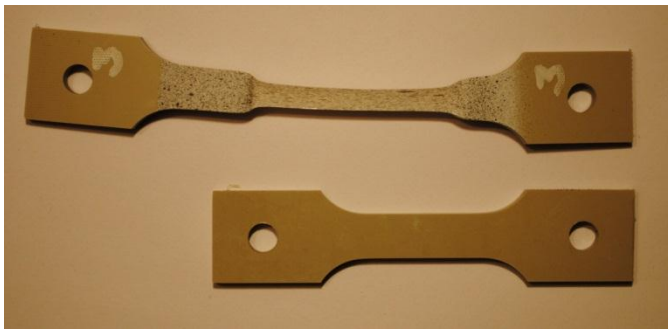

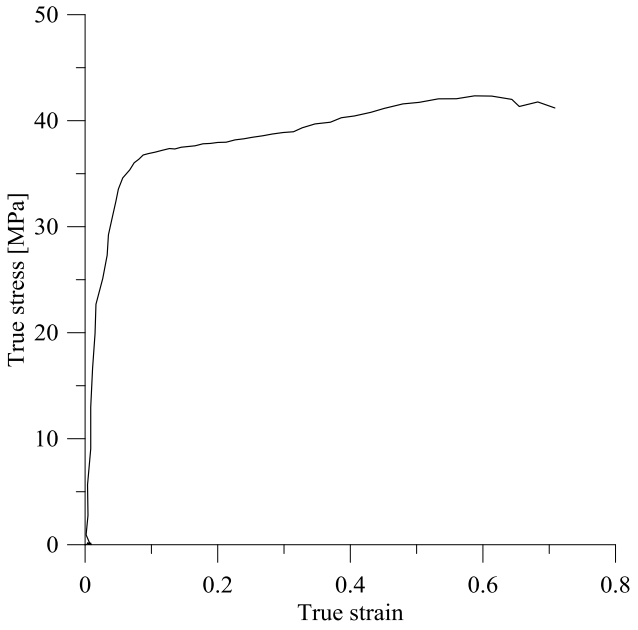

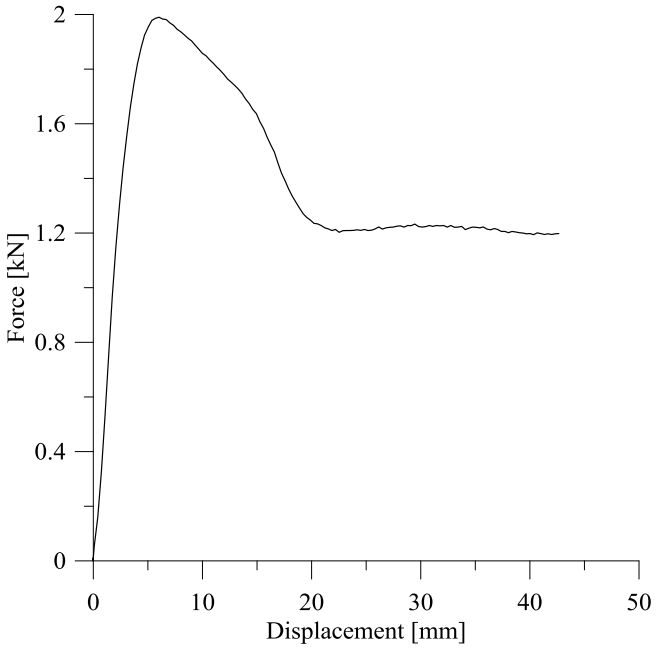

Initial thickness	4.9	mm
Thickness after testing	2.03	mm
Initial width	11.95	mm
Width after testing	5.75	mm
Velocity	0.33	mm/s
Strain rate	0.01	s^{-1}
Yield stress	36.8	MPa
Maximum force	1.99	kN
Poissons ratio ν	0.42	
Contraction ratio ρ	0.41	
Young's modulus	1441	MPa

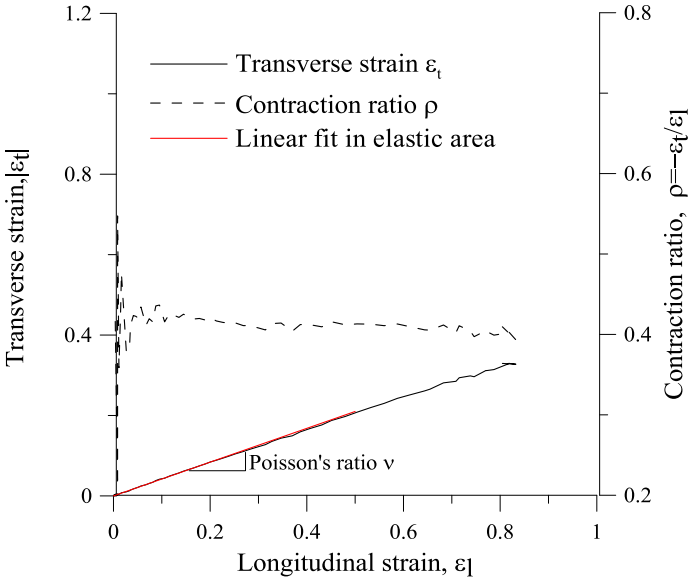

PP-T4

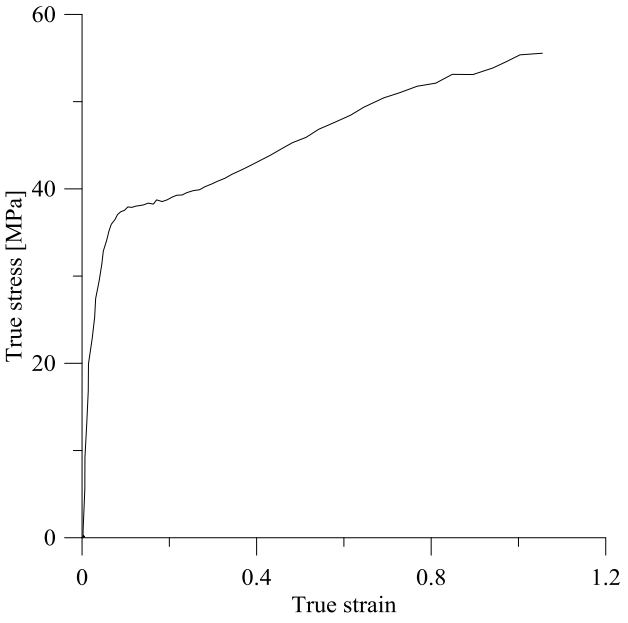

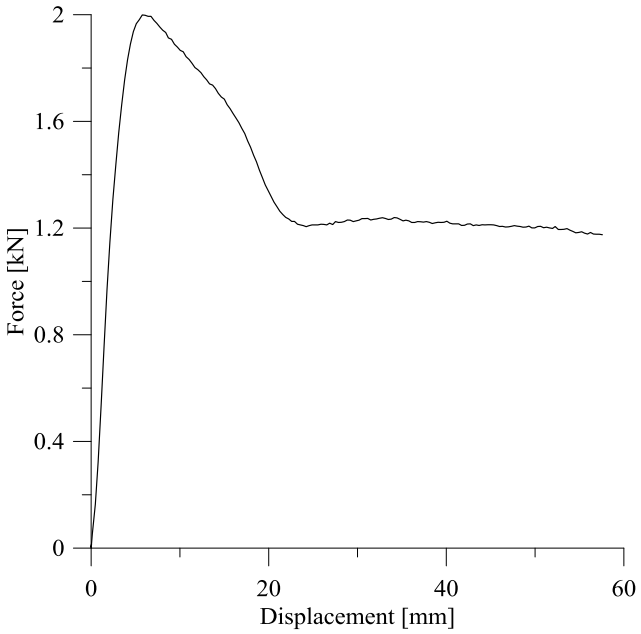

Initial thickness	4.89	mm
Thickness after testing	1.99	mm
Initial width	11.96	mm
Width after testing	5.67	mm
Velocity	0.33	mm/s
Strain rate	0.01	s^{-1}
Yield stress	37.3	MPa
Maximum force	1.99	kN
Poissons ratio ν	0.49	
Contraction ratio ρ	0.45	
Young's modulus	1465	MPa

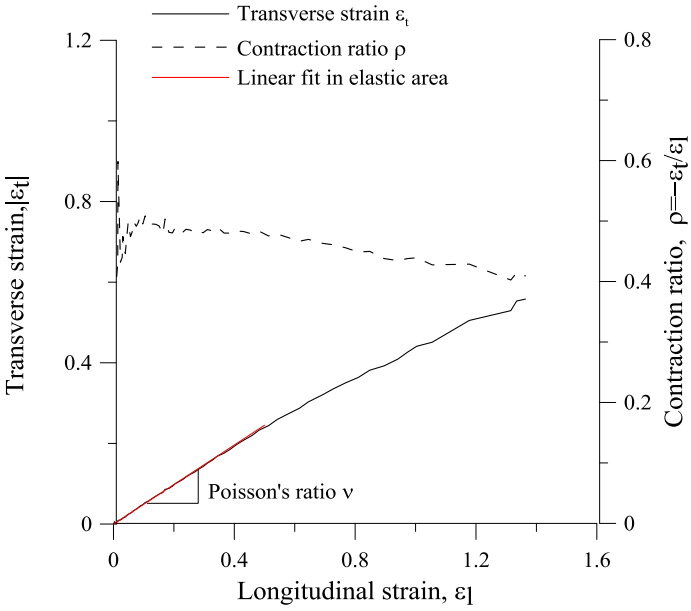

PP-T5

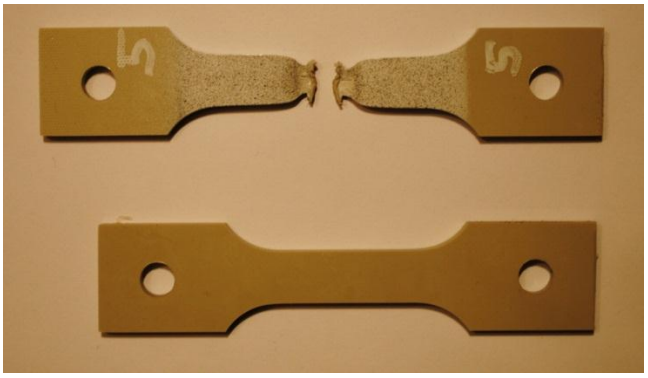

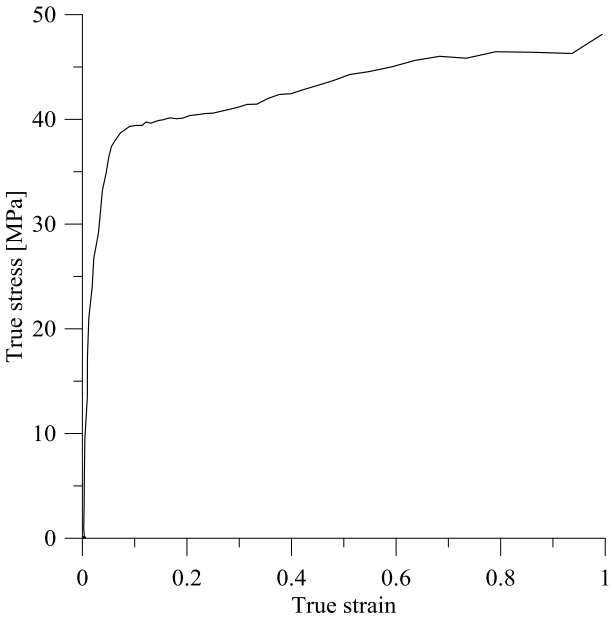

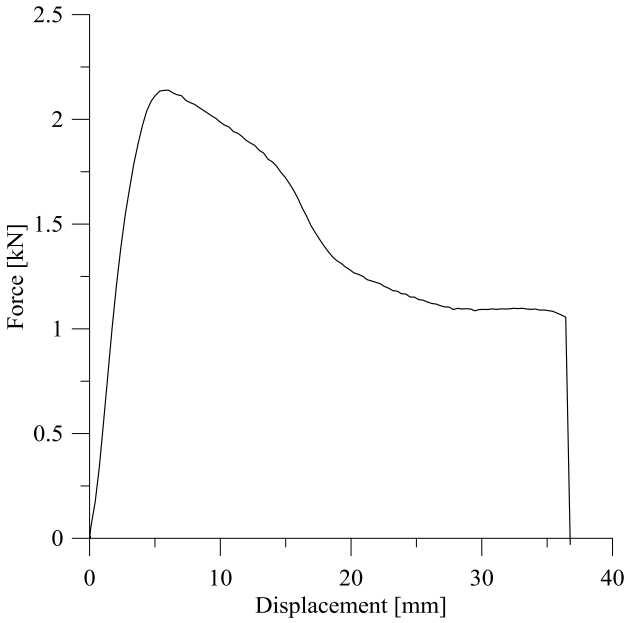

Initial thickness	4.90	mm
Initial width	11.95	mm
Velocity	3.3	mm/s
Strain rate	0.1	s^{-1}
Yield stress	38.9	MPa
Maximum force	2.14	kN
Poissons ratio ν	0.38	
Contraction ratio ρ	0.37	
Young's modulus	1789	MPa

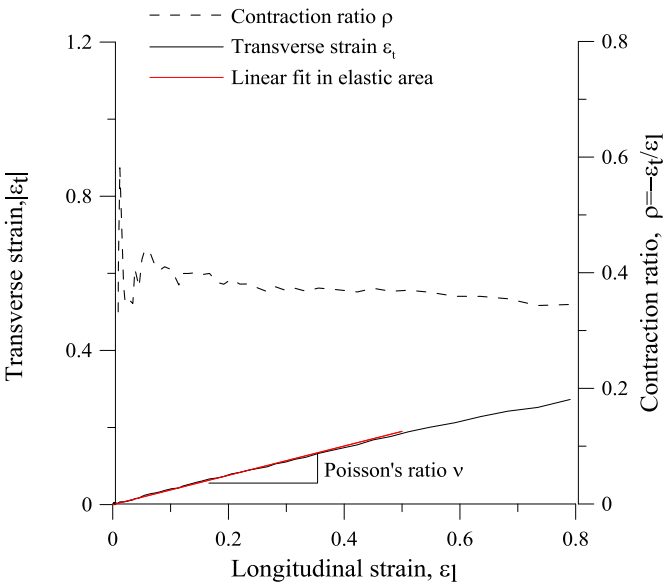

PP-T6

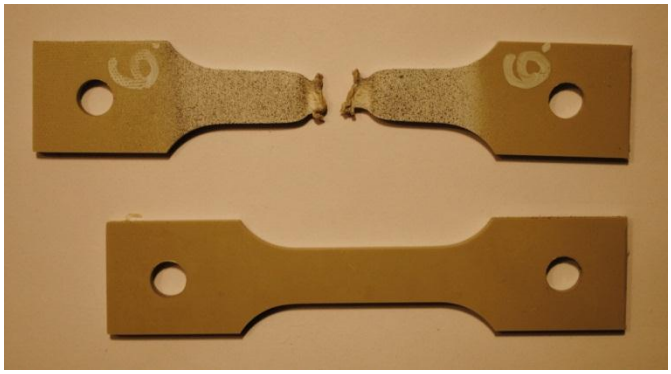

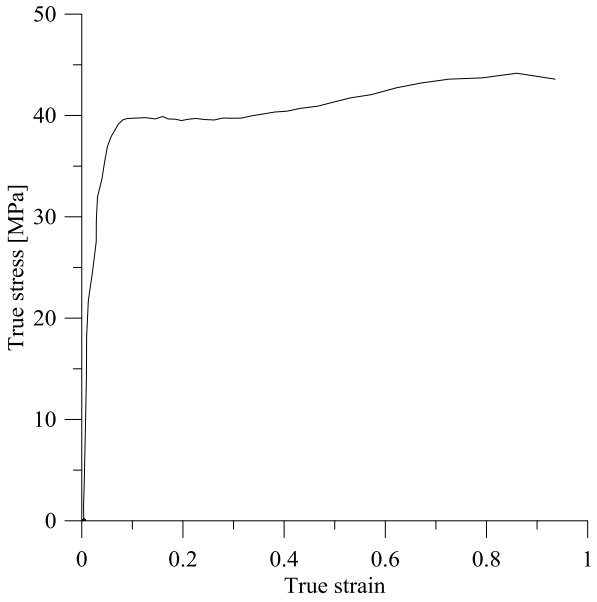

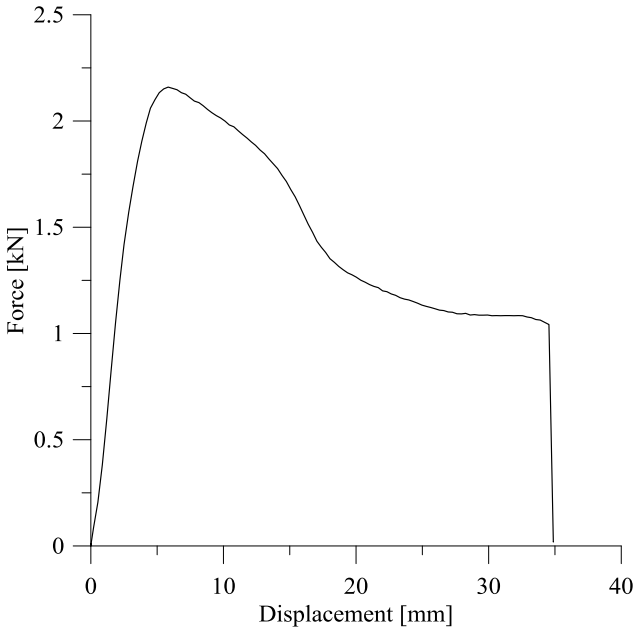

Initial thickness	4.88	mm
Initial width	11.94	mm
Velocity	3.3	mm/s
Strain rate	0.1	s^{-1}
Yield stress	39.5	MPa
Maximum force	2.16	kN
Poissons ratio v	0.36	
Contraction ratio ρ	0.30	
Young's modulus	1839	MPa

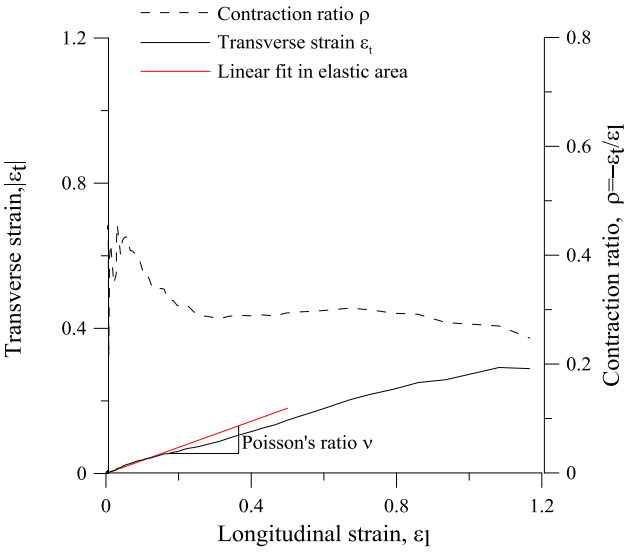

PP-T7

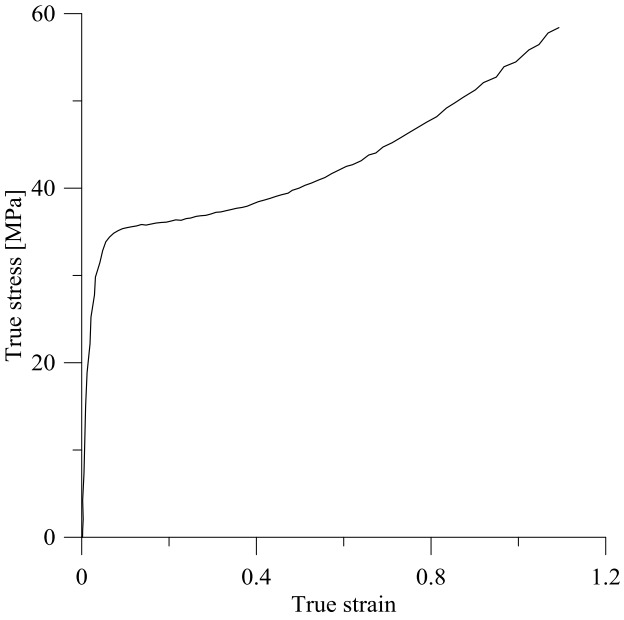

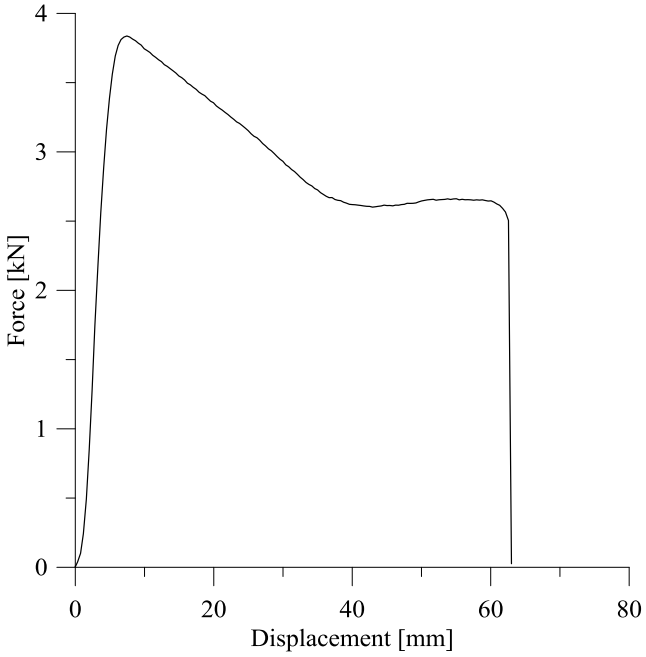

Initial thickness	9.75	mm
Initial width	11.97	mm
Velocity	0.104	mm/s
Strain rate	$10^{-2.5}$	s^{-1}
Yield stress	34.9	MPa
Maximum force	3.84	kN
Poissons ratio v	0.38	
Contraction ratio ρ	0.38	

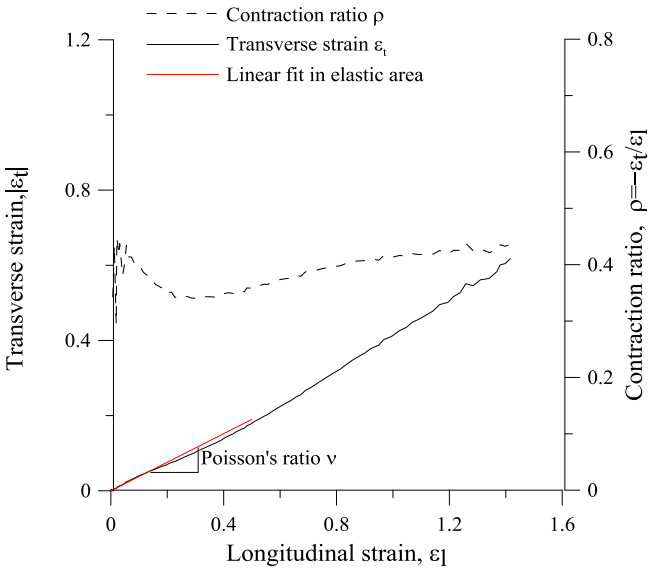

PP-T8

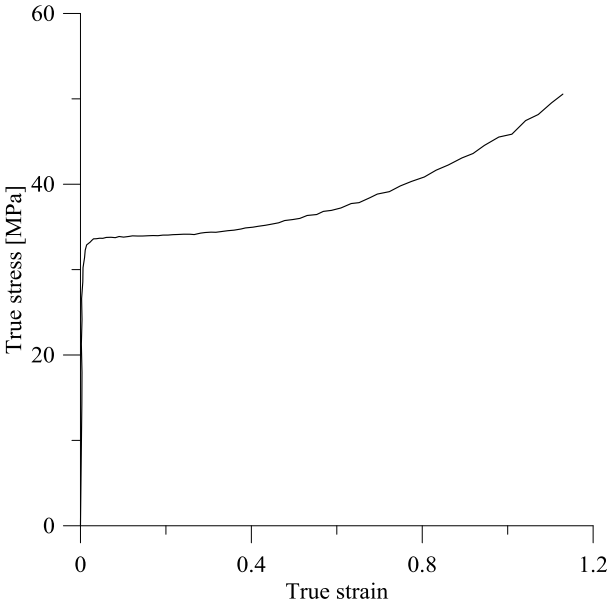

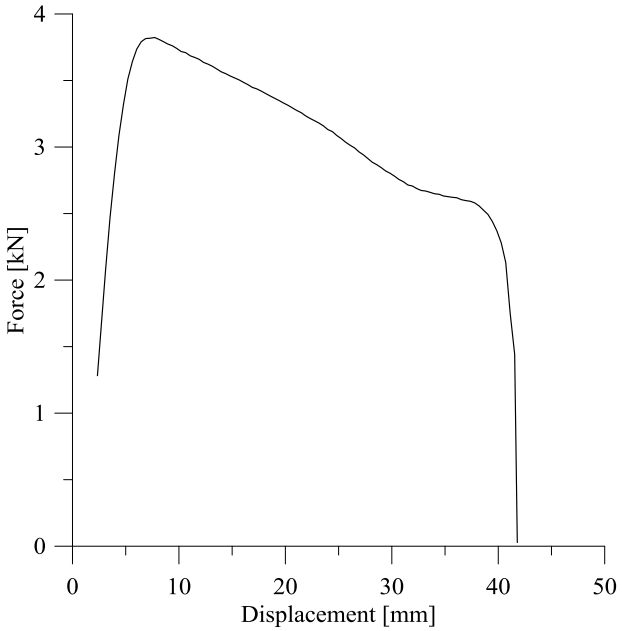

Initial thickness	9.74	mm
Initial width	11.97	mm
Velocity	0.104	mm/s
Strain rate	$10^{-2.5}$	s^{-1}
Yield stress	33.5	MPa
Maximum force	3.82	kN
Poissons ratio ν	0.34	
Contraction ratio ρ	0.30	

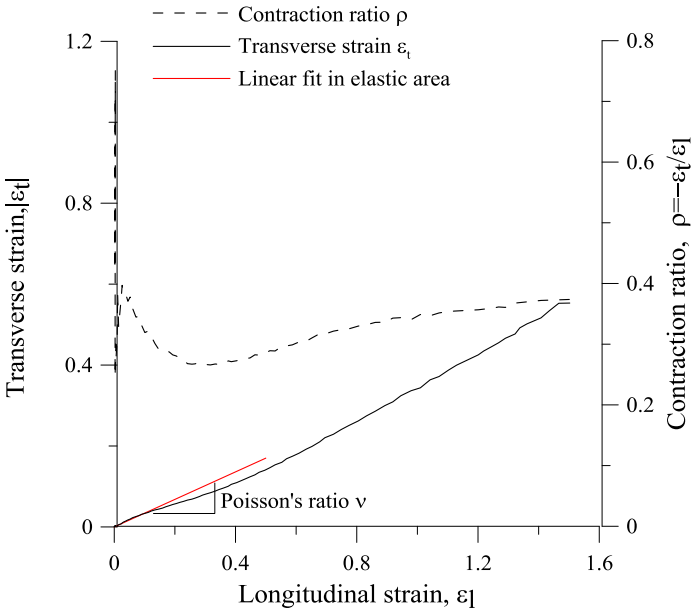

PP-T9

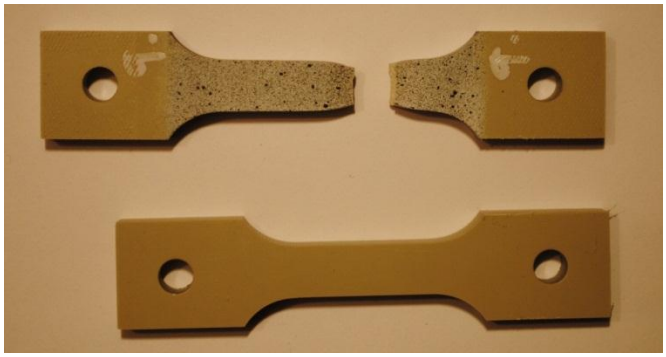

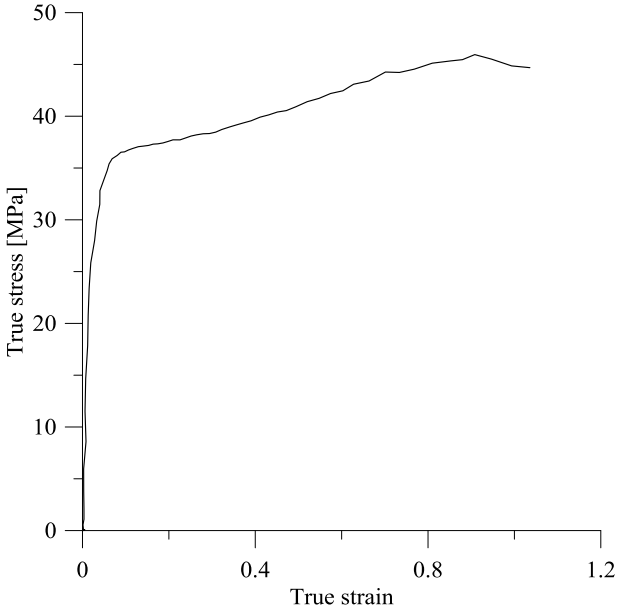

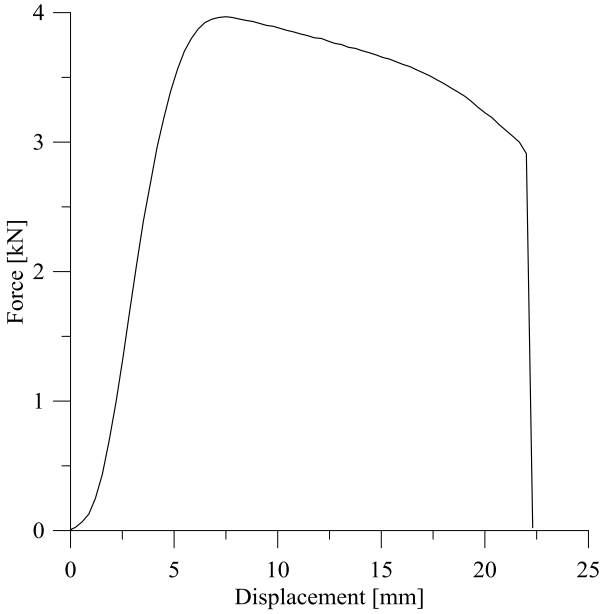

Initial thickness	9.73	mm
Initial width	11.97	mm
Velocity	0.33	mm/s
Strain rate	0.01	s^{-1}
Yield stress	36.1	MPa
Maximum force	3.97	kN
Poissons ratio ν	0.36	
Contraction ratio ρ	0.31	

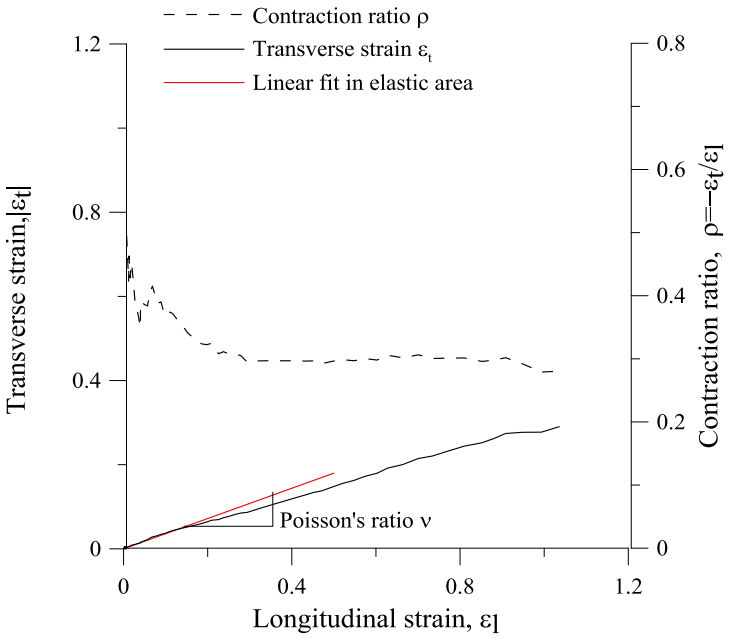

PP-T10

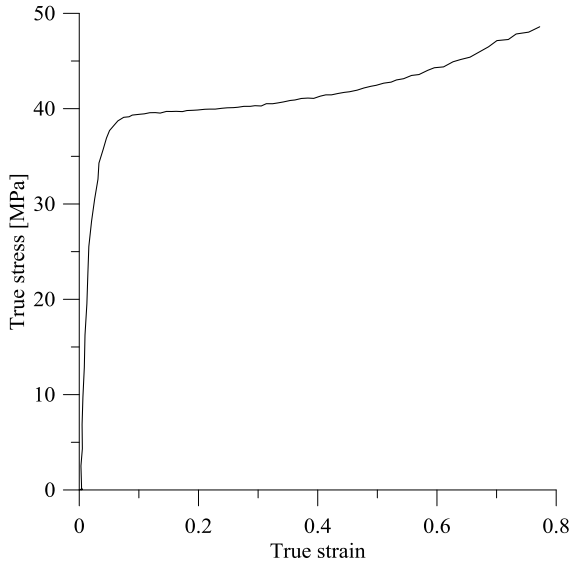

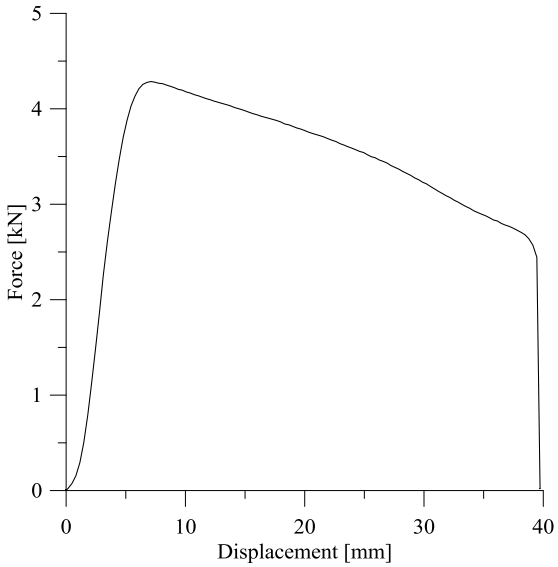

Initial thickness	9.71	mm
Initial width	11.96	mm
Velocity	3.3	mm/s
Strain rate	0.1	s^{-1}
Yield stress	38.9	MPa
Maximum force	4.28	kN
Poissons ratio v	0.37	
Contraction ratio ρ	0.32	

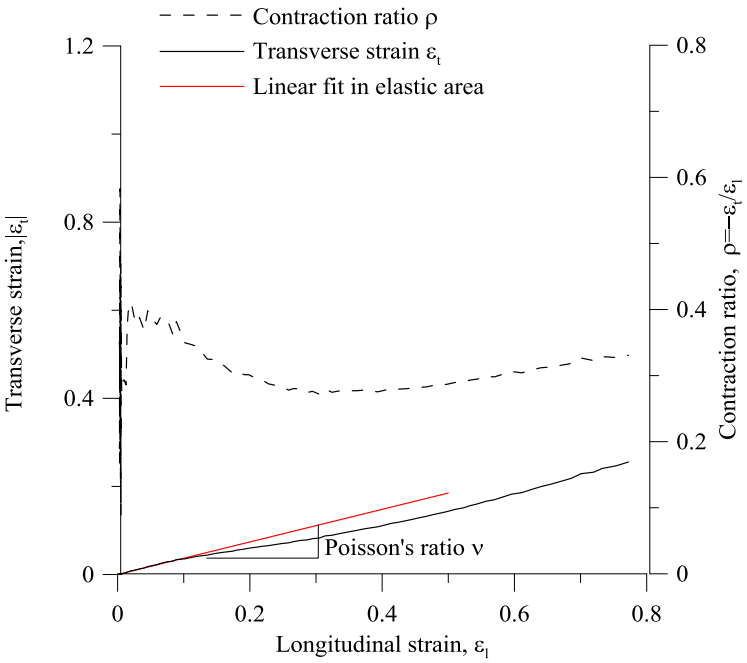

PP-11

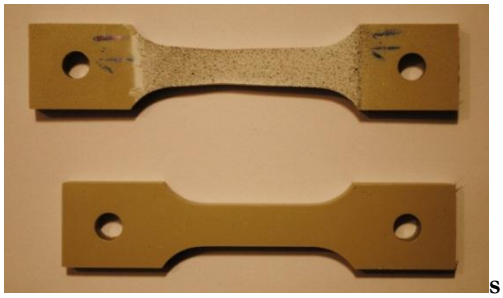

s

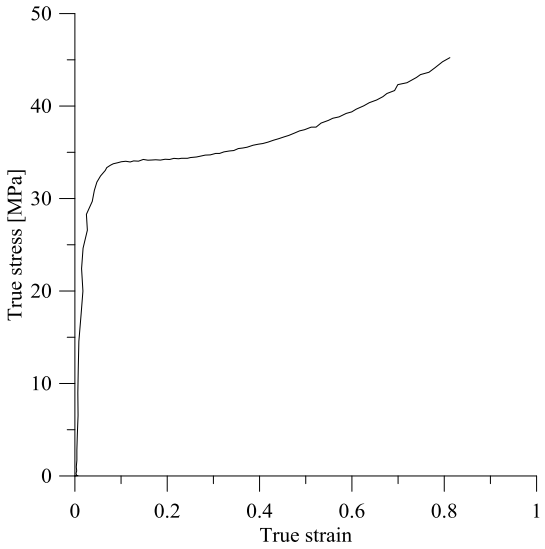

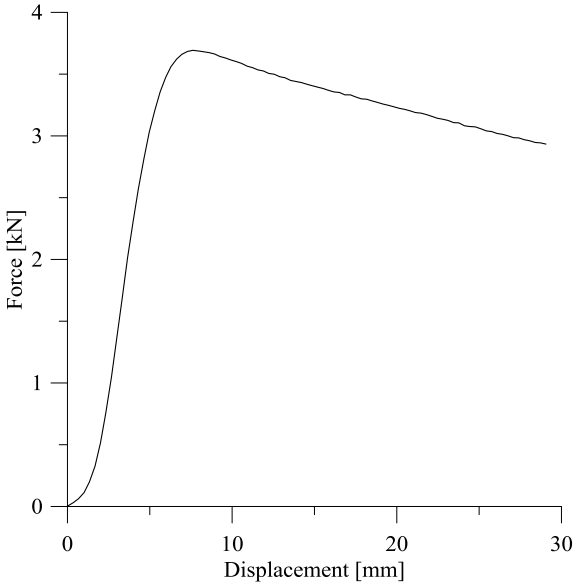

Initial thickness	9.74	mm
Thickness after testing	8.3	mm
Initial width	11.98	mm
Width after testing	10.38	mm
Velocity	0.033	mm/s
Strain rate	0.001	s^{-1}
Yield stress	33.6	MPa
Maximum force	3.69	kN
Poissons ratio ν	0.32	
Contraction ratio ρ	0.35	

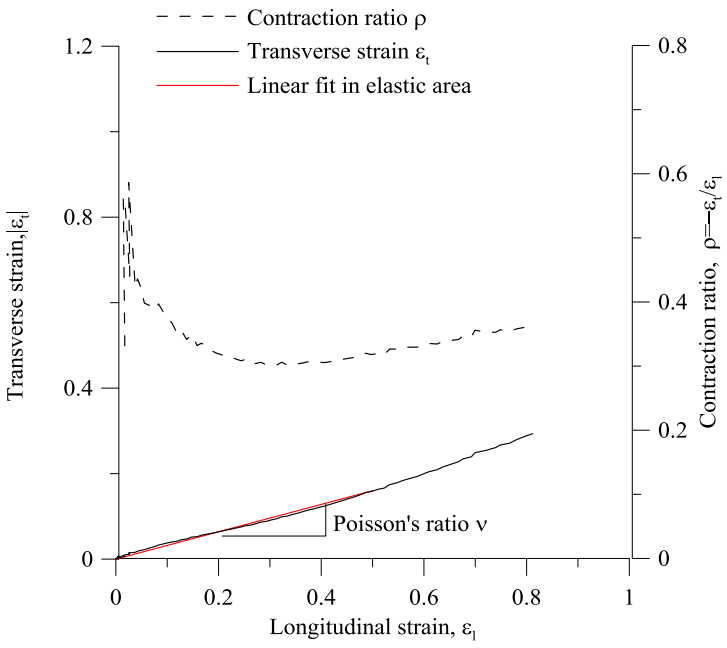

Appendix B

Compression tests

Compression tests

5 compression tests were carried out in a servo-hydraulic Dartec M1000/RK testing machine with a capacity of 20 kN on the test specimens seen in Figure 1 and 2. The test sample of height 8 mm had the longitudinal axis in the extrusion direction, while the test specimen of height 5 mm had the longitudinal axis perpendicular to the extrusion direction. A list of the compression tests carried out, their strain rate, velocity and geometry is seen in Table 1. This appendix presents results from the material tests, including force-displacement curves and stress-strain curves. In addition, pictures of the test specimens after testing and plots of transverse and longitudinal strains are presented. The force and displacements were obtained from the Dartec machine, and the strains were obtained using the DIC technique and MATLAB scripts.

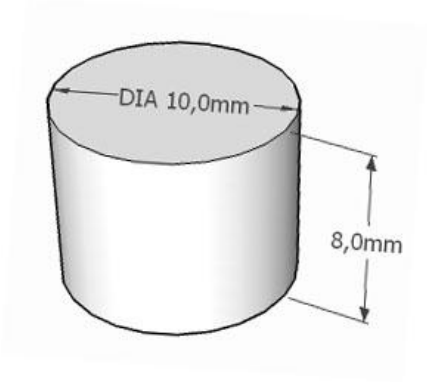

Figure 1. Test sample number 1.

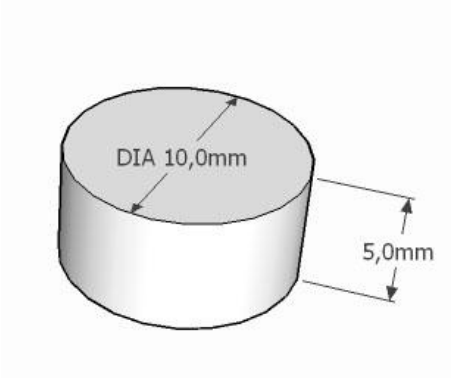

Figure 2. Test sample number 2.

Table 1. List of test specimens.

	Strain rate [s^{-1}]	Velocity [mm/s]	Test sample
PP-C1	10^{-3}	0.008	1
PP-C2	10^{-3}	0.008	1
PP-C3	10^{-2}	0.08	1
PP-C4	10^{-1}	0.8	1
PP-C5	10^{-2}	0.05	2

PP-C1

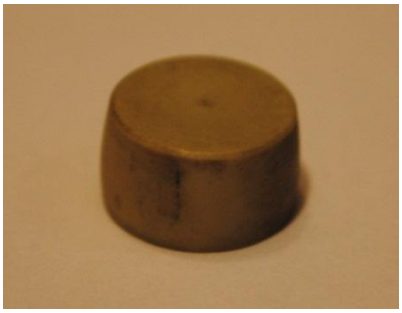

Initial diameter	9.55	mm
Diameter after testing	11.27	mm
Initial height	8.04	mm
Height after testing	6.09	mm
Cross head velocity	0.008	mm/s
Strain rate	0.001	s^{-1}
Yield stress	45.75	MPa

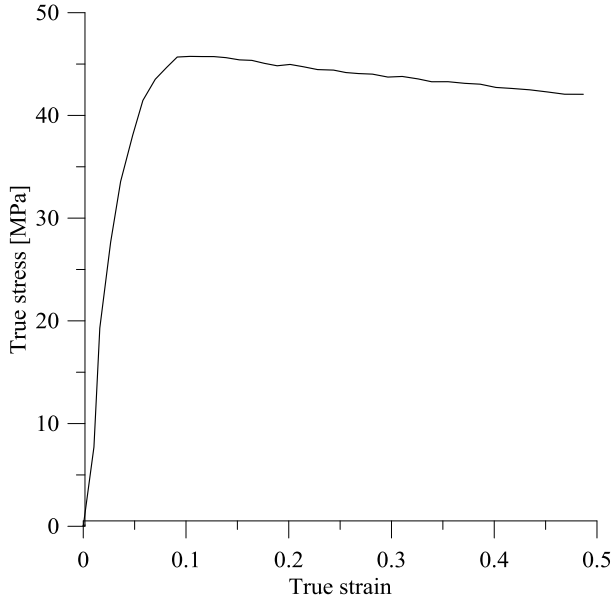

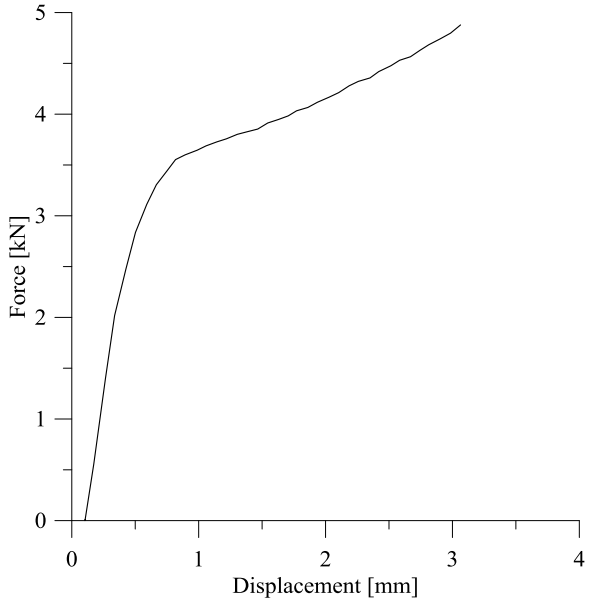

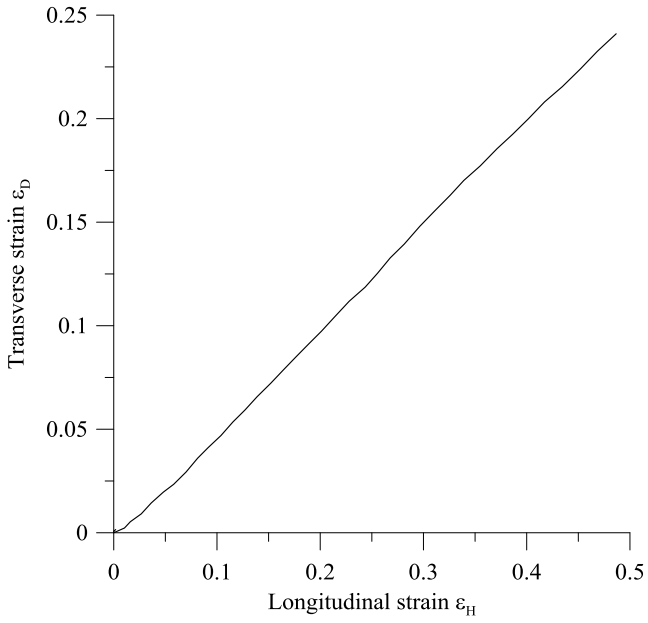

PP-C2

Initial diameter	9.56	mm
Diameter after testing	11.4	mm
Initial height	8.02	mm
Height after testing	6.00	mm
Cross head velocity	0.008	mm/s
Strain rate	0.001	s^{-1}
Yield stress	45.18	MPa

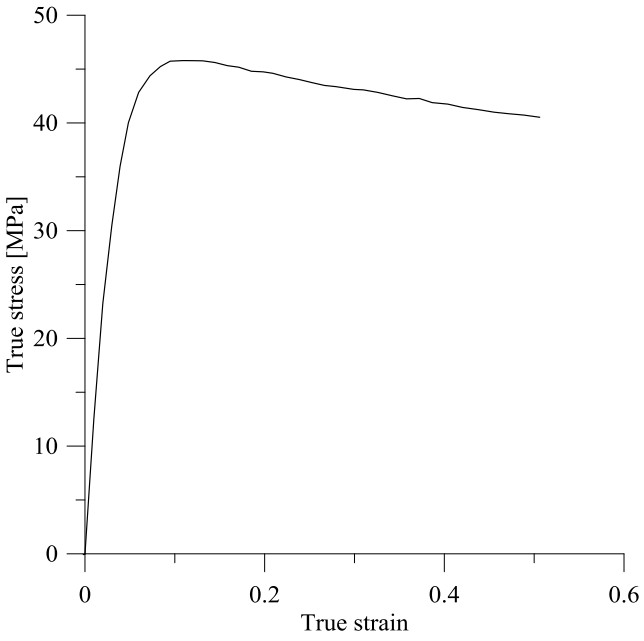

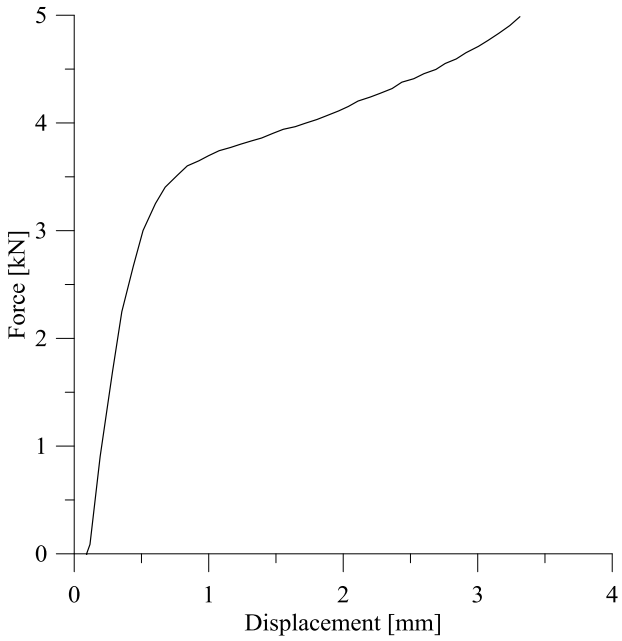

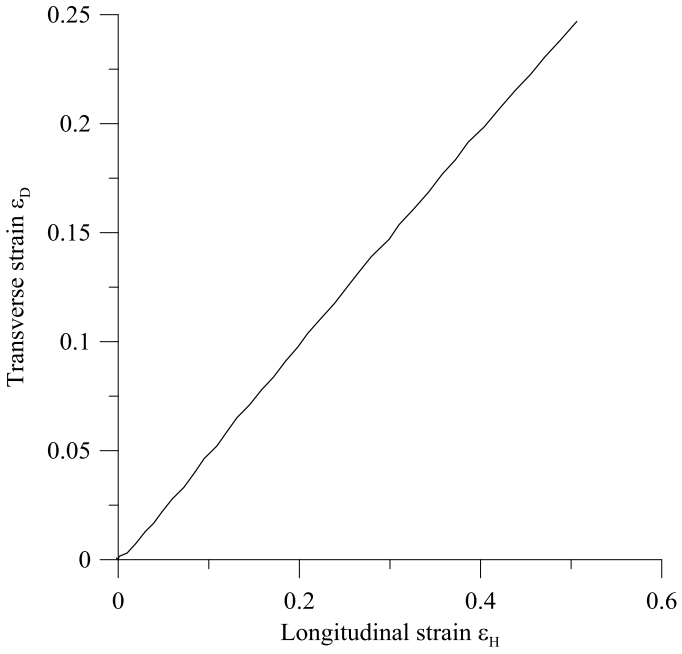

PP-C3

Initial diameter	9.56	mm
Diameter after testing	12.35	mm
Initial height	8.02	mm
Height after testing	5.18	mm
Cross head velocity	0.08	mm/s
Strain rate	0.01	s^{-1}
Yield stress	51.61	MPa

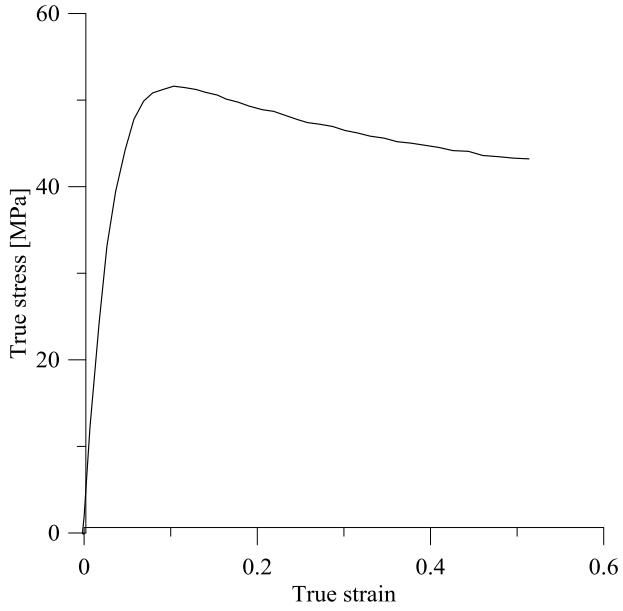

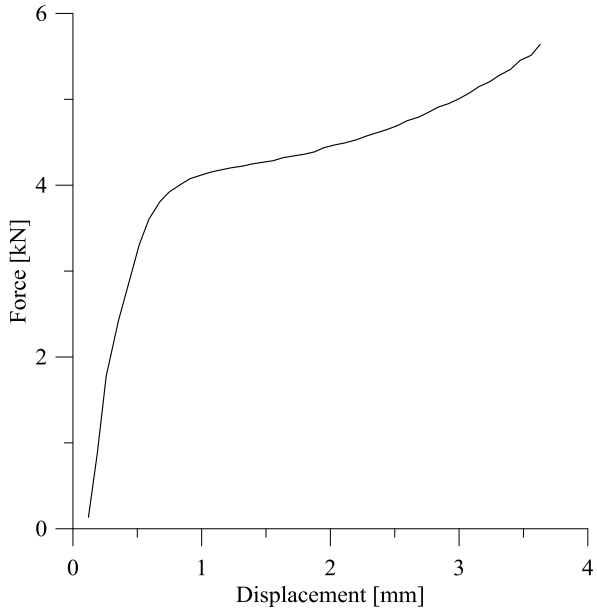

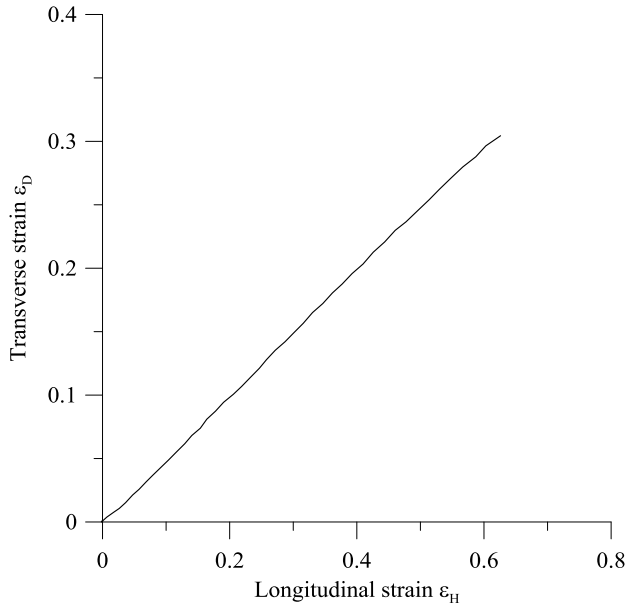

PP-C4

Initial diameter	9.56	mm
Diameter after testing	13.10	mm
Initial height	7.99	mm
Height after testing	4.70	mm
Cross head velocity	0.8	mm/s
Strain rate	10^{-1}	s^{-1}
Yield stress	57.74	MPa

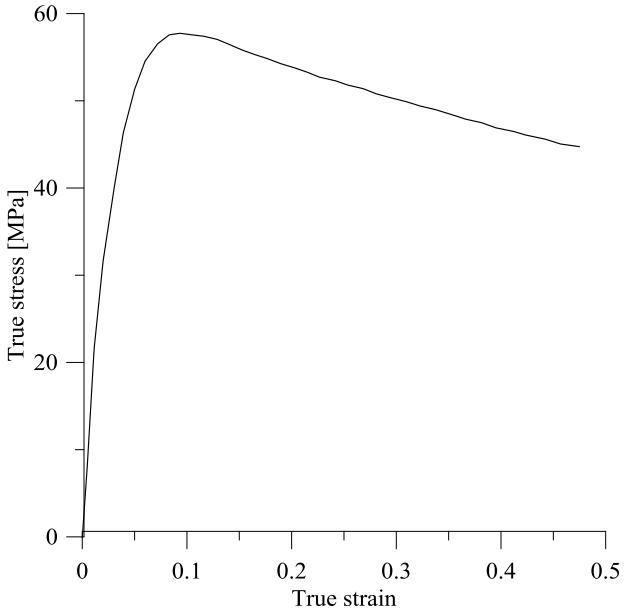

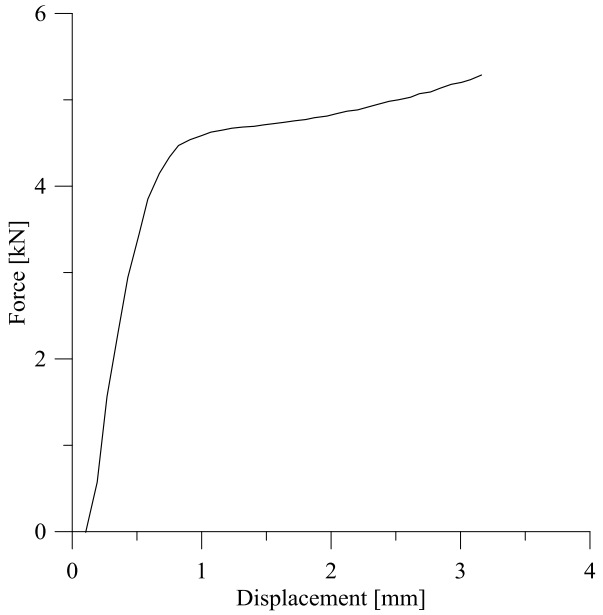

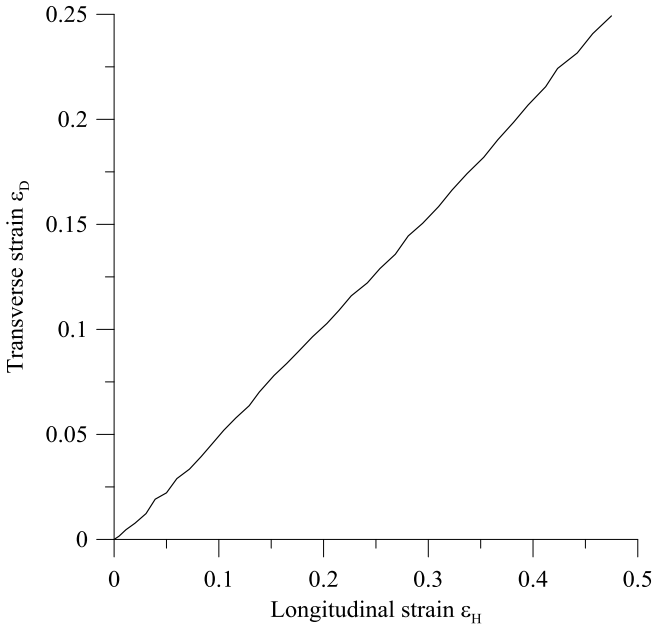

PP-C5

Initial diameter	9.99	mm
Diameter after testing	13.12	mm
Initial height	4.89	mm
Height after testing	3.03	mm
Cross head velocity	0.05	mm/s
Strain rate	0.01	s^{-1}
Yield stress	47.10	MPa

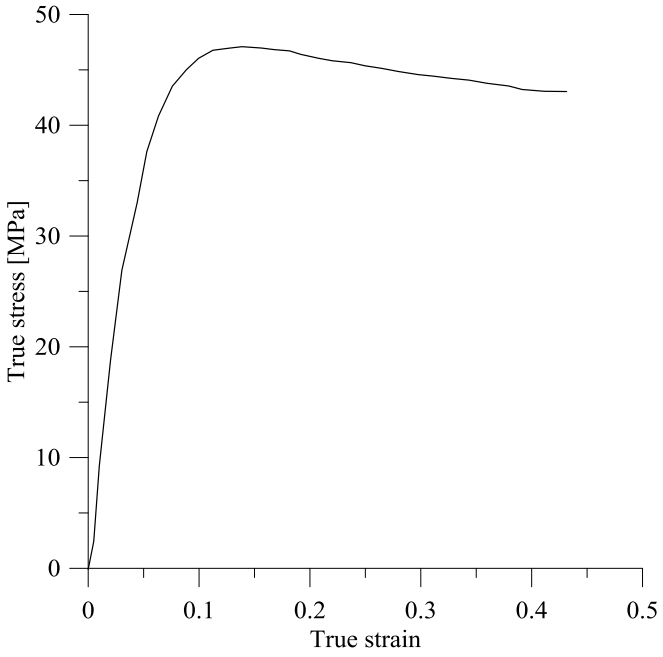

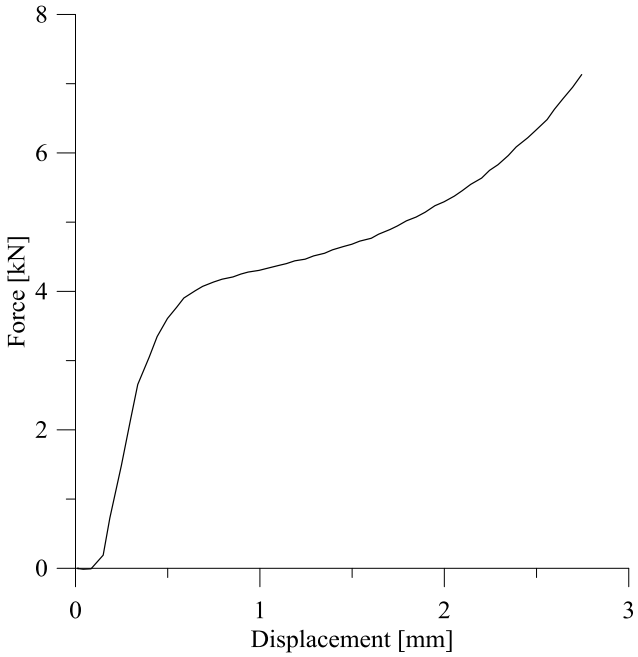

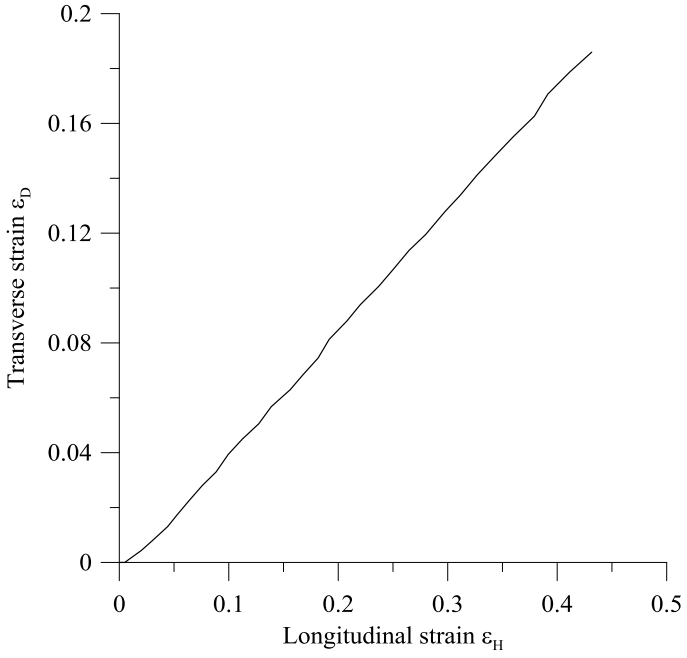

Appendix C

Stretching of a plate with a hole

Stretching of a plate with a hole

4 tension tests on a plate with a hole were carried out in a servo-hydraulic Dartec M1000/RK testing machine with a capacity of 20 kN. The plates had geometries like in Figure 1. Table 1 shows the tests that were carried out.

This appendix will present force and displacement curves from the tests. The forces were obtained from the Dartec machine, and the displacements were obtained from a cross section 40 mm above the center of the hole using the DIC technique. A picture of the test specimens after the testing is presented as well, and for test PP-H1, the dimensions seen in Figure 2 are shown.

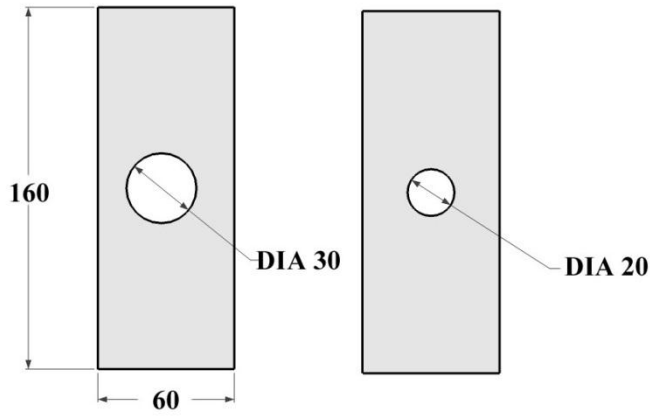

Figure 1. Geometry of plates with a hole, where all dimensions are in millimeters.

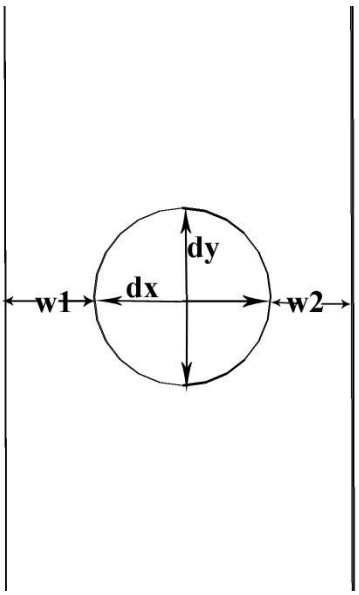

Figure 2. Dimensions that were obtained from test PP-H1.

Table 1. Overview of tension tests carried out on a plate with a hole.

Test number	Cross-head velocity [mm/s]	Initial diameter of hole [mm]
PP-H1	0.05	29.85
PP-H2	0.05	19.71
PP-H3	0.5	29.87
PP-H4	0.5	19.58

PP-H1

Cross head velocity	0.05	mm/s
Initial diameter of hole	29.85	mm
Maximum force	4.8	kN
Maximum displacement	24.2	mm

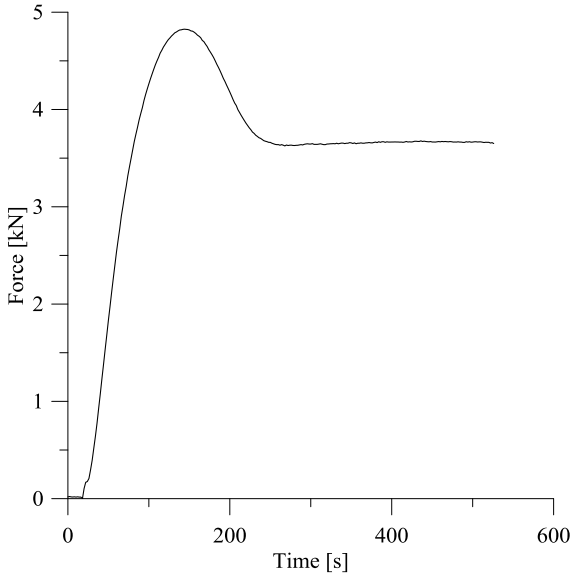

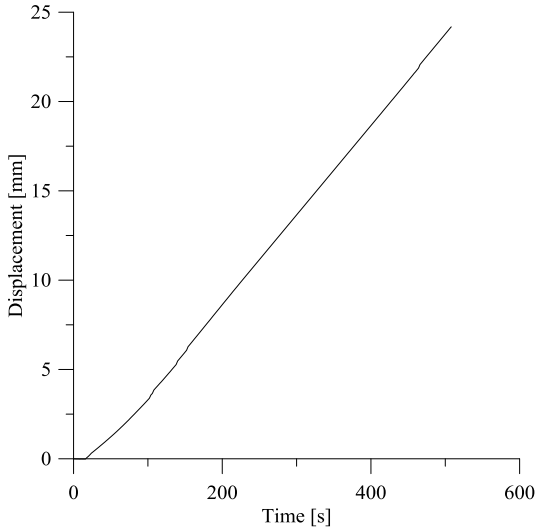

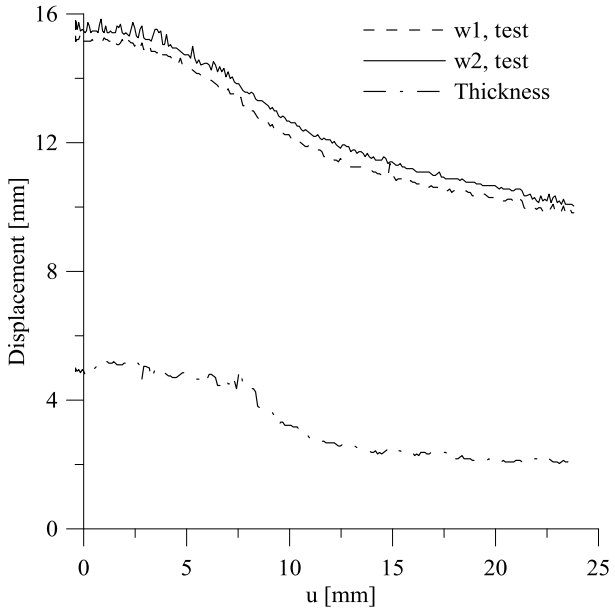

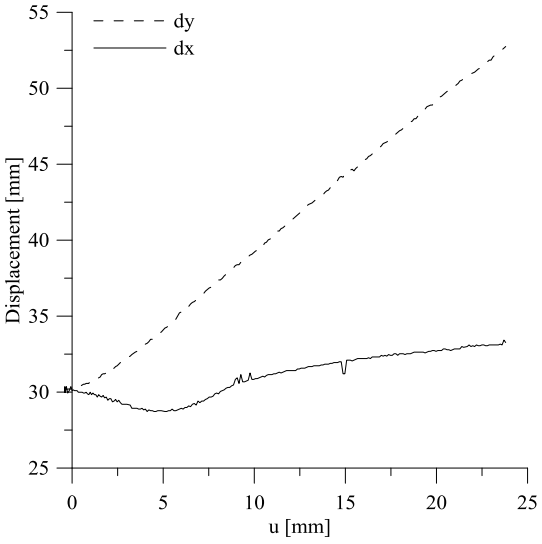

PP-H2

Cross head velocity	0.05	mm/s
Initial diameter of hole	19.71	mm
Maximum force	6.1	kN
Maximum displacement	28.4	mm

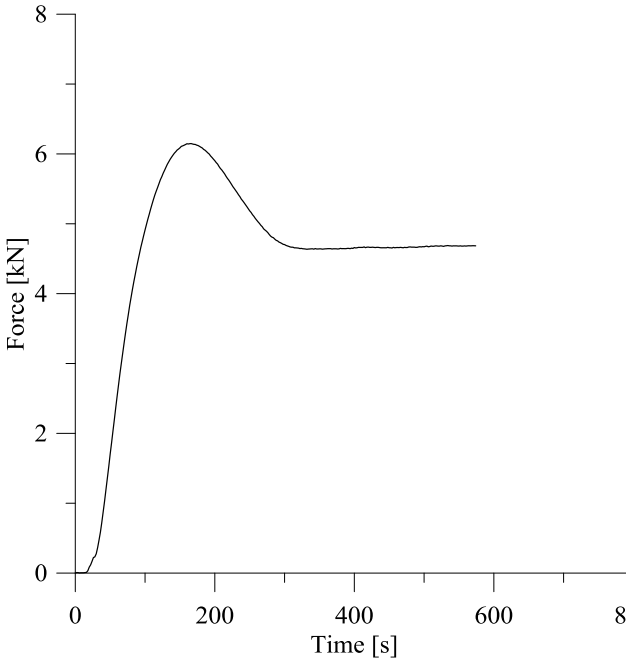

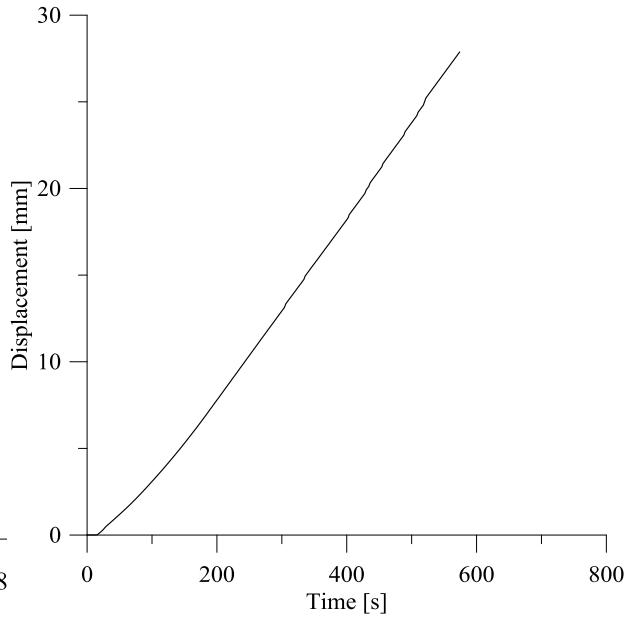

PP-H3

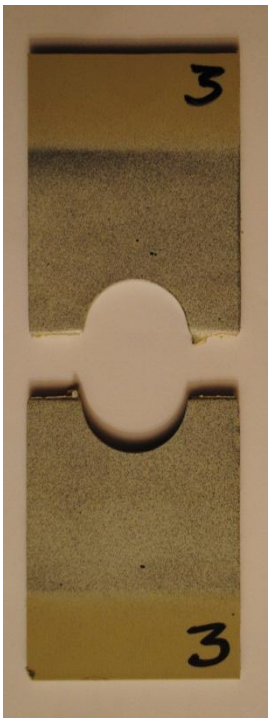

Cross head velocity	0.5	mm/s
Initial diameter of hole	29.87	mm
Maximum force	5.3	kN
Maximum displacement	8.5	mm

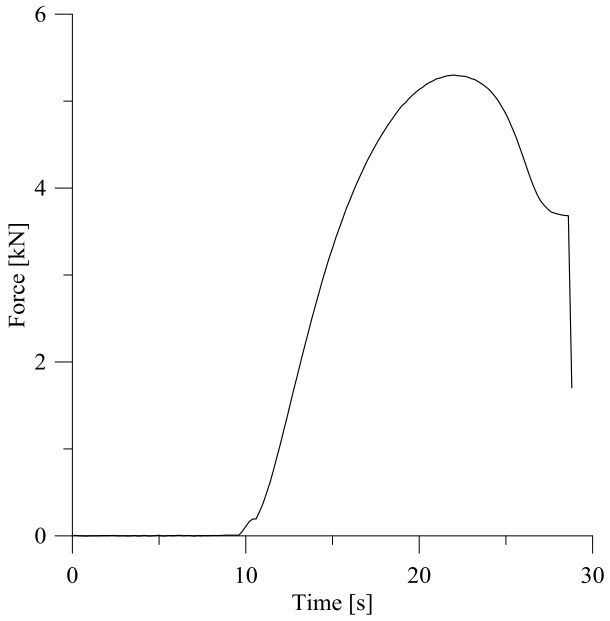

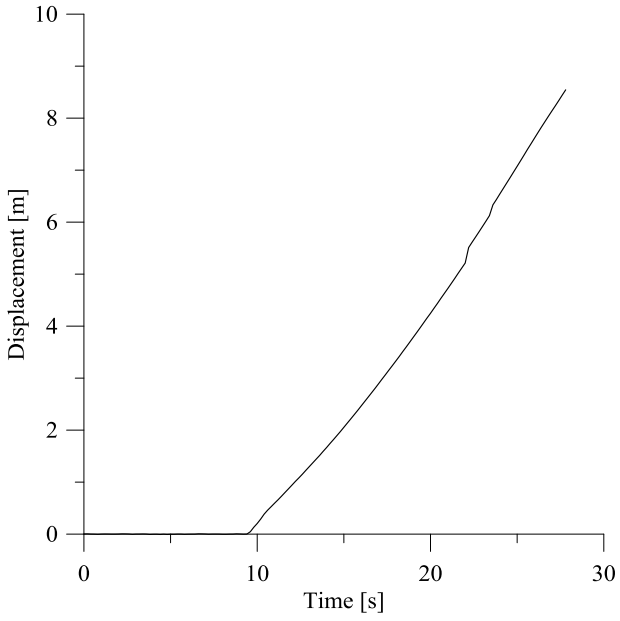

PP-H4

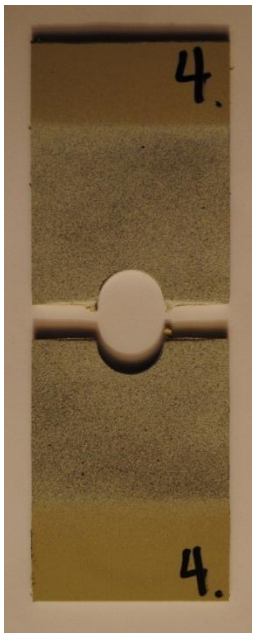

Cross head velocity	0.5	mm/s
Initial diameter of hole	19.58	mm
Maximum force	6.9	kN
Maximum displacement	8.4	mm

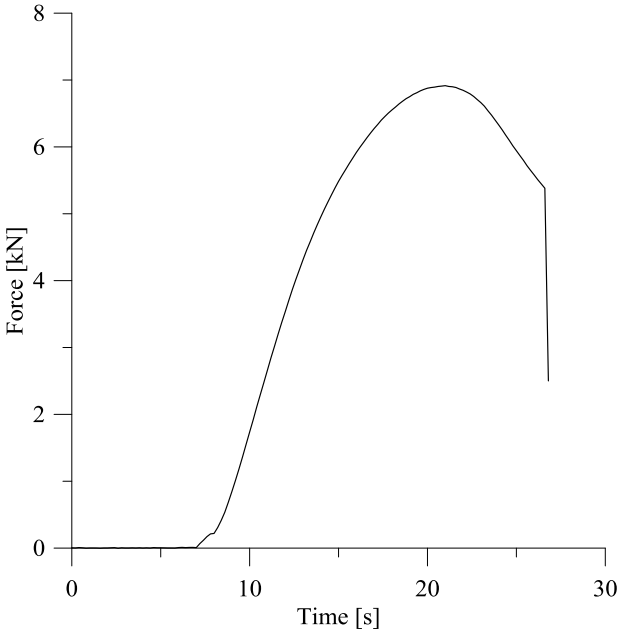

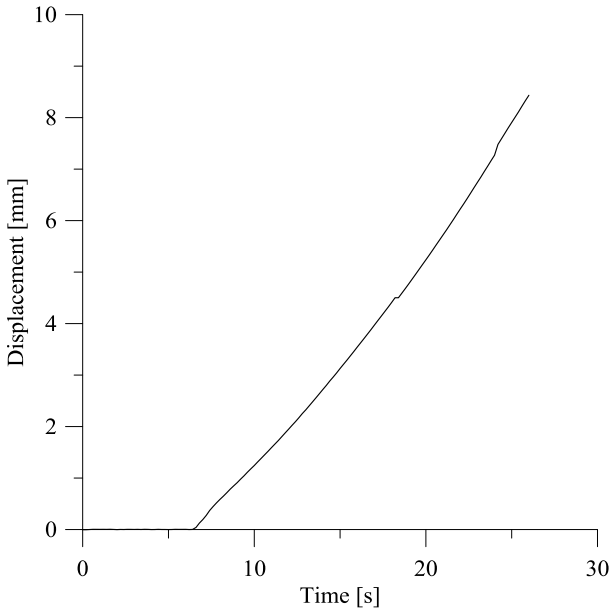

Appendix D

Plate impact tests

Plate impact tests

A total of 6 plate impact tests, all seen in Table 1, were carried out in an Instron CEAST 9350 Drop Tower machine. The test setup is seen in Figure 1. This appendix presents data obtained from the machine during the plate impact testing, including force, displacement and velocity. Pictures of the test specimens after the impact tests are shown as well.

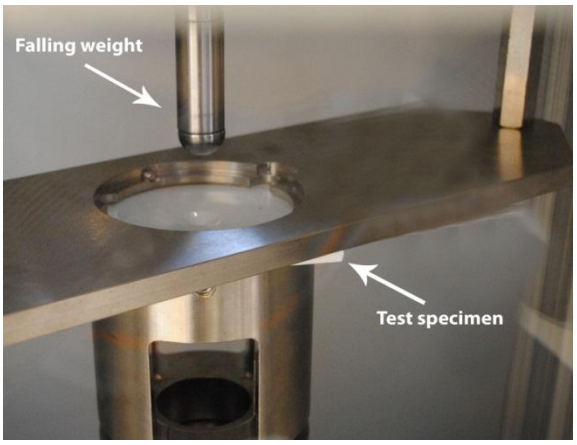

Figure 1. Test setup of plate impact tests.

Table 1. List of plate impact tests carried out.

	Mass [kg]	Velocity [mm/s]	Energy [kJ]
PP-D1	5.045	4430	50
PP-D2	5.045	6263	100
PP-D3	10.045	4430	100
PP-D4	10.045	6263	200
PP-D5	10.045	5424	150
PP-D6	10.045	5774	170

PP-D1

Initial thickness	4.94	mm
Energy	50	J
Mass	5.045	kg
Velocity	4430	mm/s
Height	1	m

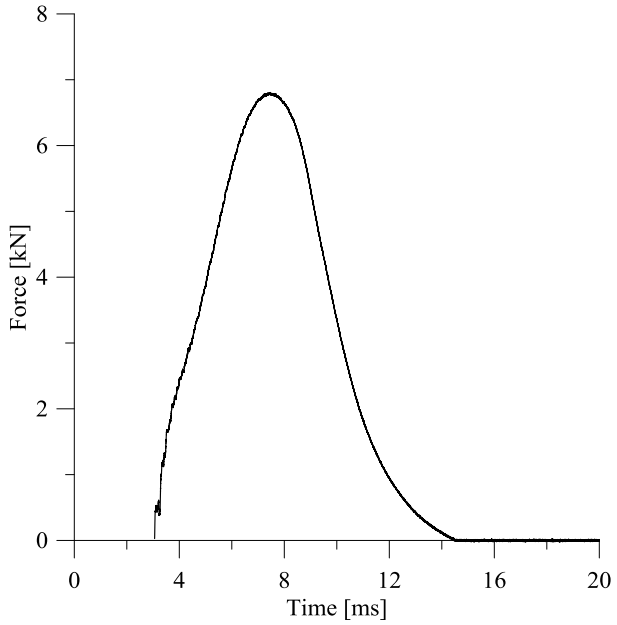

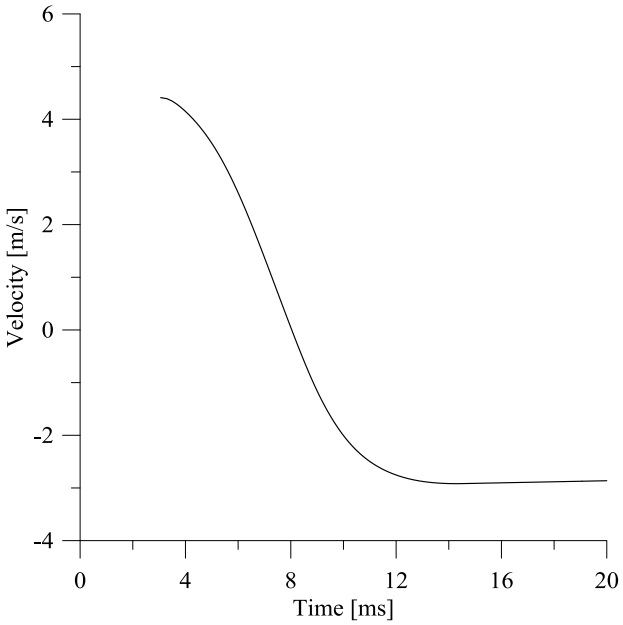

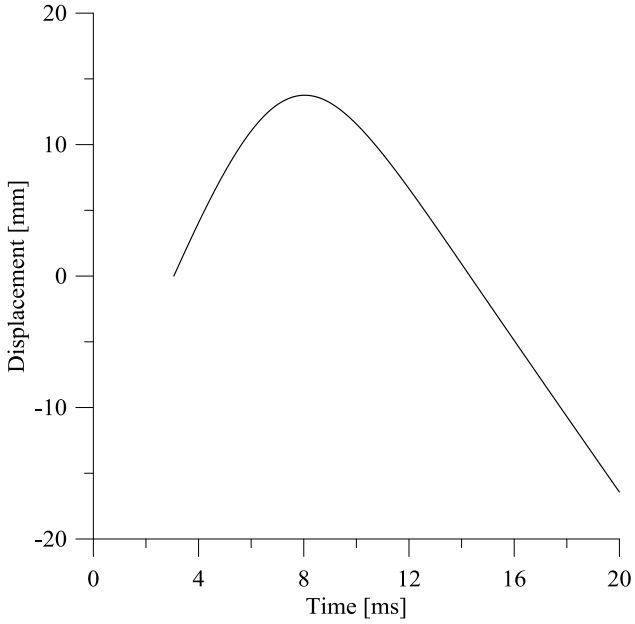

PP-D2

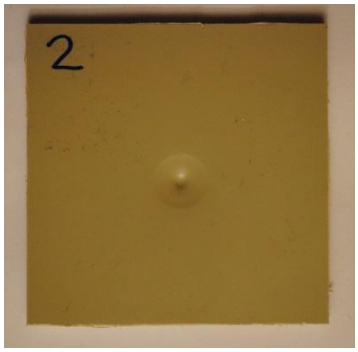

Initial thickness	4.94	mm
Energy	100	J
Mass	5.045	kg
Velocity	6230	mm/s
Height	2	m

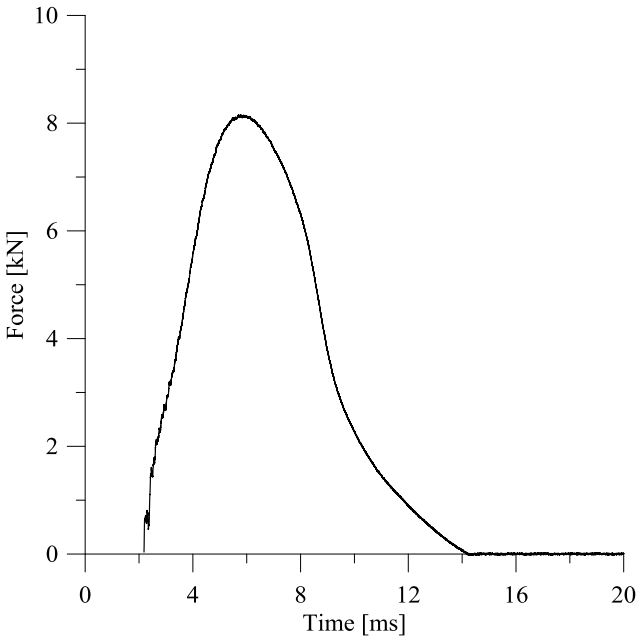

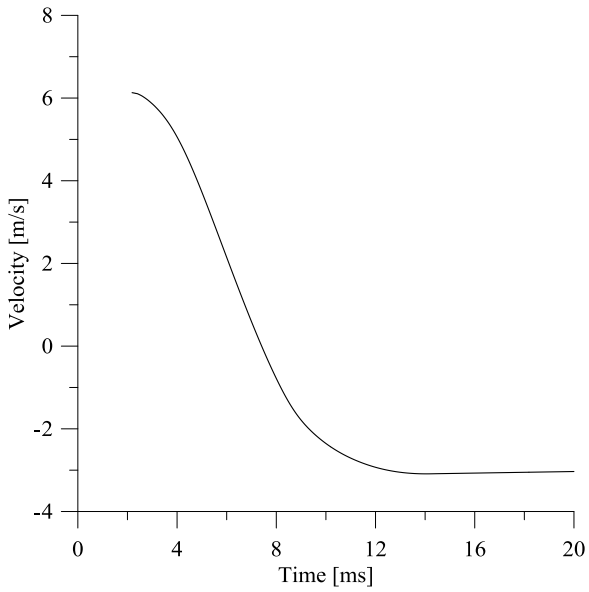

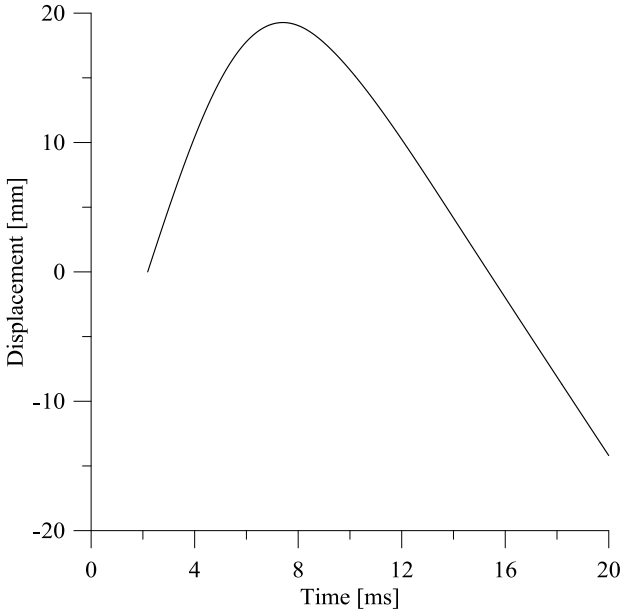

PP-D3

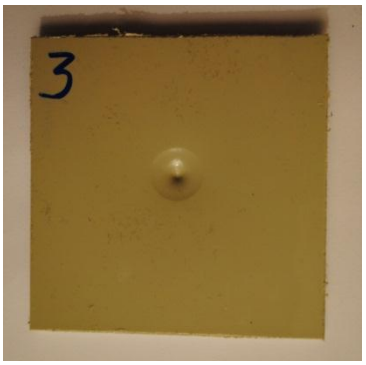

Initial thickness	4.94	mm
Energy	100	J
Mass	10.045	kg
Velocity	4430	mm/s
Height	1	m

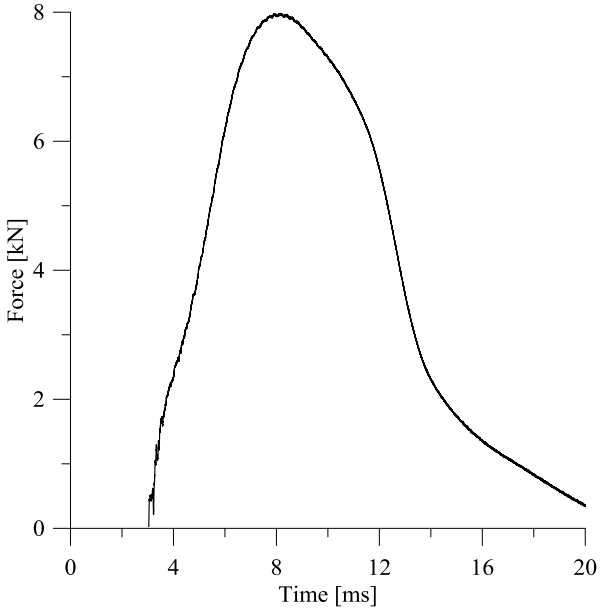

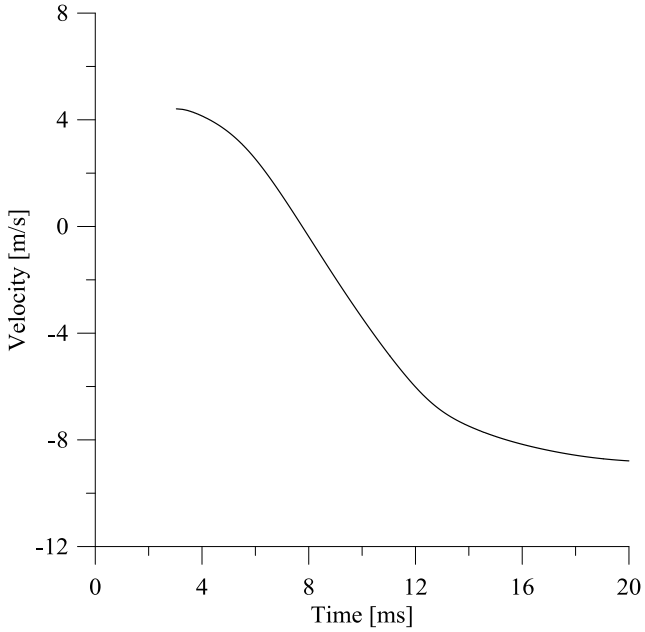

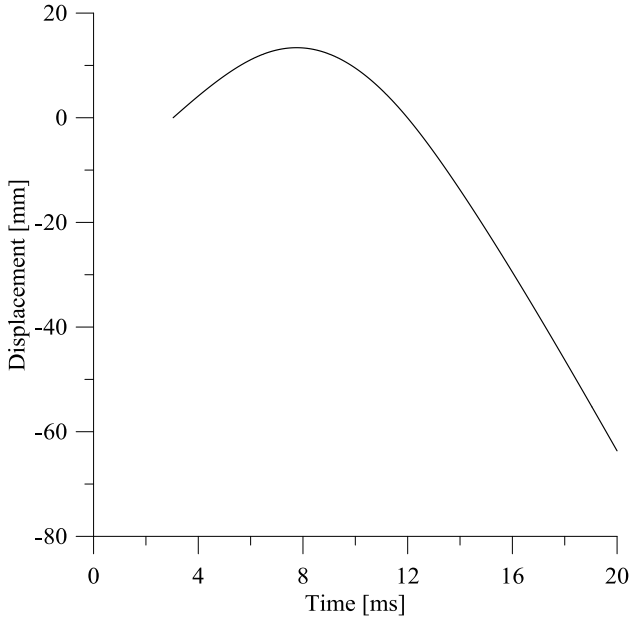

PP-D4

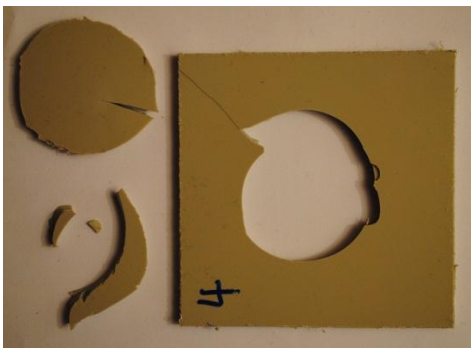

Initial thickness	4.95	mm
Energy	200	J
Mass	10.045	kg
Velocity	6230	mm/s
Height	2	m

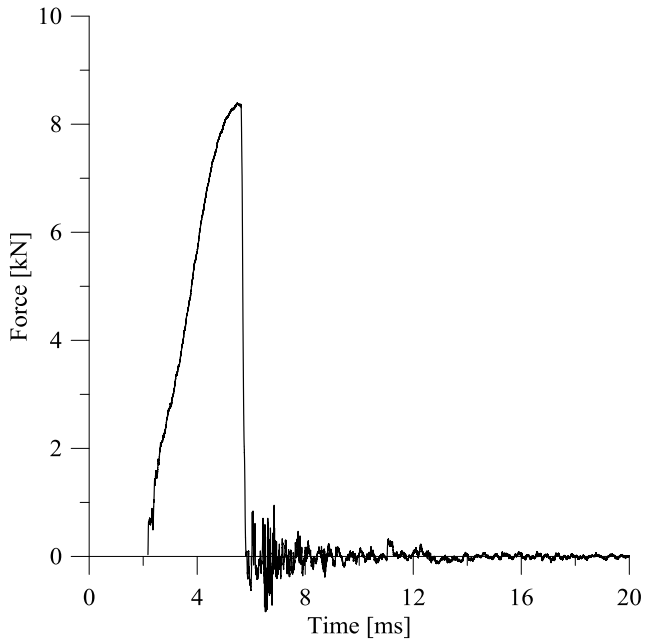

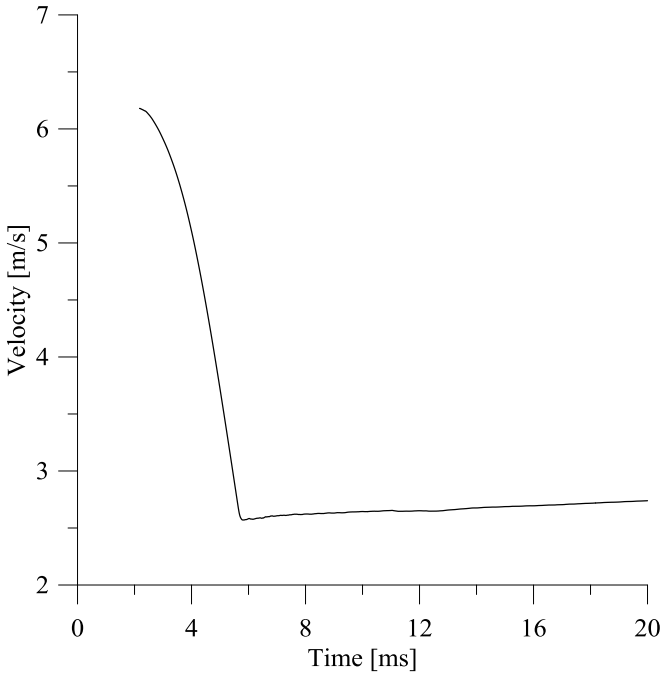

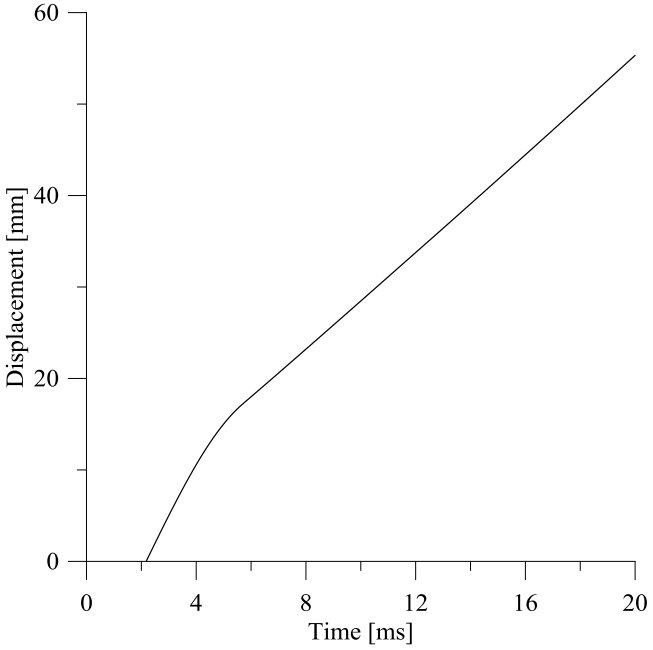

PP-D5

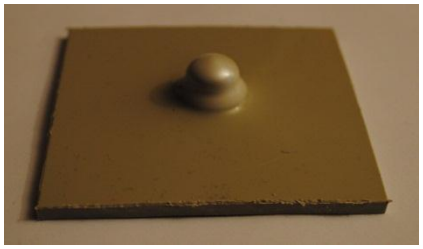

Initial thickness	4.94	mm
Energy	150	J
Mass	10.045	kg
Velocity	5424	mm/s
Height	1.5	m

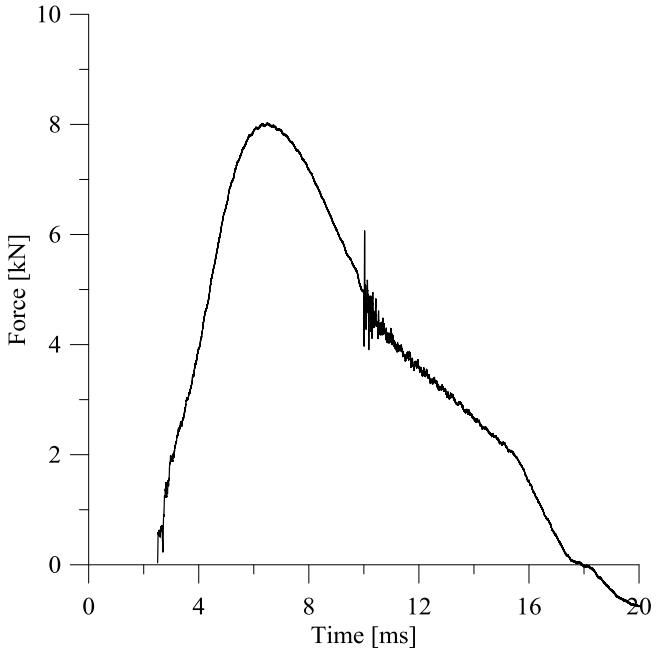

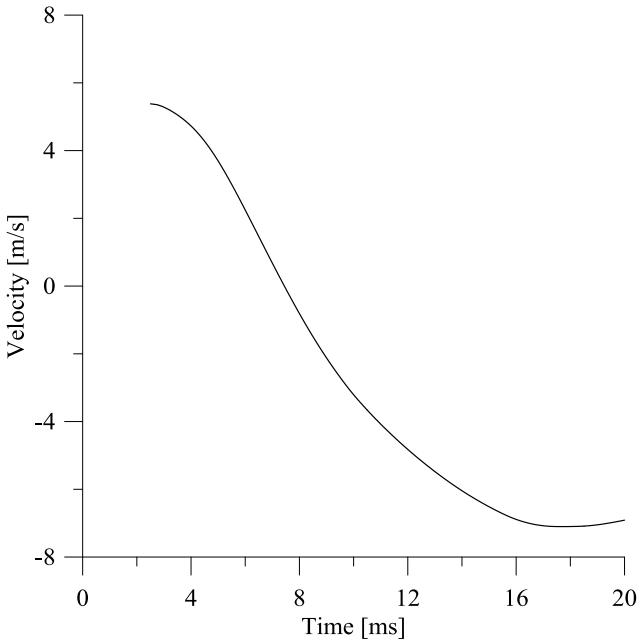

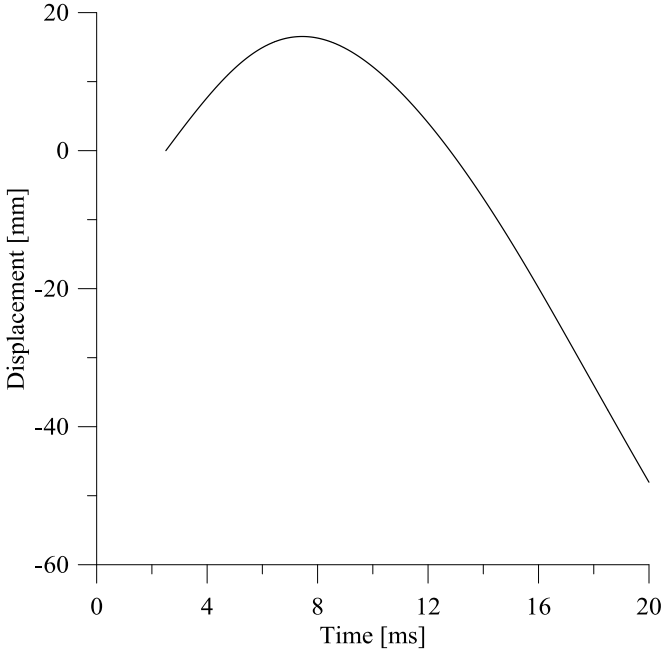

PP-D6

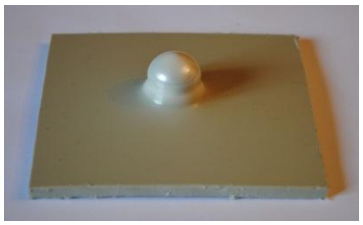

Thickness	4.94	mm
Energy	170	J
Mass	10.045	kg
Velocity	5774	mm/s
Height	1.7	m

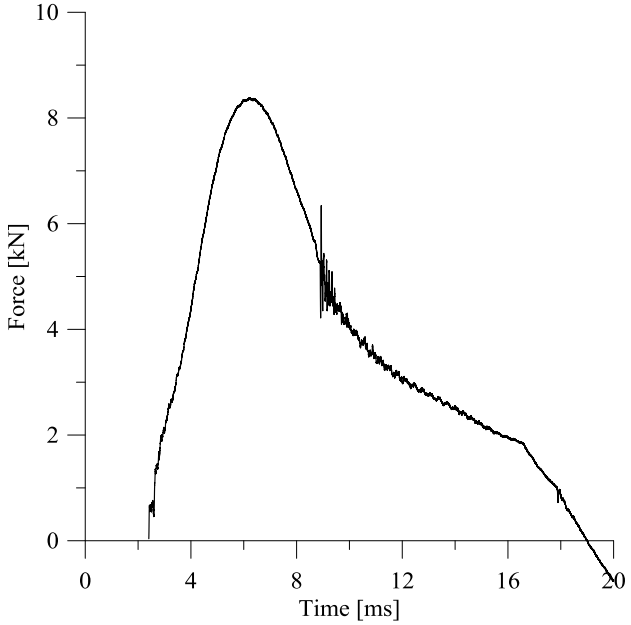

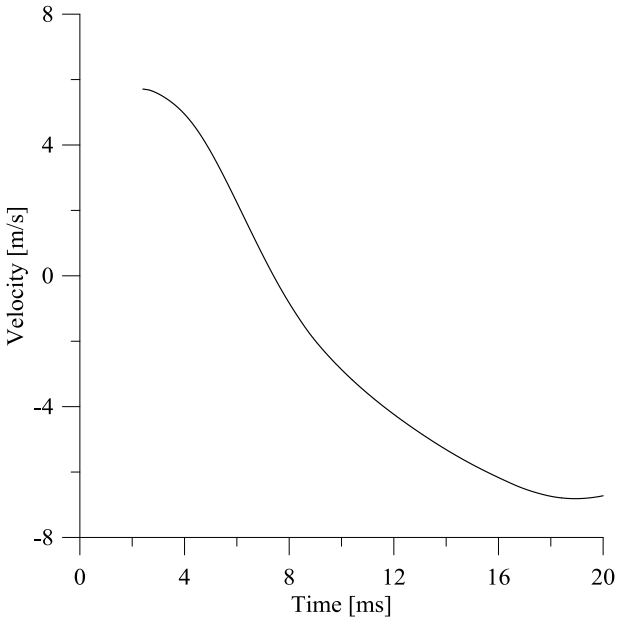

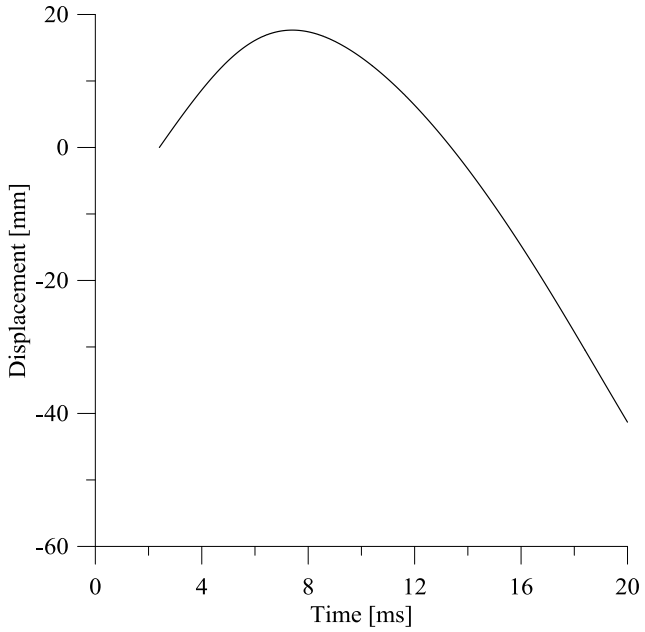

Appendix E

MATLAB scripts

Determination of strains in tension tests

```
%Finding the strain from the matrices from 7D
%Test PP-T1

ant=130; %enter number of pictures

X=13; %input('enter x value in area where necking starts  ')
Y=30; %input('enter y value in area where necking starts  ')

%First strain is 0
elnmini(1)=0;
elnmaxi(1)=0;

for A=1:ant; %go through all pictures
B=eval(sprintf('elnmaxi%.3d',A));


%Finding where necking starts:
%Looking at a belt of 40 pixels in y-direction. Determine at what row
%the strain is biggest. Use this row in further calculation
for i=Y-20:Y+20;
      m=1;
       for j= X-8:X+7;

          a(m)=B(i,j);
          m=m+1;
       end
       K(i,1)=mean(a);
end
b=max(K);
[rad(A)]=find(K==b);
end

figure(1) % figure of row-picture
plot(rad,'-r');
xlabel('Picture')
ylabel('Row')
title('Overview of what row that has most strain')

%% find from the figure that row 31 is the one with most strain.

row=31;

% Calculate the mean of row number 31 from all pictures and save in the
% vector "elnmaxi"

            for k=1:ant
               n=1;
                 for p= X-4:X+5
                     M_elnmaxi(n)=eval(sprintf('elnmaxi%.3d(row,%d)',k,p));
                     M_elnmini(n)=eval(sprintf('elnmini%.3d(row,%d)',k,p));
                     n=n+1;
                end
       elnmaxi(k+1,1)=mean(M_elnmaxi);
       elnmini(k+1,1)=mean(M_elnmini);
            end

figure (2)
subplot(1,2,1)
plot(elnmaxi)
title('elnmaxi, longitudinal strain')
subplot(1,2,2)
plot(-1*elnmini)
title('elnmini, transverse strain')
```

Determination of diameter and height of compression tests

```
%Determining the diameter and height of compression test samples:

no_pics=40; % enter number of pictures.

for k=1:no_pics;
 filename=['PP-C1_2012_02_07_13h32m03s_Cam1_Frame_' num2str(k,'%08d')
'.bmp'];
 image=imread(filename);
 K=im2bw(image,0.8);
 D=1-K;  % convert matrix so black = a nonzero value

 %Find the row in the middle of the test specimen:
  row_first_nonzero=find(K(:,1),1,'first');
  row_last_nonzero=find(K(:,1),1,'last');
  row_dia(k)=round(row_first_nonzero+(row_last_nonzero-
row_first_nonzero)/2);

 %Find first and last nonzero pixel at the row called row_dia:
   col_first_nonzero=find(D(row_dia(k),:),1,'first');
   col_last_nonzero=find(D(row_dia(k),:),1,'last');

height_pixels(k)=row_last_nonzero-row_first_nonzero;
diameter_pixels(k)=col_last_nonzero-col_first_nonzero;
end

diameter_pixels=transpose(diameter_pixels);
height_pixels=transpose(height_pixels);

%1 pixel corresponds to 9,55mm/1310 pixels =191/26200 mm:
diameter_mm=diameter_pixels*191/26200;
height_mm=height_pixels*191/26200;
```

Determination of dimensions in the plate with a hole

The MATLAB script presented is determining the dimensions w1, w2, dx and dy. The dimensions w1 and w2 are named b1 and b2 in the script.

```
%Finding b1, b2, btot and dx from the pictures
%PP-H1 cam1
clear all
clc

no_pics=264; % number of pictures
files = dir('PPS-01*.bmp');

%Convert to black-white picture:
for k=1:no_pics;
image=imread(files(k).name);
if k>=236 %need different contrast in the pictures
      K=im2bw(image,0.26);
else
    K=im2bw(image,0.18);
end

%Divide the test specimen in two vertical pieces:
K_left=K(:,1:length(K)/2);
K_right=K(:,length(K)/2:length(K));
```

```
%Find the row in the middle of the test specimen:
a_l=size(K_left);
length_l=a_l(1,1);
row_left=round(length_l/2);
a_r=size(K_right);
length_r=a_r(1,1);
row_right=round(length_r/2);

%Find the row where necking is highest in each picture:
for i=row_left-250:row_left+250;
b1_sum(i)=sum(K_left(i,:));
b2_sum(i)=sum(K_right(i,:));
end

min_b1=min(b1_sum(row_left-250:row_left+250));
min_b2=min(b2_sum(row_right-250:row_right+250));

Row_left(k)=round(mean(find(b1_sum==min_b1)));
Row_right(k)=round(mean(find(b2_sum==min_b2)));

b1(k)=b1_sum(Row_left(k));
b2(k)=b2_sum(Row_right(k));

row_mean(k)=round((Row_left(k)+Row_right(k))/2);
col_first_nonzero=find(K(row_mean(k),:),1,'first');
col_last_nonzero=find(K(row_mean(k),:),1,'last');
b_tot(k)=col_last_nonzero-col_first_nonzero;

%Finding dx at row_mean too:
b1_row_mean(k)=b1_sum(row_mean(k));
b2_row_mean(k)=b2_sum(row_mean(k));
dx(k)=b_tot(k)-b1_row_mean(k)-b2_row_mean(k);

end

b1=transpose(b1);
b2=transpose(b2);
b_tot=transpose(b_tot);
dx=transpose(dx);
%in picture no 1: 1 pixel corresponds to 0.0528mm
mm=0.0528;
b1_mm=b1*mm;
b2_mm=b2*mm;
b_tot_mm=b_tot*mm;
dx_mm=dx*mm;

%plot of b1 og b2:
figure(1)
plot(b1_mm,'r');
hold on
plot(b2_mm,'m');
hold on
plot(b_tot_mm,'b');
hold on
plot(dx_mm,'g');
xlabel('foto');
ylabel('bredde');
legend('b1','b2','b total','dx');

%plot of row -picture
figure(2)
plot(Row_left,'b')
hold on
plot(Row_right,'r')
xlabel('foto')
ylabel('rad')
legend('b1','b2')
```

Appendix F

LS-DYNA keyword file

LS-DYNA keyword file for a representative tension test (PP-T2)

```
*KEYWORD
*INCLUDE
geometri.k
*HOURGLASS
$#hgid    ihq        qm  ibq       q1      q2  qb/vdc     qw
     1      5  0.150000     0    0.000   0.000   0.000   0.000
*BOUNDARY_PRESCRIBED_MOTION_SET
$ nsid    dof    vad    lcid       sf      vid   death  birth
     2      1         0     1 0.033000     01.0000E+28   0.000
*BOUNDARY_SPC_SET
$#   nsid    cid    dofx   dofy   dofz   dofrx   dofry  dofrz
     1      0         1     1        1       0       0       0
*DEFINE_CURVE_SMOOTH
$#lcid    sidr      dist    tstart      tend     trise    v0
     1      0 10000.000     0.000  10000.000 5.0000E-3 1.000
*SECTION_SOLID
$#   secid  elform   aet
     1      2         0
*PART
$# title
$# pid   secid     mid   eosid    hgid    grav  adpopt    tmid

     2      1         1      0       0       0       0       0
$
$$$$$$$$$$$$$$$$$$  MATERIAL MODEL  $$$$$$$$$$$$$$$$$$$$$$$$$$$$
$
*MAT_USER_DEFINED_MATERIAL_MODELS
$ MID    rho   User mat #   LMC   # Hist var      IBULK    IG

     1 910E-3        49     16       50      0       15     16
$IVECT     IFAIL ITHERM   IHYPER     IEOS
     0      0         0      1
$    E    Poisson    eps0    C   sigma_T    Cr lamda_L   alfa
  1600 0.4458   0.00075 0.0483    17.00   1.30    1.938 1.3817
$ beta    kappa   sigma_0     H                     K       G
1.142857   0.00    32.3  48.93                     4920    553
$
$$$$$$$$$$$$$$$$$  CONTROL OPTIONS  $$$$$$$$$$$$$$$$$$$$$$$$
$
*CONTROL_ENERGY
       2      2       2      1
*CONTROL_TIMESTEP
  0.0000 0.9000       0   0.00   0.00000
*CONTROL_ACCURACY
       0      3
*CONTROL_TERMINATION
$#endtim  endcyc   dtmin    endeng    endmas
1300.000      0  0.000     0.000     0.000
*CONTROL_CPU
 0.0000000
*CONTROL_PARALLEL
$   NCPU
       1      0     2         0
$
$$$$$$$$$$$$$$$$$$    DATABASE OPTIONS  $$$$$$$$$$$$$$$$$$$$ $
*DATABASE_SECFORC
```

```
$#      dt    binary  lcur     ioopt
0.020000    1       0         1
*DATABASE_NODAL_FORCE_GROUP
       1
*DATABASE_NODFOR
   2E-02
*DATABASE_BINARY_D3PLOT
20.0E-01
*DATABASE_EXTENT_BINARY
      59    0       3        1        0       0       0       0
       0    0       4        0        0       0
*DATABASE_NODOUT
2.0000E-02
*DATABASE_HISTORY_NODE_SET
$#  id1    id2      id3     id4     id5     id6     id7     id8
       2    0       0        0       0       0       0       0
*DATABASE_CROSS_SECTION_SET_ID
$#   csid
       1
$#  nsid    hsid    bsid    ssid    tsid    dsid     id   itype
       3       1       0       0       0       0      0      0
*END
```